Supplementary Materials for

Direct in Vivo RNAi Screen Unveils Myosin IIa as a Tumor Suppressor of Squamous Cell Carcinomas

Daniel Schramek, Ataman Sendoel, Jeremy P. Segal, Slobodan Beronja, Evan Heller, Daniel Oristian, Boris Reva, Elaine Fuchs*

*Corresponding author. E-mail: fuchslb@rockefeller.edu

Published 17 January 2014, *Science* **343**, 309 (2014)
DOI: 10.1126/science.1248627

This PDF file includes:

Materials and Methods

Mice and lentiviral transductions

TβRII floxed mice (*17*) were crossed to K14-Cre (*18*) and/or Rosa26YFPlox/stop/lox (*19*) mice and or K14-CreER mice (*18*). *Myh9* floxed mice were purchased form EMMA (EM:02572). CD1 mice were from Charles River laboratories. Large-scale production and concentration of lentivirus ($6x10^9$ cfu/ml) as well as ultrasound-guided lentiviral injection were performed as previously described. (*20, 21*) As controls for knock-down mice, littermates were infected with a non-targeting scrambled-shRNA, which activates the endogenous microRNA processing pathway but is not known to target any gene. *Myh9*fl/fl K14CreER mice were injected i.p. with 2mg tamoxifen (20mg/ml stock solution in corn oil) for 5 consecutive days at 6-8 weeks of age. DMBA/TPA treatment was performed as previously described. (*22*) Briefly, 7-8 week old CD1 mice in second telogen were shaved and treated with 400nmol DMBA in 100ul aceton one week later. Thereafter, mice were treated with 17nM TPA in 100ul aceton wice weekly for 20 weeks. All animals were maintained in an AAALAC-approved animal facility and procedures were performed with protocols approved by IACUC and in accordance with the National Institutes of Health.

Constructs and RNAi

shRNA constructs for the shRNA pool were obtained from The Broad Institute's Mission TRC-1 mouse library. (*23*) We tested and used especially the following shRNAs targeting *Brca1, Trp53* and *Myh9*:

Brca1 #560	TRCN0000042560	5'-CCCATCATACTTTAATGTGTA-3'
Trp53 #361	TRCN0000012361	5'-CCACTACAAGTACATGTGTAA-3'
Myh9 #503	TRCN0000071503	5'-GCCCTGGAACTGTGTTTAGAA-3'
Myh9 #504	TRCN0000071504	5'-CGGTAAATTCATTCGTATCAA-3'
Myh9 #505	TRCN0000071505	5'-GCACACATTGACACAGCCAAT-3'
Myh9 #506	TRCN0000071506	5'-GCCATACAACAAATACCGCTT-3'
Myh9 #507	TRCN0000071507	5'-GCGATACTACTCAGGGCTTAT-3'

The scrambled shRNA 5'-CAACAAGATGAAGAGCACCAA-3' was used as the scrambled control. These hairpin sequences were cloned from the library vectors into pLKO-H2B-RFP vector. (*20*) All other hairpins were obtained from the TRC library and are listed in Supplementary Table 1.

In vivo Screen

We used non-invasive, ultrasound-guided *in utero* lentiviral-mediated delivery of RNAi, which selectively transduces single-layered surface ectoderm of living E9.5 mouse embryos as previously described (*24*). Our prior applications of *in utero* lentiviral RNAi transductions have been restricted to rapidly growing mouse embryos, where one can screen effectively for oncogenic regulators. (*20, 24, 25*) However, there are caveats to using embryonic growth as a measure for tumor growth, particularly since cancers often develop in adult tissues, which are not as proliferative. Hair follicle development is also ongoing throughout embryogenesis, potentially confounding results. By lowering the titer and using less potent tumor-susceptibility mouse models such as *TGFbRII*-cKO, *Trp53* mutants and oncogenic *HRas*, we carried out an *in vivo* RNAi tumor-suppressor screen in adult mice. We titered our pool such that ~15-20% of the ~150,000 surface ectoderm progenitors were infected (fig. S2A). Based upon library size, ≥20 cells/embryo should be transduced with each shRNA, which if inconsequential should expand clonally 40X by adulthood.

Tumor free survival.

Control and *TβRII*-cKO animals were transduced at E9.5 with low-titer shRNA pool targeting orthologs of putative HNSCC genes, including *Brca1, Trp53* or *Myh9*. Scrambled shRNA was used as control. Transductions and knockdowns were confirmed by real-time PCR of mRNAs isolated from newborn skin epidermis or by fluorescence microscopy of a lentiviral reporter fluor, H2B-RFP or H2B-GFP. Animals were assessed biweekly for signs of tumorigenesis, and were considered positive if lesions grew to be larger than 2mm in diameter.

Deep Sequencing: Sample preparation, preamplification and sequence processing

Epidermal and tumor cells were subjected to genomic DNA isolation with the DNeasy Blood & Tissue Kit (Qiagen), and each sample was analyzed for target transduction using real-time PCR. 6μg genomic DNA of each tumor was used as template in a pre-amplification reaction with 25 cycles and Phusion High-Fidelity DNA Polymerase (NEB). PCR products were run on a 2% agarose gel, and a clean ~200 bp band was isolated using QIAquick Gel Extraction Kit as recommended by the manufacturer (Qiagen). Final samples were then sent for Illumina HiSeq 2000 sequencing. Illumina reads were trimmed to the 21 nt hairpin sequence using the FASTX-Toolkit and aligned to the TRC 2.x library with BWA (v 0.6.2)44 using a maximum edit distance of 3. Hits were ranked based on (a) numbers of shRNAs that targeted the gene and scored positively in the screen, with 2 out of 5 shRNAs being considered meaningful; and (b) numbers of tumors enriched for a specific shRNA.

Immunofluorescence staining.

The following primary antibodies were used for immunofluorescence: chicken anti-GFP (1:2000; Abcam); guinea-pig anti-K5 (1:500; E. Fuchs); rat anti-K14 (1:500; E. Fuchs); rabbit anti-K6 (1:500; E. Fuchs); rabbit anti-K18 (1:500; E. Fuchs); rat anti-CD104 β4-integrin (346-11A, 1:300; BD); rabbit anti loricin (1:500; E. Fuchs); rabbit anti-Caspase 3 (AF835, 1:1000; R&D), rabbit anti-K10 (PRB-159P, 1:1000; Covance); rabbit anti-Myh9 (HPA001644, 1:500 Sigma); rabbit anti-SMA (ab5694 1:300; Abcam) and rabit anti-p53 (NCL-p53-CM5p, 1:300; Leica). Secondary antibodies were conjugated to Alexa-488, 546, or 647 (1:1000, Life Technologies). Cells and tissues were processed as previously reported (*20*), and mounted in Vectashield HardSet mounting medium with DAPI (Life Technologies). Confocal images were captured by a scanning laser confocal microscope (LSM510 and LSM780; Carl Zeiss, Inc.) using Plan-Apochromat 20x/0.8 oil and C Apochromat 40x/1.2 water lenses. Images were processed using ImageJ and Adobe Photoshop CS3. For quantifications of nuclear p53, images were captured using an inverted Zeiss LSM 780 laser scanning microscope, powered by Zen software. Quantitative image analysis was performed using ImageJ software. To quantify p53 nuclear staining, the following formula was used: CTCF (corrected total cell fluorescence) = whole nucleus signal – (mean background signal (measured in the suprabasal layer) x area of the nucleus measured).

Immunohistochemistry and histological analyses of mouse and human tumors

Immunohistochemistry was performed as previously described (*26*). Briefly, 5-μm sections were cut, stained with H&E or processed for immunohistochemistry/immunofluorescence microscopy. Whole-mount staining of mammary glands was performed as described (*26, 27*). For immunoperoxidase staining, paraffin-embedded sections were dehydrated and antigenic epitopes exposed using a 10-mM citrate buffer (pH 6.0) in a pressure cooker. Sections were incubated with the following primary antibodies at 4°C overnight: rabbit anti-K14 (1:500; E. Fuchs) and rabbit anti-Myh9 (HPA001644, 1:500 Sigma). Primary antibody staining was visualized using peroxidase-conjugated anti-rabbit IgG followed by the DAB substrate kit for peroxidase visualization of secondary antibodies (Vector Laboratories). The following human tissue microarray comprising 48 healthy human skin samples, 30 hyperplastic skin lesions and 206 human skin SCCs as well as from 156 HNSCCs were obtained from US Biomax, Rockeville, MD: SK244a, SK241, SK242, SK801, SK802, SK2081, SK801b and HN803a, HN811a, HN483.

Western Blot analysis

Protein blotting was carried out using standard protocols. Briefly, total cell lysates were prepared using RIPA buffer (20 mM Tris-HCl (pH 8.0), 150 mM NaCl, 1mM EDTA, 1mM EGTA, 1% Triton X-100, 0.5% Deoxycorate, 0.1 % SDS, 25 mM β-glycerophosphate, 10 mM NaF, 1 mM Na3VO4) supplemented with protease inhibitors

(Complete mini, Roche). Blots were blocked with 5% BSA in 1 × TBS 0.1% Tween-20 (TBST) for 1 h and incubated with the primary antibody overnight at 4 °C (diluted in TBST according to the manufacturer's protocol). Primary antibodies were reactive to rabbit anti-Myh9 (1:500, HPA001644, Sigma); phosphorylated (P) Erk1/2 (1:1000, #9101, Cell Signaling), Erk1/2 (1:1000, #9102, Cell Signaling), mouse anti-p53 (1:500, #2524, Cell Signaling), mouse anti-p21(F5) (1:500; sc-6246, Santa Cruz), mouse anti-GAPDH (ab8245, 1:5000; Abcam), mouse anti-Chk2 (1:500, #611570, BD); rabbit anti-P-Chk1 (1:500, #12302P, Cell Signaling); mouse anti-Chk1 (1:1000, 2360S, Cell Signaling); rabbit anti-pSmad2 (Ser465/467) (1:1000, Cell Signaling) and mouse anti-Smad2/3 (610843, 1/500; BD). Blots were washed three times in TBST for 30 min, incubated with HRP-conjugated secondary antibodies (1:2,000; Promega) for 1h at room temperature, washed 3 times in TBST for 30 min and visualized using enhanced chemiluminescence (ECL).

p53/DNA damage responses.

For measurement of DNA damage response and p53 activation primary mouse keratinocytes were seeded at a cell density of 100,000 cells per well in a 6-well plate and allowed to grow for 24 h at 3% O2 till importantly 100% confluency. Cells were then treated with doxorubicin (1mM) as previously reported (*26, 27*). For experiments using blebbistatin, cells were pretreated with blebbistatin (4μM final concentration, Sigma B0560) 30 min prior to doxorubicin treatment. The Rock inhibitor Y27632 was used at 10μM (Sigma Y0503) (*28*), LatrunculinA was used at 2μM (Sigma L5163), LeptomycinB was used at 20nM (Sigma #9676) and the proteasome inhibitor MG132 was used at 3μM (Sigma M7449).

mRNA quantifications.

Newborn mouse epidermal keratinocytes were cultured in 0.05 mM Ca++ E-media supplemented with 15% serum (*29*). For lentiviral infections, cells were plated in 6-well dishes at 200,000 cells/well and incubated with lentivirus in the presence of polybrene (100mg/ml) overnight. After 2 days, infected cells were positively selected with puromycin (1mg/ml) for 3 days, and then processed for mRNA analysis. cDNAs were generated from 1μg of total RNA using the SuperScript Vilo cDNA synthesis kit (Life Technologies). Real-Time PCR was performed using the 7900HT Fast Real-Time PCR System (Applied Biosystems) and gene-specific and Ppib as well as Hprt1 control primers as well as the following primers for p53 target genes:

p21 (Cdkn1a) fwd primer	5'– GTGGCCTTGTCGCTGTCTT -3'
p21 (Cdkn1a) rev primer	5'– GCGCTTGGAGTGATAGAAATCTG -3'
Fas fwd primer	5'–CTGCGATGAAGAGCATGGTTT-3'
Fas rev primer	5'–CCATAGGCGATTTCTGGGAC-3'
Bax forward primer	5'–ATGCGTCCACCAAGAAGCTGA-3'

Bax reverse primer	5'–AGCAATCATCCTCTGCAGCTCC-'
Mdm2 forward primer	5'–TTCGGCCTTCTCCTCGCTGTCGTC -3'
Mdm2 reverse primer	5'–TGGCGTAAGTGAGCATTCTGGTGA -3'
Bax forward primer	5'–TGTGTGCGACACTGTGCTC-3'
Bax reverse primer	5'–TCGGCTAGGTAGCGGTAGTAG-3'
Hprt1 for primer	GATCAGTCAACGGGGGACATAAA
Hprt1 rev primer	CTTGCGCTCATCTTAGGCTTTGT
Ppib for primer	GTGAGCGCTTCCCAGATGAGA
Ppib rev primer	TGCCGGAGTCGACAATGATG

Explant and Migration/Invasion Assay

Explant outgrowth migration assays were performed as described previously (*30*). Briefly, explants were cut using a 3-mm dermal biopsy punch (Miltex), placed on fibronectin-coated 35-mm, glass-bottomed plates (MatTek), and submerged in E-media containing 0.6 mM Ca++. Explant outgrowth was monitored daily.

Transwell migration assays were performed on 24-well plates. The underside of each Boyden chamber well was coated with 10 µg/ml fibronectin and placed atop fibroblast-conditioned E-media containing 0.05 mM Ca++. A total of 50,000 keratinocytes/well were plated in 100µl E-medium containing 0.05 mM Ca++. Eight hours later, cells were washed off the top membrane and fixed on the bottom membrane. Cells were stained using H&E and counted under the microscope. Similarly, invasion assays were performed in precoated Matrigel invasion chamber (BD Biosciences).

Analysis of human HNSCC patient data

We analysed the publicly available data sets of the **The Cancer Genome Atlas** (TCGA: http://cancergenome.nih.gov). The cBioPortal for Cancer Genomics developed and maintained by the Computational Biology Center at Memorial Sloan-Kettering Cancer Center was used to mine the publicly available TCGA dataset on HNSCC (*31, 32*). To re-trace the exact Kaplan-Meyer analysis please visit http://bit.ly/13xxPuh for the analysis of HNSCC patients stratified by the lowest (<5th percentile) *MYH9* expression versus the rest (≥5th percentile).

Statistical Analysis

All data were collected from experiments performed at least three times, and expressed as mean ± standard deviation (s.d.) or standard error of the mean (s.e.m.). Differences between groups were assayed using two-tailed student t-test and Prism 5 (GraphPad Software). Differences were considered significant if $p<0.05$. Data were analyzed and statistics performed (unpaired two-tailed Student's t-test) in Prism5 (GraphPad). Significant differences between two groups are noted by asterisks or p-values.

Predicting functional impact score of mutations (Mutataion Assessor):

To assess the functional impact of *MYH9* mutations, we used the score of Mutation Assessor. This score assesses a mutation impact by a value of the entropic disordering caused by mutation in evolutionary conserved postions of multiple alignments of protein sequences (*33*). The score of Mutation Assessor have been compared in independent tests to the scores of many others prediction methods including the oldest and well recognized methods - Polyphen and Sift. It was shown that "MutationAssessor consistently provided the highest accuracies. For certain combinations metapredictors slightly improved the performance of included individual methods, but did not outperform MutationAssessor as stand-alone tool" (*34*). Additional studies showed that predicted high-scoring functional mutations as well as truncating mutations tend to be evolutionarily selected as compared to low-scoring and silent mutations. This result justifies prediction of mutations-drivers using a shorter list of predicted high-scoring functional mutations, rather than the "long tail" of all mutations (*35*).

For all mutated genes, we assessed a number of functional mutations and computed a probability (Fisher test) of obtainting the observed numbers of predicted functional mutations by chance taking as a background distribution the distribution of predicted functional mutations and predicted non-functional mutations in all other genes. This approach was used recently (*36*).

The obtained P-values were adjusted for false discovery rate using Benjamini and Hochberg method. The statistically significant enrichment of the predicted functional mutations in a given gene as compared to the distribution of functional mutations across all other genes demonstrates the positive selection in tumor evolution and suggests that a given gene is a driver (*35*).

Among 302 sequenced HNSCCs, 16 missense MYH9 mutations surfaced (fig. S20A). Three quarters of these mutations were assessed as functional (fig. S20, B and C) by Mutation Assessor. We also assessed a probability to observe the predicted functional mutations by chance taking the distribution of predicted functionality of mutations in all other genes as a background. The significant enrichment of the predicted functional mutations demonstrates the positive selection in tumor evolution and suggests that a given gene is a driver (*35*). MYH9 was ranked 16th in the list of ~15,000 genes mutated in HNSCCs ($p=0.000026$, false discovery rate $q=0.024$) (Supplementary Table 2 and 3; fig. S21A).

MutationAssessor was used for example by the following projects:

The Cancer Genome Atlas Research Network. Nature (2011) "Integrated Genomic Analyses of Ovarian Carcinoma" (*37*)

The Cancer Genome Atlas Network. Nature (2008) "Comprehensive genomic characterization defines human glioblastoma genes and core pathways"(*38*)

Taylor et al. Cancer Cell (2010) "Integrative genomic profiling of human prostate cancer" (*39*)

Barretina et al. Nature Genetics (2010) "Subtype-specific genomic alterations define new targets for soft-tissue sarcoma therapy"(*40*)

MutationAssessor was highlighted in: Lynda Chin, William Hahn, Gad Getz and Matthew Meyerson; Genes Dev. (2011) "Making sense of cancer genomic data" (*41*)

Supplementary Figures

Fig. S1. Strategy for using lentiviral-mediated *in utero* delivery of shRNAs to screen and study the effects of tumor suppressors on squamous cell carcinoma formation *in vivo*

(**A**) Kaplan-Meier analysis of tumor-free survival of mice of the indicated genotype transduced with an shRNA that efficiently targets *Brca1* #560. (n=6 for each genotype, $p<0.0062$, log-rank test between *TβRII*-cKO vs. *TβRII* fl/fl mice infected with shRNA targeting *Brca1*-#560). Note that on a *TβRII*-cKO background, *Brca1* shRNA-mediated initiation of tumor growth is greatly accelerated. (**B**) Representative images of *Brca1* shRNA-transduced *TβRII* fl/fl and *TβRII*-cKO mice showing lesions on backskin as well as in oral cavity, respectively. (**C**) Representative section of a *Brca1* knockdown tumor isolated from a *TβRII* fl/fl animal showing a well-differentiated SCC. (**D**) In vivo knockdown efficiency of *Brca1* shRNA #560 in skin and in SCC tumors as measured by quantitative RT-PCR. (n=3 ± SEM * $p<0.05$).

Fig. S2. Determining suitable viral titer and measuring lentiviral shRNA library representation

(**A**) Control lentivirus (pLKO), harboring an H2B-GFP reporter transgene and a U6-driven scrambled shRNA control (Scr) expression vector was used in a dilution series to determine the appropriate dilution/titer required to selectively and stably transduce about 15-20% of surface ectoderm keratinocytes *in vivo* by ultrasound-guided *in utero* delivery to the amniotic sacs of living E9.5 embryos. Fluorescence activated cell sorting (FACS) analyses of epidermal keratinocytes isolated from transduced pups at E18.5 were used for quantifications. Comparative quantitative RT-PCR was then used to estimate the required dilution of the test lentiviral shRNA library needed to give rise to 15-20% of infection. Control lentivirus as well as the test lentiviral shRNA library had an initial titer of ~$6x10^9$ cfu/ml and were diluted 40X for all subsequent infections. (**B**) Scatter plot of Illumina sequencing data, illustrating good correlation between the number of reads per shRNA in DNA isolated from the lentiviral plasmid library versus the actual shRNA representation in DNA isolated from transduced epidermal keratinocytes of mouse embryos 3 days after infection with the lentiviral library (R=non-parametric (Spearman) correlation coefficient).

Fig. S3. SCC formation in *TβRII*-cKO mice infected with the shRNA library

(**A**) Histological sections of invasive SCC from oral cavity/lip of a transduced TβRII-cKO mouse. Different magnifications accentuate tumor heterogeneity, with well-differentiated areas (typified by keratin pearls) adjacent to poorly-differentiated areas. Note invasion into subcutaneous muscle (arrowheads) as well as moderate atypia characterized by anisokaryosis and anisocytosis, hyperchromasia, and frequent large and

prominent nucleoli. Mitoses were on average 10X more frequent than the surrounding WT tissue (arrows). (**B**) Representative immunofluorescence analyses for basal markers Keratin 5 and β4-integrin, differentiation marker Loricrin, and proliferation marker Ki67 on tumor sections from adult *TβRII*-cKO mice that had been infected with the lentiviral shRNA library at E9.5 in utero.

Fig. S4. SCC formation in adult *TβRII*-cKO mice derived from embryos whose surface ectoderm was infected with the shRNA library

(**A** to **D**) Representative H&E images of tumor sections showing invasive SCC arising from various transduced epithelial tissues as indicated. (**A**) At the mucocutaneous junction, a poorly demarcated neoplasm has invaded the dermis. The SCC is composed of nests and cords of basal cells exhibiting signs of squamous differentiation, notably eosinophilic keratin pearls. Some nests show evidence of stroma invasion associated with a desmoplastic stroma. Cellular atypia are minimal and mitoses are not observed within well-differentiated areas. The overlying epidermis is moderately hyperplastic and hyperkeratotic. The tumor is infiltrated by numerous neutrophils. (**B**) Backskin squamous cell carcinoma invading the underlying dermis and subcutaneous tissue. The SCC is well-demarcated, but in several areas, cells have detached from the main tumor and invaded into subcutaneous tissues. Invasive regions are characterized by small nests and cords of basal cells that have broken through the basement membrane and invaded adjacent stroma and muscle. This contrasts with nests of well-differentiated stratified squamous epithelium in the infundibular regions that are replete with keratinization. Throughout the tumor are scattered moderate to marked atypia characterized by fourfold anisokaryosis and anisocytosis, hyperchromasia, and variation in nucleolar size with frequent large and prominent nucleoli. Mitoses are prevalent at ~38/ ten 400x fields. (**C**) In this example, both cornea and eyelid are enlarged and their architecture is distorted by a poorly demarcated neoplasm composed of nests and cord of basal cells showing squamous differentiation and formation of keratin pearls. Some nests show evidence of stromal invasion associated with a desmoplastic stroma. Cellular atypia are minimal and mitoses are not observed. The overlying epidermis is moderately hyperplastic and hyperkeratotic. The tumor is infiltrated by numerous neutrophils. The cornea and conjunctiva are infiltrated by numerous neutrophils. In one eye, the lens is present in the section and shows swelling and liquefaction of lens fibers and posterior migration of lens epithelium. These tumors were often large, with involvement of both cornea and eyelids. The conjunctivitis and keratitis are ocular changes that appear to be secondary to expansion of the eyelid. (**D**) An SCC that has invaded subcutaneous tissues and the salivary gland. The tumor is a poorly demarcated and infiltrative neoplasm, composed of basal-like cells forming nests and cords supported by desmoplastic stroma. Cells are polygonal, have indistinct borders, and display a moderate amount of eosinophilic cytoplasm. They have ovoid nuclei with finely stippled chromatin and small nucleoli. There is threefold anisokaryosis, and an average of 12 mitoses per 400x fields. The skin shows a focally

extensive area of epidermal hyperplasia, with focal epidermal ulceration with serocellular crusting. The dermis is infiltrated by moderate numbers of neutrophils and macrophages, and fewer lymphocytes.

Fig. S5. Formation of benign lesions in *TβRII*-cKO mice derived from embryos whose surface ectoderm was infected with the shRNA library

(**A** to **C**) Representative H&E images of sections from affected *TβRII*-cKO epithelial tissues of mice that were transduced as embryos with the lentiviral shRNA library. (**A**) Neoplasm of basal cell tumor that appeared to be benign based on histologic features. Note the well-demarcated epidermal neoplasm that extends deep into the underlying dermis. It is composed of thin cords and nests of basaloid cells surrounded by fibrous stroma. Epithelial cells display indistinct borders, a small amount of amphophilic cytoplasm, and oval nuclei with finely stippled chromatin and multiple small nucleoli. An average of 3 mitoses were seen for every ten 400x fields. Overlying epidermis and infundibular epithelium show moderate hyperplasia and orthokeratotic hyperkeratosis. A few mm from this tumor is a well-demarcated region of deep dermal and subcutaneous fibrosis. (**B**) This squamous papilloma displays an exophytic, well demarcated neoplasm, composed of a branching papillary structure and markedly proliferative, but well differentiated, epidermis. Note marked orthokeratotic hyperkeratosis supported by thin stalks of fibrovascular stroma. The proliferative epidermis shows occasional mild dysplasia. The stroma is focally infiltrated by moderate numbers of melanophages and/or melanocytes, and moderate numbers of lymphocytes. (**C**) Some lesions showed no signs of malignancy. In this example, only ulceration is seen, with moderate neutrophilic and histiocytic dermatitis and weak signs of epidermal hyperplasia, indicating that these lesions are likely to be preneoplastic. Note focally extensive areas of mild epidermal hyperplasia, with multifocal epidermal ulceration associated and serocellular crusting and dermal necrosis. The superficial, mid and deep dermis is multifocally infiltrated by small to moderate numbers of neutrophils and macrophages, and fewer lymphocytes.

Fig. S6. *Trp53* knockdown triggeres SCC development in *TβRII*-cKO mice

(**A**) In vivo knockdown efficiency of *Trp53* shRNAs in skin as measured by quantitative RT-PCR. (n=3 ± SEM * $p<0.05$; ** $p<0.001$). (**B**) Kaplan-Meier analysis of tumor-free survival of mice of the indicated genotype transduced with an shRNA that efficiently targets *Trp53* (#361). Of note, *Trp53* shRNA-transduced TβRII-cKO mice show a median tumour-free survival of 147 days. (n=6 for each genotype, $p<0.0047$, log-rank test).

Fig. S7. *Myh9* knockdown delays hair follicle downgrowth and impedes eyelid closure.

(**A**) Quantitative RT-PCR of *Myh9* mRNA in primary murine keratinocytes infected with various *Myh9*-shRNA lentiviruses. (n=3 ± SEM * $p<0.005$) (**B**) Immunoblot analysis of protein lysates from epidermal keratinocytes of newborn mice transduced in utero with indicated *Myh9*-shRNAs. (**C**) Myosin-IIa immunohistochemistry of skin sections from

these mice transduced at E9.5 with scrambled-control or *Myh9* #504 shRNAs, and examined at birth. Note loss of myosin-IIa and impaired hair follicle down-growth in *Myh9*-knockdown animals. (**D**) Newborn mice reveal "Open Eyes at Birth" phenotype indicative of an impediment to eyelid closure during embryonic development. Inset shows that mice were efficiently transduced with the lentivirus, as judged by expression of the reporter H2B-RFP fusion protein. (**E**) 8 day-old *Myh9* shRNA-transduced mice show sparse and delayed hair growth compared to scrambled shRNA transduced littermate controls.

Fig. S8. *Myh9* knockdown does not interfere with tissue homeostasis in skin in young animals

(**A** to **D**) Fluorescence microscopy of frozen skin sections from *Myh9* knockdown *TβRII*-cKO and *TβRII* fl/fl mice at one (**A** and **B**) or three (**C** and **D**) months of age. Mice had been transduced *in utero* at E9.5 with lentivirus expressing an H2B-RFP reporter and either Myh9 #504 or scrambled shRNAs. Note that transduced regions (RFP+) show grossly normal immunolabeling for (**A**) Keratin 14 (K14) in the basal cells of interfollicular epidermis and hair follicles, and (**B**) Keratin 10 (K10) specific for terminally differentiating epidermis. In older animals, sparse areas of epithelial thickening were noted, concomitant with expanded K14 expression (**C**) and induction of K6, associated with a hyperproliferative state (**D**).

Fig. S9. Validation of *Myh9* as a tumor suppressor

(**A**) Sections of tumors from *TβRII*-cKO mice, transduced with shRNAs targeting *Brca1* or *Myh9*, respectively, and immunolabeled for myosin-IIa (absent in the epithelium of *Myh9* #504 shRNA-targeted SCCs). (**B** to **D**) Immunofluorescence microscopy of frozen tissue sections from tumors arising spontaneously in *TβRII*-cKO mice that had been transduced as embryos with *Myh9* shRNAs. Note architecture of poorly differentiated SCCs with (**B**) β4-integrin and K5-expressing nodules, (**C**) high proliferation rates in the basal layer as indicated by nuclear Ki67 and (**D**) reduced expression of differentiation markers such as Loricrin. (**E** to **H**) H&E of paraffin sections of these tumors confirmed their identity as poorly differentiated squamous cell carcinomas that invade into (**E**) subcutaneous fat, (**F**) skeletal muscle, (**G**) salivary gland and (**H**) locally draining lymph node.

Fig. S10. Genetic ablation of *Myh9* phenocopies *Myh9* shRNA knock-down

(**A**) Western Blot analysis of keratinocytes purified from *Myh9* fl/fl K14-Cre (*Myh9*-cKO) mice and control littermates shows target-specific reduced expression of myosin-IIa. (**B**) Anti-myosin-IIa immunolabeling of skin sections of wild-type and K14-Cre conditionally targeted Myh9-cKO animals. Note the antibody specificity and the recapitulation of the impediment to hair follicle down-growth, also seen with *Myh9* knock-down animals. (**C**) Histology of skin sections of double mutant (*Myh9/TβRII* iKO)

mice generated by inducing K14-driven CreER with topical application of tamoxifen. Note grossly normal skin morphology. (**D**) Representative *Myh9/TβRII* iKO animal as well as H&E section showing a poorly differentiated skin SCC that has invaded through the skeletal muscle into the deep subcutaneous structures and lymph nodes. (**E**) Representative *Myh9/TβRII* iKO animal as well as H&E section showing a moderately differentiated invasive anogenital squamous cell carcinoma that has invaded the colonic epithelium. The colonic epithelium is not neoplastic, but is ulcerated and inflamed with some reactive changes.

Fig. S11. Myh9 regulates epidermal outgrowth from skin explants

(**A** and **B**) Representative phase-contrast and epifluorescence images of (**A**) *TβRII* fl/fl and (**B**) *TβRII*-cKO skin explants from E18.5 embryos infected at E9.5 with scrambled-control or shRNAs construct targeting *Myh9*. Viral constructs harbored reporter genes encoding either membranous GFP (mGFP) or H2B-RFP. Epidermal outgrowth was monitored for 48 hr and was significantly increased in *Myh9* shRNA-transduced keratinocytes compared to scrambled control transduced explants of *TβRII*-proficient and deficient cells. White dotted lines mark leading edges; red arrows denote distance between explant and its leading edge. (**C** and **D**) Quantifications of epidermal outgrowth from skin explants of (**C**) *TβRII* fl/fl and (**D**) *TβRII*-cKO mice transduced with indicated knock-down constructs. (n=3 ± SEM * $p<0.05$, two-tailed t test between scrambled and each *Myh9* knock-down construct)

Fig. S12. *Myh9* knockdown enhances keratinocyte migration in a scratch wound assay *in vitro.*

(**A**) Shown are representative temporal phase-contrast and RFP epifluorescence images of scratch wound assays on keratinocytes infected in vitro with scrambled-control or *Myh9* shRNAs #504. Yellow arrows indicate the extent of wound closure. H2B-RFP marks transduced keratinocytes as shown in the last panel. (**B** and **C**) Transwell migration assays through Boyden chambers coated with (**B**) fibronectin (migration assay) or with (**C**) Matrigel ECM (invasion assay). *Myh9*-deficiency markedly increases migration and invasion towards fibroblast-conditioned medium (bottom chamber), irrespective of TβRII-cKO status. (n=3 ± SEM * $p<0.05$ and ** $p<0.005$, two-tailed t test between scrambled and each Myh9- knockdown construct).

Fig. S13. *Myh9* regulates oncogenic *H-Ras*-driven but not *Trp53*-driven tumorigenesis

(**A**) Kaplan-Meier analysis of tumor-free survival of DMBA/TPA treated (*H-Ras*-induced) syngenic CD1 mice transduced with the indicated shRNA. (n=6 for each genotype, $p<0.0005$, log-rank test between scrambled control and each Myh9 shRNA infected mice). (**B**) Representative images of CD1 mice, transduced *in utero* with either scrambled control or *Myh9* shRNA #504 12-weeks after DMBA-treatment. (**C**) Tumor

multiplicity of DMBA/TPA-treated CD1 mice transduced with the indicated shRNA. (n=6 for each genotype). (**D**) SCC conversion frequency in syngenic CD1 mice transduced with the indicated shRNA 20-weeks after DMBA-treatment. (**E**) Representative H&E as well as myosin-IIa IHC images of tumors from CD1 mice transduced in utero with either scrambled control or *Myh9* shRNAs #504 20-weeks after DMBA-treatment. (**F**) Kaplan-Meier analysis of tumor-free survival of mice of the indicated genotype transduced with two shRNAs that efficiently target *Myh9*. (n=6 for each genotype, p=ns, log-rank test*)*. Note that whether mice are singly mutant for *Trp53*, singly deficient for *Myh9* or doubly mutant for *Trp53/Myh9,* their Kaplan-Meier profiles for SCCs are comparable. (**G**) Kaplan-Meier analysis of tumor-free survival of mice of the indicated genotype transduced with shRNAs that efficiently target *Myh9* or *Trp53*. (n<6 for each genotype*)*. Note that whether mice conditionally null for *TβRII* are also singly deficient for *Trp53*, singly deficient for *Myh9* or doubly deficient for *Trp53/Myh9,* their Kaplan-Meier profiles for SCCs are comparable.

Fig. S14. *Myh9* regulates p53.
(**A**) p53 and p21 expression after treatment with DNA damage response drug doxorubicin (Dox; 1μM). Primary mouse epidermal keratinocytes were transduced with the different Myh9 shRNAs as indicated. Myosin-IIa and GAPDH levels are indicated as control. (**B**) p53 and p21 expression after treatment with DNA-damage-response inducer doxorubicin (1μM) in Myh9fl/fl keratinocytes after adenoviral-Cre-mediated *Myh9* ablation (KO). Myosin-IIa and GAPDH levels are shown as controls. (**C**) Quantification of p53 in nuclei of the skin of *Myh9* cKO and control mice 6 hours after treatment g-irradiation (5Gy) as shown in Fig. 3B. Plotted is the corrected total cell fluorescence (CTCF) per cell and the median with interquartile range. ($p < 0.0001$; Mann Whitney test). (**D**) Represetative images showing p53 expression in the skin of *Myh9* knock-down (H2B-RFP labeled) mice either left untreated or 6 hours after γ-irradiation (5Gy). Note that p53 staining is only observed in basal, keratin 5 positive cells. Note also that H2B-RFP labeled *Myh9* shRNA #507-infected cells do not show efficient nuclear p53 staining. Mosaic analysis shows that the effect shown is cell-intrinsic.

Fig. S15. *Myh9* ablation does not affect EGF signaling.
(**A**) *Myh9* knockdown keratinocytes efficiently respond to EGF. Western Blot of phosphorylated (activated) Erk after EGF stimulation (20ng/ml) of *TβRII* fl/fl (wt) and *TβRII*-cKO (KO) keratinocytes infected in vitro with various *Myh9* knockdown constructs.

Fig. S16. *Myh9* but not Myh10 or Myh14 regulates p53 in *TβRII*-wt and also in *TβRII*-cKO keratinocytes.
(**A**) p53 and p21 expression after treatment with DNA-damage-response inducer doxorubicin (1μM) in wt keratinocytes after shRNA-mediated knockdown of *Myh9,*

Myh10 and *Myh14*. GAPDH levels are shown as controls. (**B**) qRT-PCR analysis confiming efficient shRNA-mediated knockdown of *Myh9, Myh10* and *Myh14*. (**C**) p53 and p21 expression after doxorubicin (Dox; 1μM) treatment of *TβRII*-cKO keratinocytes transduced by lentiviral delivery of Myh9 shRNAs and Cre recombinase. Myosin-IIa and GAPDH levels are indicated as control. (**D**) Western Blot of phosphorylated (activated) P-SMAD2 in *TβRII* fl/fl keratinocytes transduced with indicated lentiviral constructs. Note that as expected, LV-Cre mediated targeting of *TβRII* resulted in loss of P-SMAD2 activity downstream of TGFβ Receptor signaling. Myosin-IIa, total SMAD2, activated phosphorylated P-ERK and total ERK are shown as controls. (**E**) qPCR analysis of *TβRII* to verify LV-Cre mediated ablation of *TβRII* gene expression.

Fig. S17. Optimal p53 activity following DNA damage depends upon myosin-IIa's ATPase activity and its role in p53 nuclear retention

(**A**) p53 expression in mouse keratinocytes treated with myosin ATPase inhibitor blebbistatin (4μM) and with doxorubicin (Dox; 1μM). GAPDH levels are indicated as control. **(B**) Western Blot of p53 in mouse keratinocytes treated with vehicle, blebbistatin, Rock inhibitor Y27632 or latrunculinB. Activated phosphorylated H2AX (γH2AX) as well as activated phosphorylated Chk1 and Chk2 show normal initial DDR activation. Note activation-dependent mobility shift of Chk2. Total Chk1 and GAPDH are shown as controls. (**C**) MG132 rescues *Myh9* phenotype. (**D**) Nuclear export inhibitor LeptomycinB rescues the *Myh9* knockdown phenotype and restores *p53* accumulation after DNA damage.

Fig. S18. Expression of myosin-IIa in human HNSCC and skin SCCs

(**A**) Myosin-IIa Western Blot of primary *Myh9*-cKO keratinocytes to validate the efficacy of the myosin-IIa antibody. Representative images of myosin-IIa immunohistochemistry of human skin as well as representative images of myosin-IIa immunohistochemistry of human SCC samples showing variability in myosin-IIa staining ranging from negative to weak, moderate and strong. K14 immunohistochemistry internally controlled for epithelial areas and tissue quality. (**B**) Analysis of human skin SCCs with respect to tumor grading and then stratified according to presence or absence of myosin-IIa expression. (**C**) Analysis of human skin SCCs with respect to absence or presence of TGFβ signaling as assessed by immunolabeling for TβRII and active P-SMAD2 and stratified according to presence or absence of myosin-IIa expression.

Fig. S19. High *MYH9* expression does not correlate with shortned human HNSCC survival

(**A**) Raw RNAseq data of HNSCC samples in the TCGA database showing the spread of *MYH9* RNA expression in all samples across the cohort of 303 patient samples. Graph delineates the z-score of *MYH9* mRNA expression defined as the relative expression of an individual gene and tumor to the gene's expression distribution in a reference

population, which is all tumors that are diploid for the gene in question. The returned value indicates the number of standard deviations away from the mean of expression in the reference population (z-score). This measure is useful to determine whether a gene is up- or down-regulated relative to the normal samples or all other tumor samples. In Fig. 4C we used the bottom 5th percentile, which equaled samples with a z-score of -1.6 or less (all samples below the red line) to perform the Kaplan-Meier survival analysis. Interestingly, this analysis also shows quite some HNSCC cases with upregulation of *MYH9* mRNA expression – top 33 tumors (or top 11%) out of our cohort of 303 HNSCCs. (**B**) Kaplan-Meier survival analysis of of HNSCC cases with *MYH9* mRNA upregulation (above 1.6 standart deviations or more indicated by the red line in fig. S19A). In contrast to the data for the low *MYH9* expression, these patients do not show any survival disadvantage/advantage when compared to the rest of the cohort. (**C**) Kaplan-Meier survival analysis of of HNSCC cases with *MYH9* mRNA upregulation, *MYH9* amplifications or gains. Of note, amplifications are defined as larger chromosomal amplifications while gains are defined as local amplifications. No survival disadvantage/advantage. (**D**) Kaplan-Meier survival analysis of of HNSCC cases with *MYH9* hemizygousity. No survival disadvantage/advantage. (**E**) Kaplan-Meier survival analysis of of HNSCC cases with *MYH9* mutations. No survival disadvantage/advantage.

Fig. S20. Mutations in myosin-IIa in human HNSCCs

(**A**) Schematic of human myosin-IIa delineating the N-terminal SH3-like domain, the myosin head domain with the ATPase function, the ATP binding pockets P-loop (P) and switch region I and II (I and II), the IQ-calmodulin binding domain and the myosin tail. Missense mutations as well as deletions are given with their respective functional impact score overhead. Note that most of the mutations are within the ATPase domain clustering in and around the switch-II region (p=0.0015; Fisher test corrected for false discovery rate). Of note, mutations of the conserved A454 (blue) residue have been shown in Dictyostelium myosin to abrogate ATPase function. E457K (red) mutant myosin was tested and shown to have an effect on DDR-induced p53 activation (fig. S221). (**B**) List of MYH9/myosin-IIa mutations found in HNSCCs and their computed functional impact score (www.mutationassessor.org). (**C**) Multiple sequence alignment of human, dog, mouse, rat, chicken MYH9 and Dyctyostelium discoideum myosin-2 heavy chain. Multiple sequence alignment by MAFFT v7.058b (E-INSi strategy, Blosum 62, Offset value 0.123) and visualization using Jalview 2.8.

Fig. S21. Prevalence of *MYH9* somatic mutations and hemizygosity in human cancers.

(**A**) Mutational spectrum of *MYH9* across 19 human tumor types and 1000 human cancer cell lines (midified from cBioPortal: http://www.cbioportal.org/public-portal/). Statistics shown were mined from the TCGA databases.

Fig. S22. Mutations within the ATPase domain of *MYH9* impair p53 activation.
(**A**) Representative immunofluorescence images of phalloidin and anti-GFP stainined mouse keratinocytes expressing either wildtype human EGFP-*MYH9* or mutant human EGFP-*MYH9* (E457K). (**B**) p53 expression in primary mouse keratinocytes infectd with either vector control lentivirus or lentivirus harboring wildtype human EGFP-*MYH9* (wt) or mutant human EGFP-*MYH9* (E457K) or (E530K) and treated with with DDR-inducer doxorubicin (Dox; 1 μM). GAPDH levels are indicated as control.

Fig. S23. *Trp53* mutations and p53 inactivating mutations are not mutually exclusive in HNSCCs.
OncoPrints visualizing p53 pathway alterations across the TCGA data base for (**A**) HNSCCs and (**B**) glioblastomas visually identifying trends in mutual exclusivity or co-occurence between *Trp53* and its negative regulators *MDM2* and *MDM4* as well as *MYH9*. The individual genes are represented as rows, and individual patients are represented as columns. Tables present the statistics and tendency towards mutual exclusivity and co-occorance. Of note, it seems that in HNSCCs *Tp53* mutations are not necessarily mutually exclusive with other p53 inactivating mutations/alterations, such as *MDM2*, *MDM4* and *MYH9*. To re-trace the exact analysis please visit: http://bit.ly/175U255 for HNSCC analysis and http://bit.ly/1fFcqUN for gliobastoma analysis.

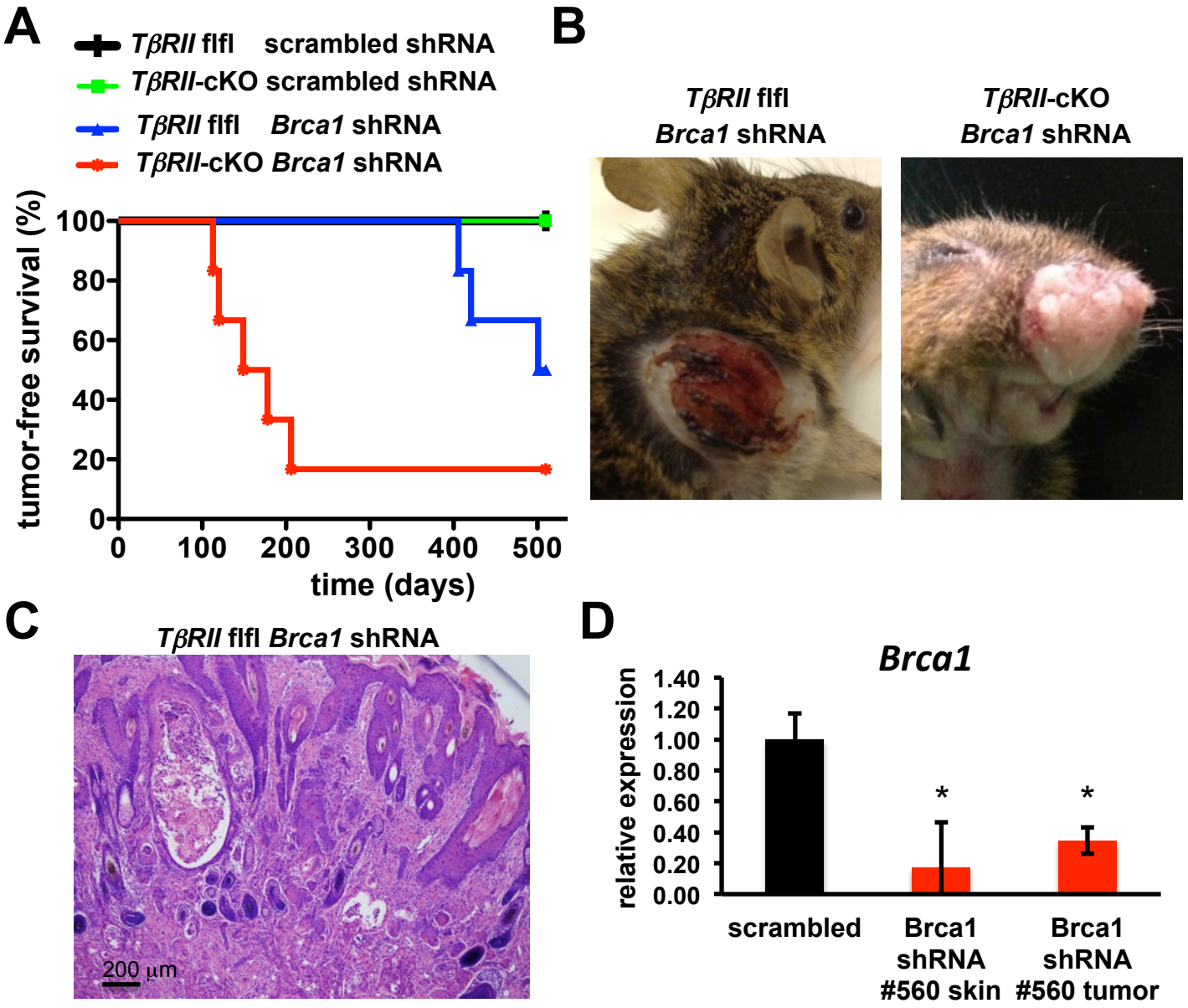
A
TβRII flfl scrambled shRNA
TβRII-cKO scrambled shRNA
TβRII flfl Brca1 shRNA
TβRII-cKO Brca1 shRNA
tumor-free survival (%)
100
80
60
40
20
0
0
100
200
300
400
500
time (days)
B
TβRII flfl
Brca1 shRNA
TβRII-cKO
Brca1 shRNA
C
TβRII flfl Brca1 shRNA
200 μm
D
Brca1
relative expression
1.40
1.20
1.00
0.80
0.60
0.40
0.20
0.00
*
*
scrambled
Brca1 shRNA #560 skin
Brca1 shRNA #560 tumor

Figure S1

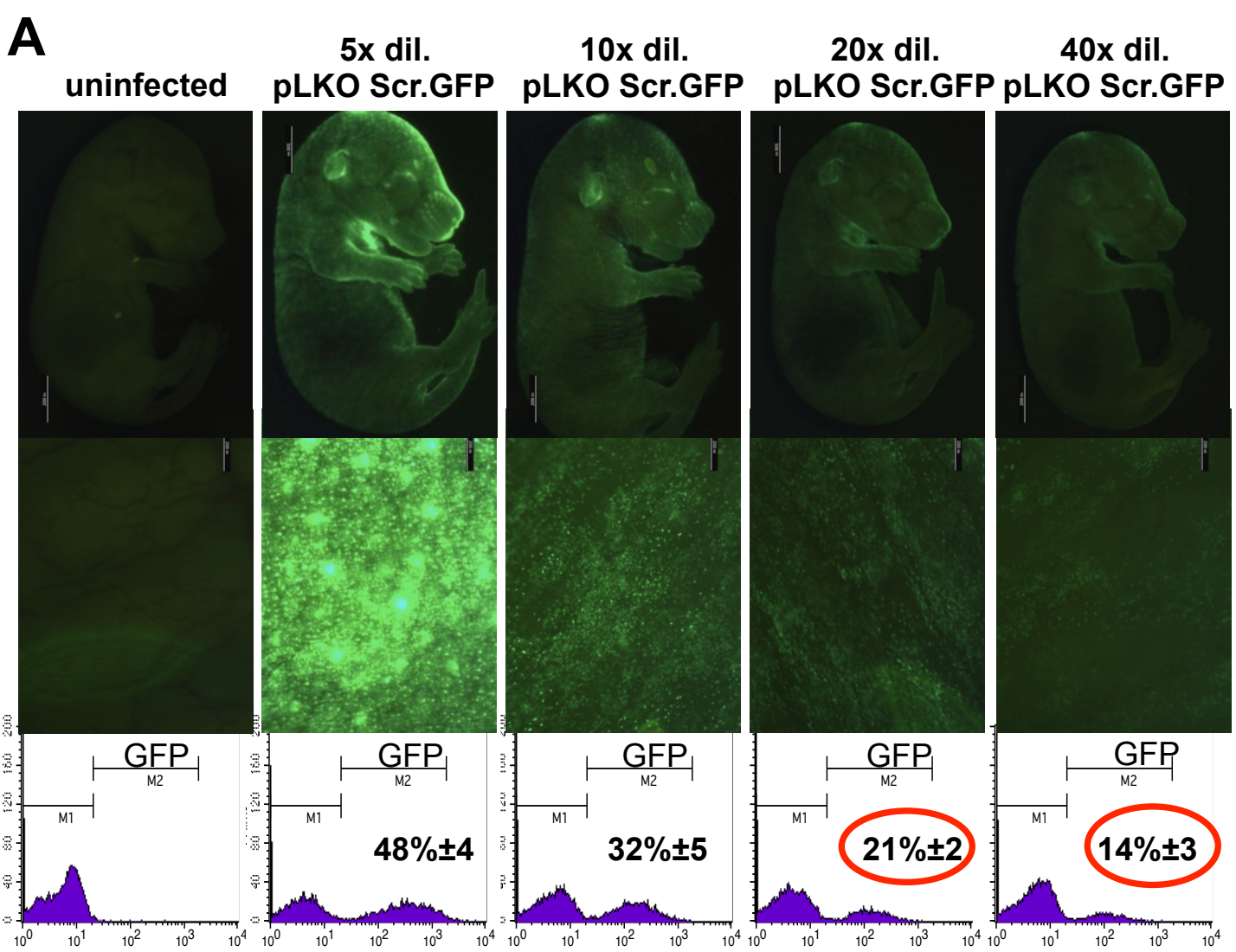
A
uninfected
5x dil. pLKO Scr.GFP
10x dil. pLKO Scr.GFP
20x dil. pLKO Scr.GFP
40x dil. pLKO Scr.GFP
GFP
M1
M2
48%±4
32%±5
21%±2
14%±3

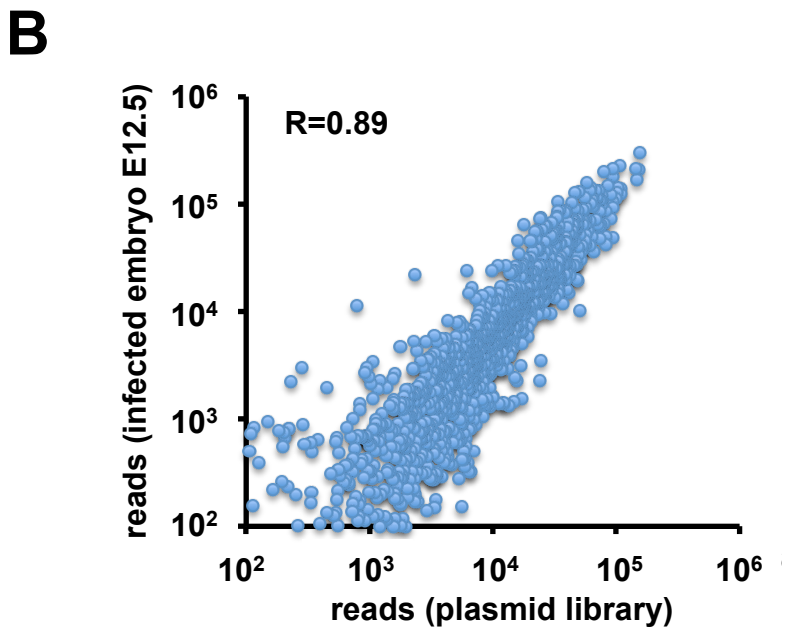
B
R=0.89
reads (infected embryo E12.5)
reads (plasmid library)

Figure S2

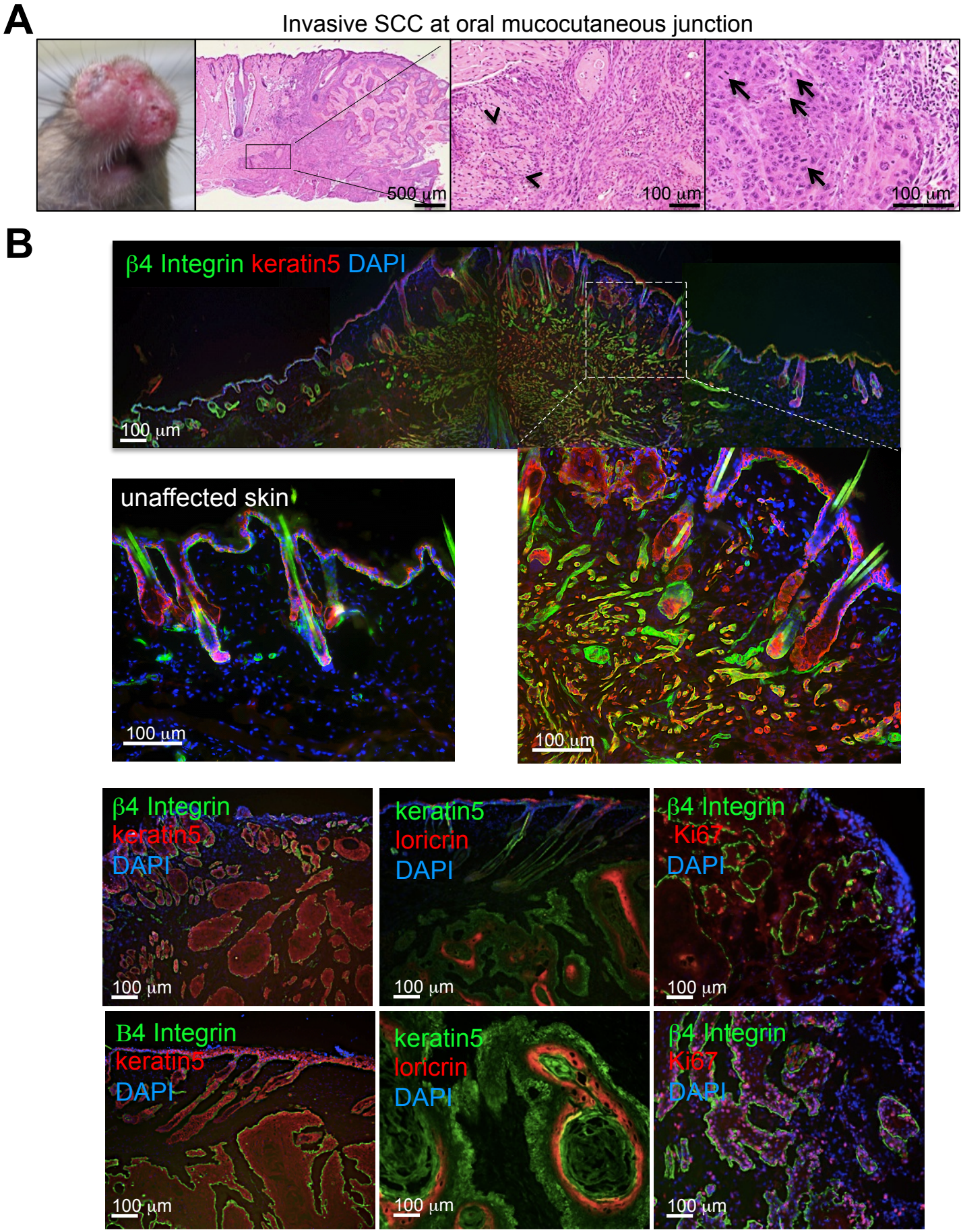
A
Invasive SCC at oral mucocutaneous junction
500 μm
100 μm
100 μm
B
β4 Integrin keratin5 DAPI
100 μm
unaffected skin
100 μm
100 μm
β4 Integrin
keratin5
DAPI
100 μm
keratin5
loricrin
DAPI
100 μm
β4 Integrin
Ki67
DAPI
100 μm
B4 Integrin
keratin5
DAPI
100 μm
keratin5
loricrin
DAPI
100 μm
β4 Integrin
Ki67
DAPI
100 μm

Figure S3

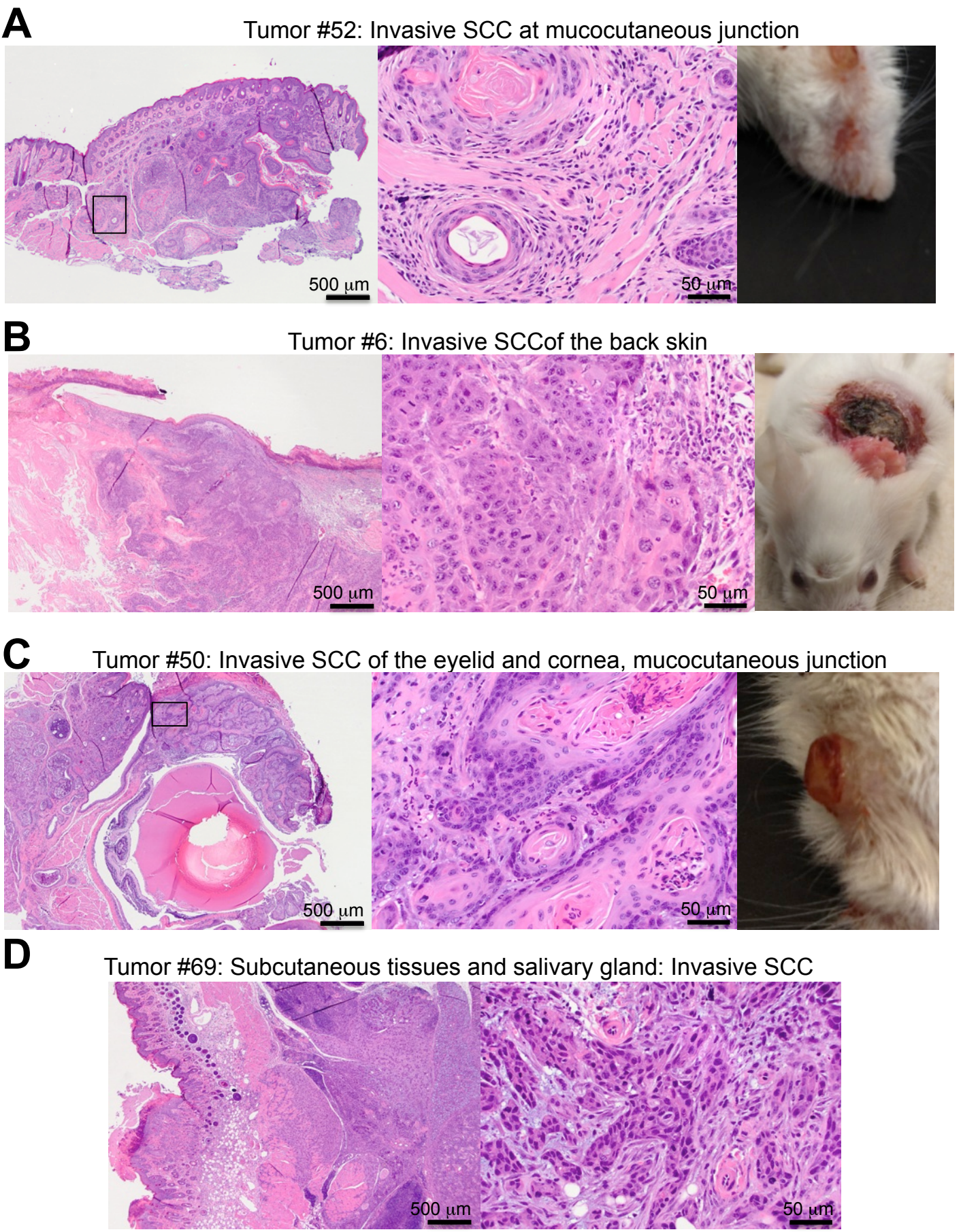
A
Tumor #52: Invasive SCC at mucocutaneous junction
500 μm
50 μm
B
Tumor #6: Invasive SCCof the back skin
500 μm
50 μm
C
Tumor #50: Invasive SCC of the eyelid and cornea, mucocutaneous junction
500 μm
50 μm
D
Tumor #69: Subcutaneous tissues and salivary gland: Invasive SCC
500 μm
50 μm

Figure S4

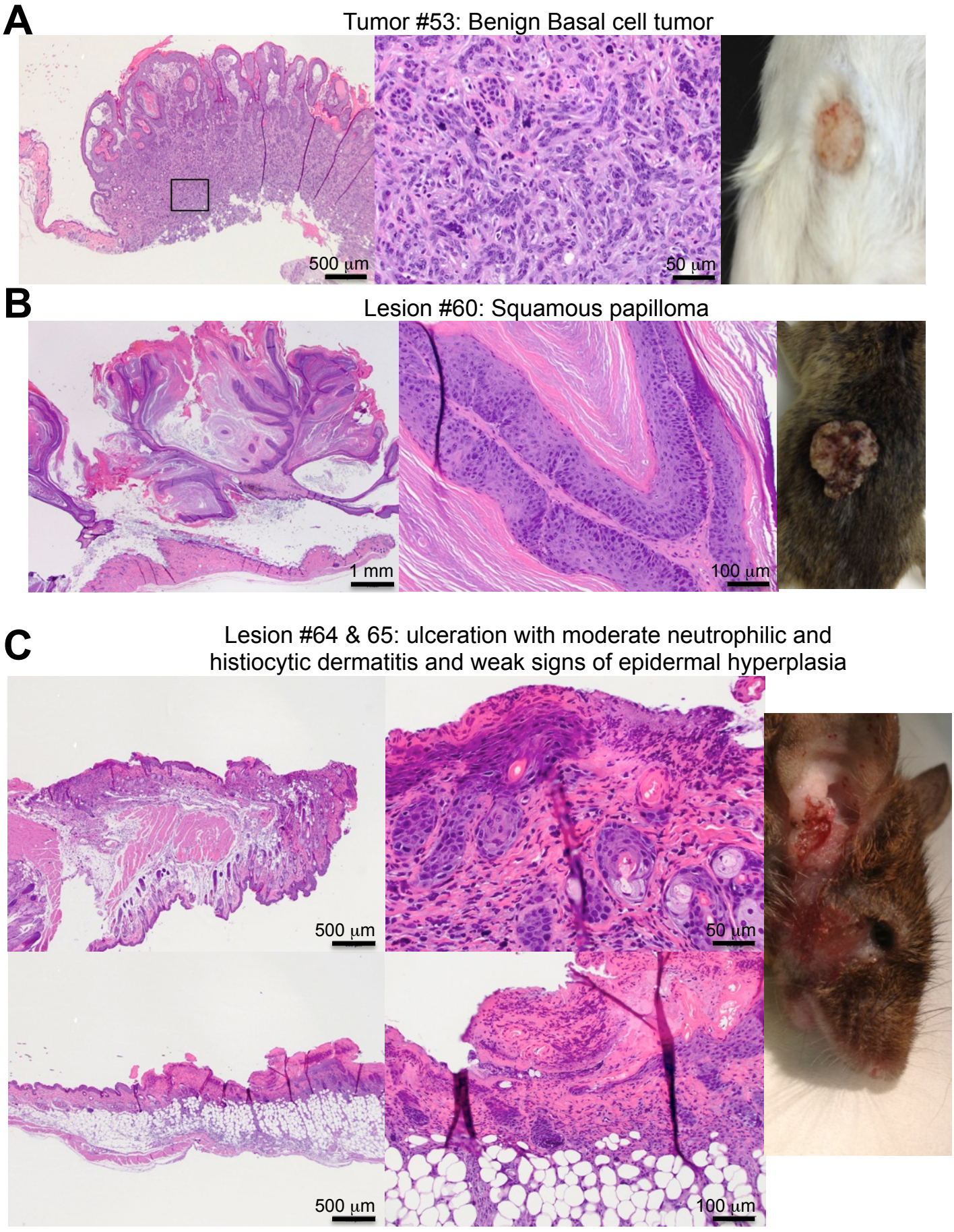
A
Tumor #53: Benign Basal cell tumor
500 μm
50 μm
B
Lesion #60: Squamous papilloma
1 mm
100 μm
C
Lesion #64 & 65: ulceration with moderate neutrophilic and histiocytic dermatitis and weak signs of epidermal hyperplasia
500 μm
50 μm
500 μm
100 μm

Figure S5

A

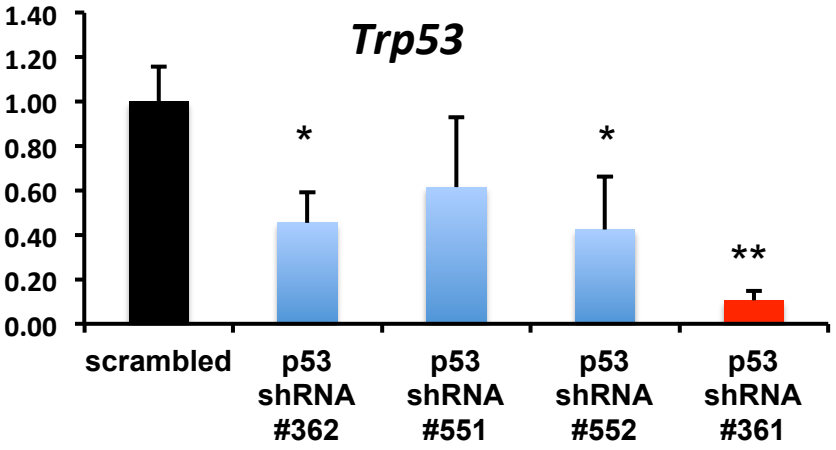
Trp53
1.40
1.20
1.00
0.80
0.60
0.40
0.20
0.00
*
*
**
scrambled
p53 shRNA #362
p53 shRNA #551
p53 shRNA #552
p53 shRNA #361

B

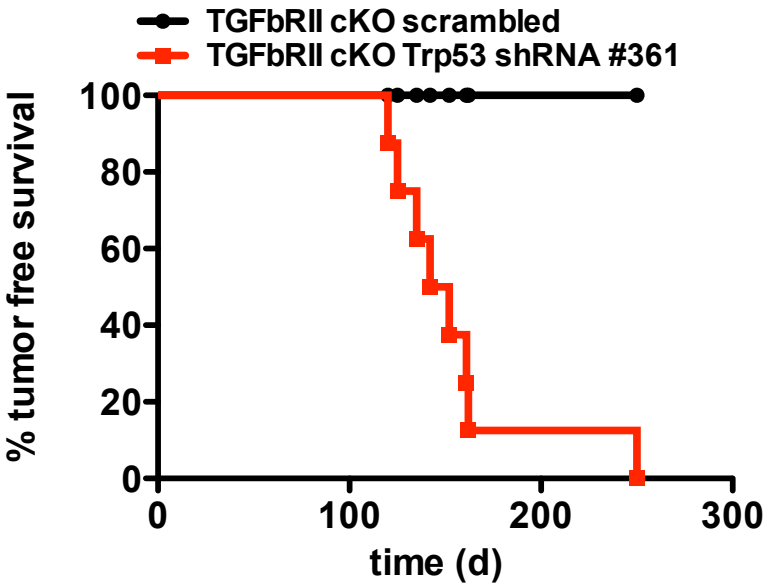
TGFbRII cKO scrambled
TGFbRII cKO Trp53 shRNA #361
% tumor free survival
100
80
60
40
20
0
0
100
200
300
time (d)

Figure S6

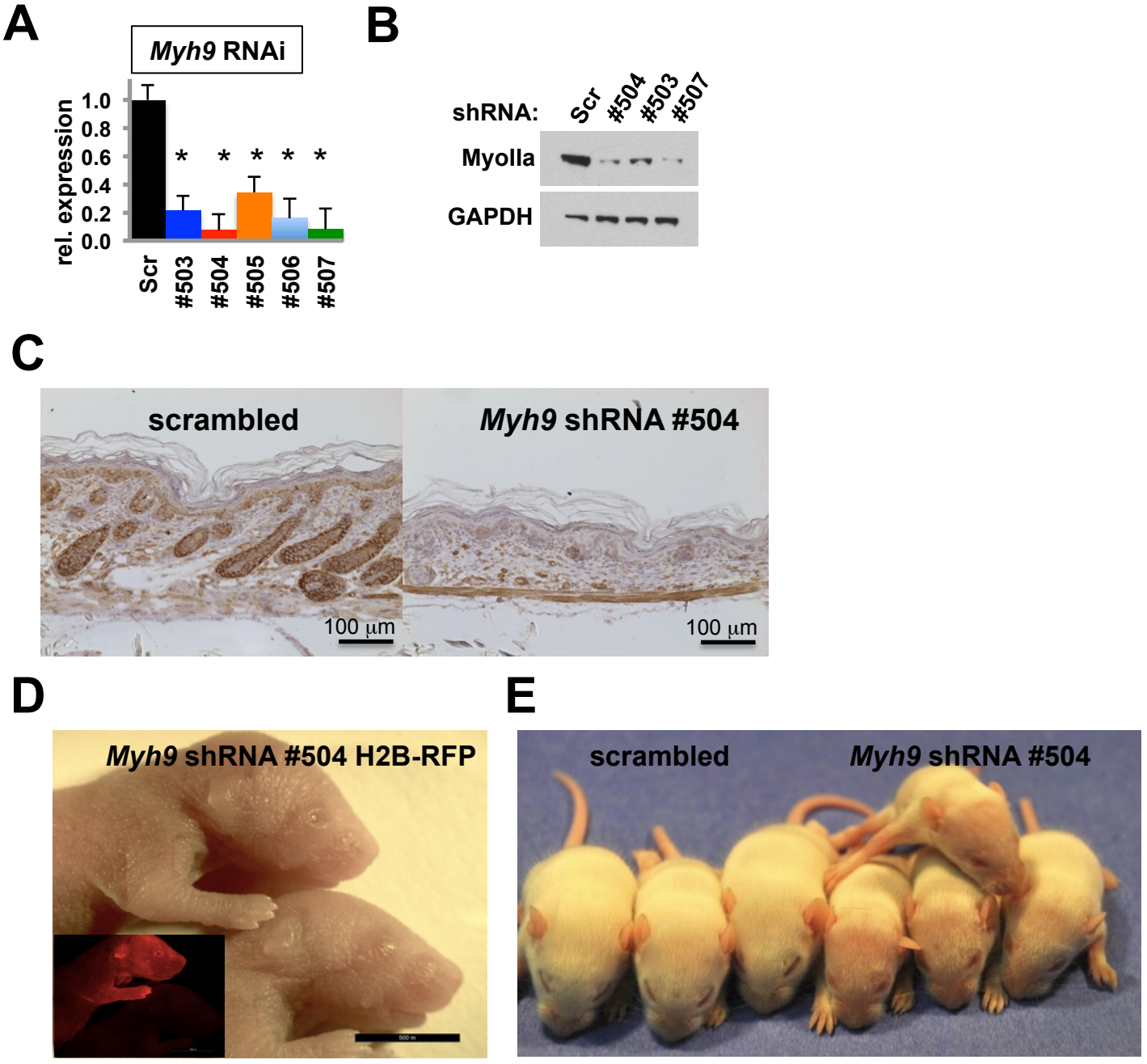
A
Myh9 RNAi
rel. expression
1.0
0.8
0.6
0.4
0.2
0.0
Scr
#503
#504
#505
#506
#507
B
shRNA:
Scr
#504
#503
#507
Myolla
GAPDH
C
scrambled
Myh9 shRNA #504
100 µm
100 µm
D
Myh9 shRNA #504 H2B-RFP
E
scrambled
Myh9 shRNA #504

Figure S7

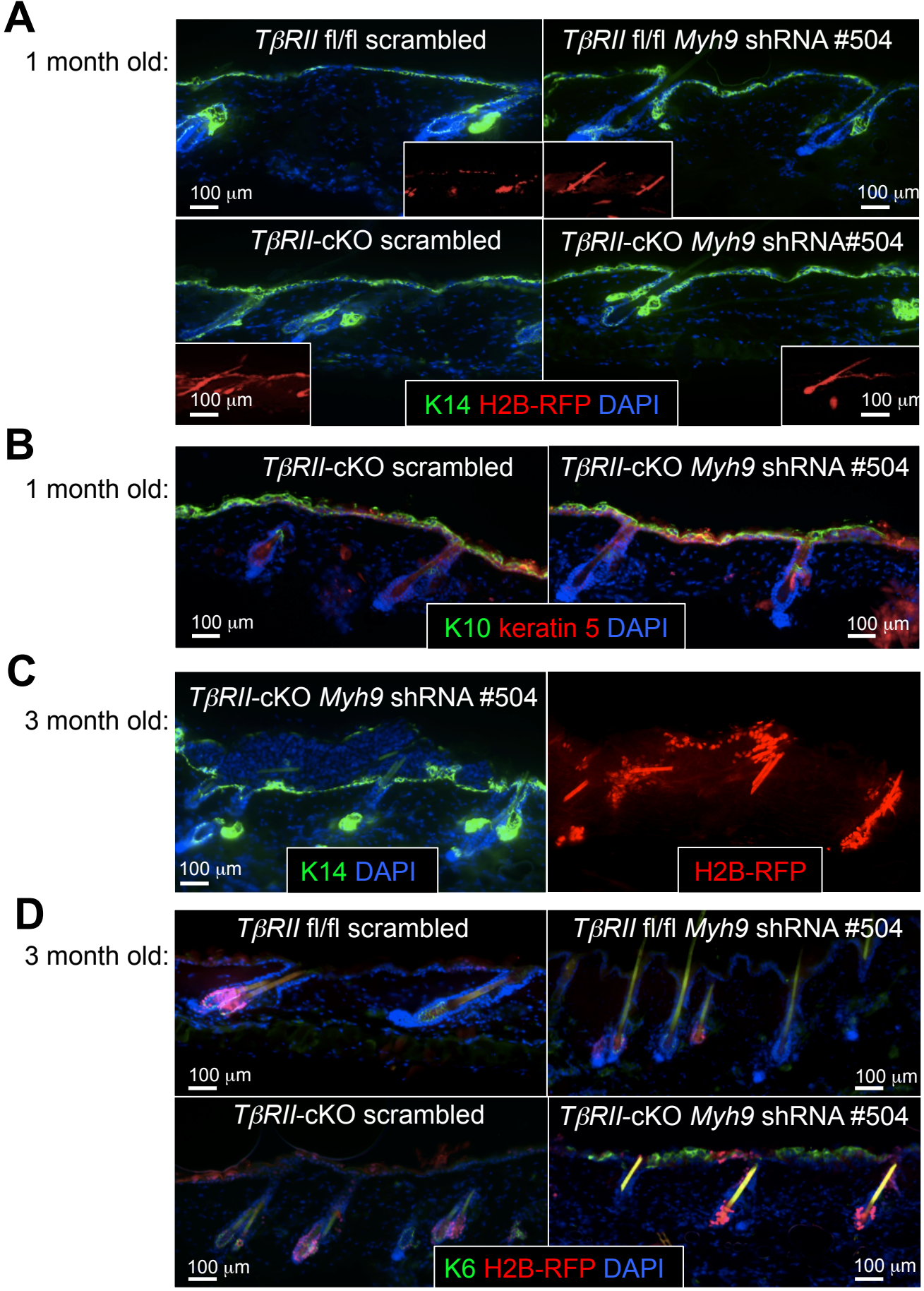
A
1 month old:
TβRII fl/fl scrambled
TβRII fl/fl Myh9 shRNA #504
100 μm
100 μm
TβRII-cKO scrambled
TβRII-cKO Myh9 shRNA#504
100 μm
K14 H2B-RFP DAPI
100 μm
B
1 month old:
TβRII-cKO scrambled
TβRII-cKO Myh9 shRNA #504
100 μm
K10 keratin 5 DAPI
100 μm
C
3 month old:
TβRII-cKO Myh9 shRNA #504
100 μm
K14 DAPI
H2B-RFP
D
3 month old:
TβRII fl/fl scrambled
TβRII fl/fl Myh9 shRNA #504
100 μm
100 μm
TβRII-cKO scrambled
TβRII-cKO Myh9 shRNA #504
100 μm
K6 H2B-RFP DAPI
100 μm

Figure S8

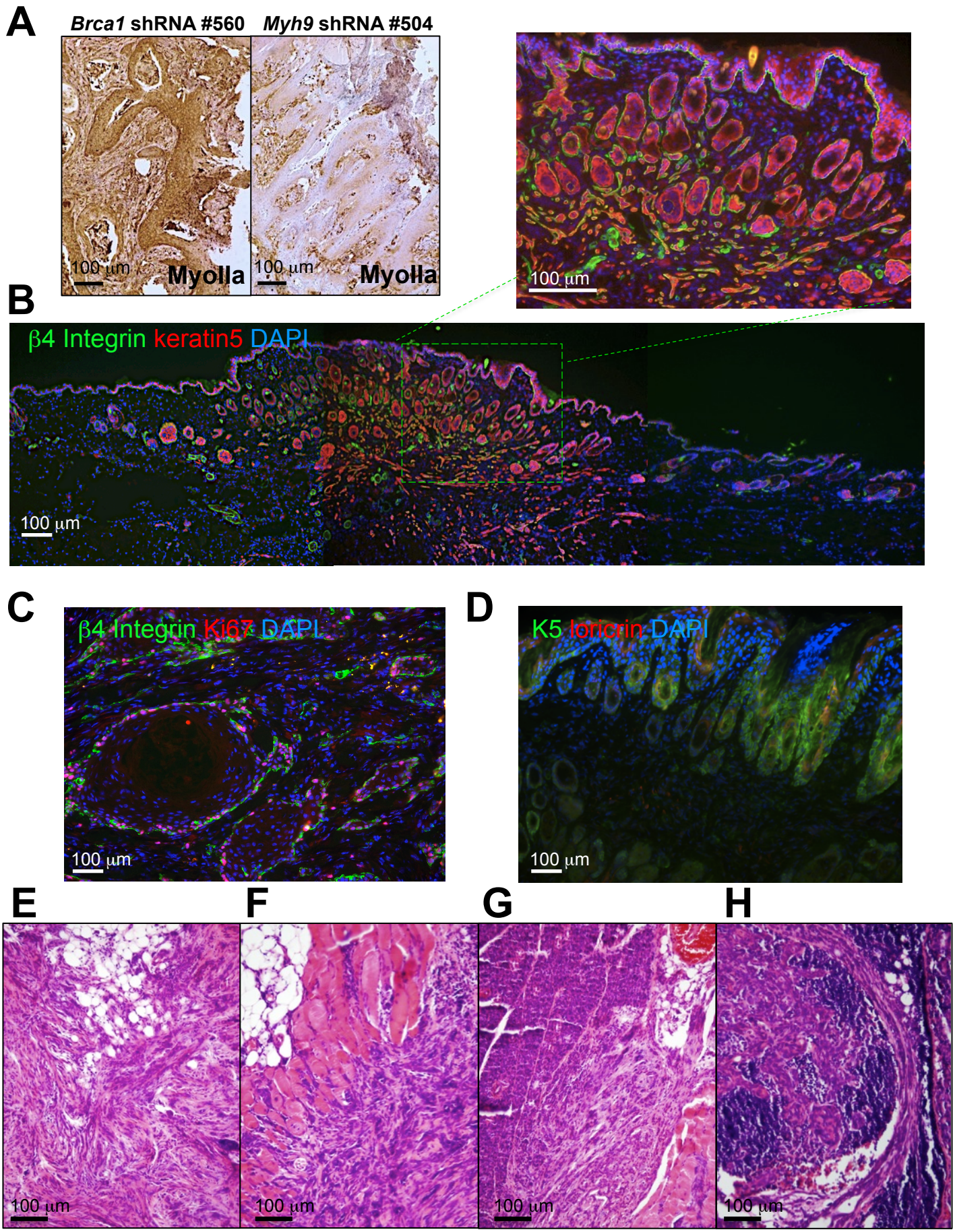
A
Brca1 shRNA #560
Myh9 shRNA #504
100 μm
Myolla
100 μm
Myolla
100 μm
B
β4 Integrin keratin5 DAPI
100 μm
C
β4 Integrin Ki67 DAPI
100 μm
D
K5 loricrin DAPI
100 μm
E
F
G
H
100 μm
100 μm
100 μm
100 μm

Figure S9

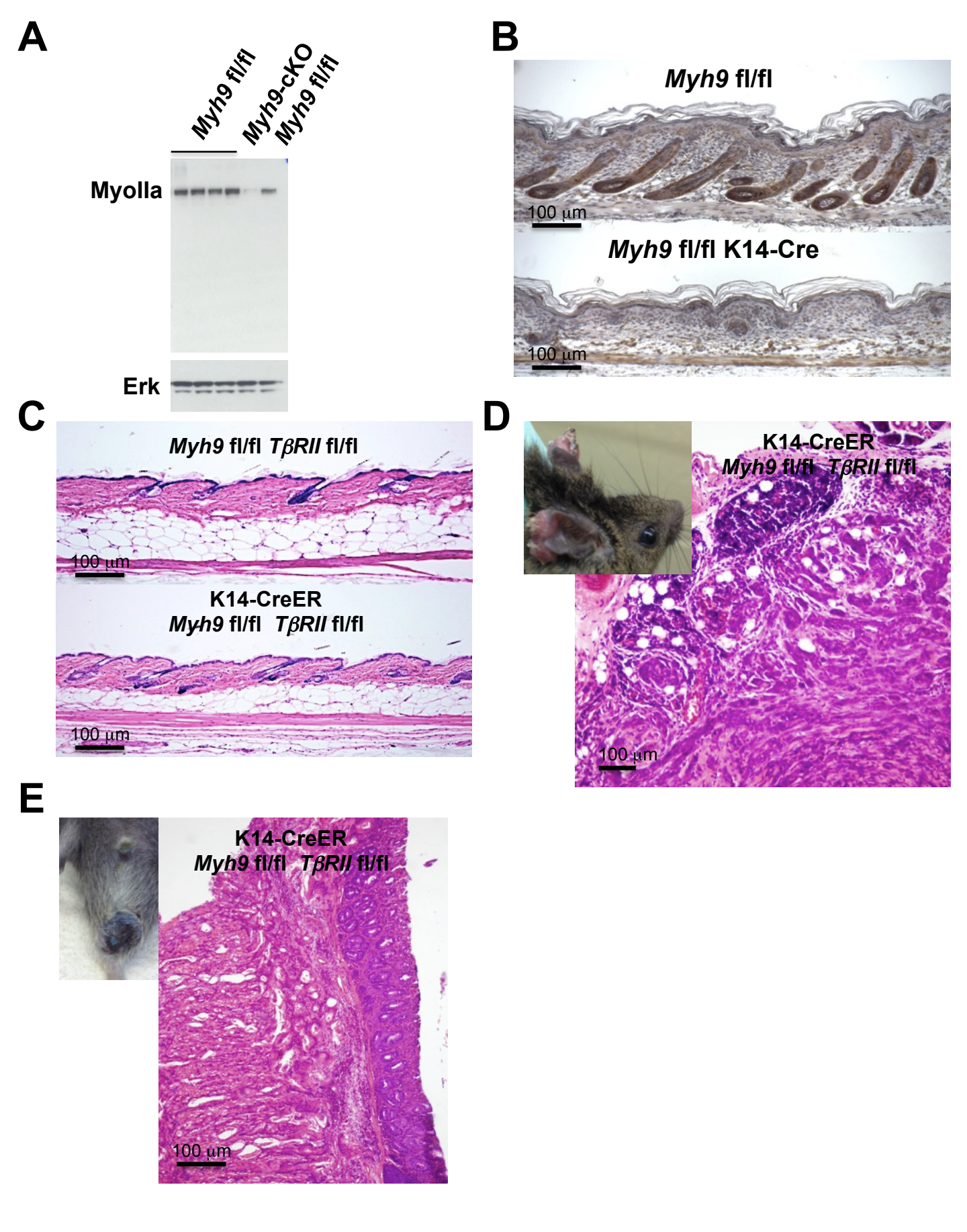
A
Myh9 fl/fl
Myh9-cKO
Myh9 fl/fl
Myolla
Erk
B
Myh9 fl/fl
100 μm
Myh9 fl/fl K14-Cre
100 μm
C
Myh9 fl/fl TβRII fl/fl
100 μm
K14-CreER
Myh9 fl/fl TβRII fl/fl
100 μm
D
K14-CreER
Myh9 fl/fl TβRII fl/fl
100 μm
E
K14-CreER
Myh9 fl/fl TβRII fl/fl
100 μm

Figure S10

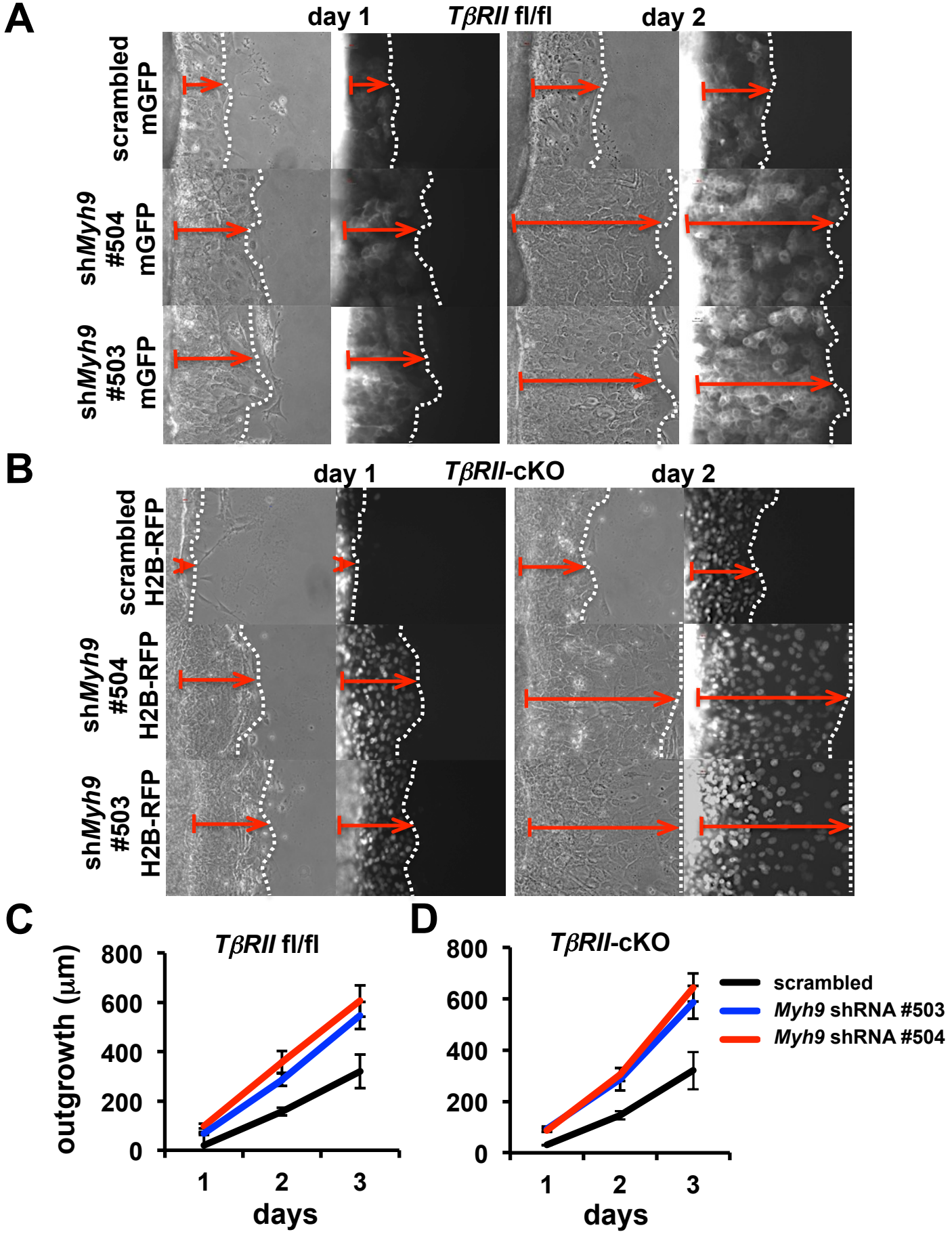
A
day 1
TβRII fl/fl
day 2
scrambled mGFP
shMyh9 #504 mGFP
shMyh9 #503 mGFP
B
day 1
TβRII-cKO
day 2
scrambled H2B-RFP
shMyh9 #504 H2B-RFP
shMyh9 #503 H2B-RFP
C
TβRII fl/fl
outgrowth (μm)
800
600
400
200
0
1
2
3
days
D
TβRII-cKO
800
600
400
200
0
1
2
3
days
scrambled
Myh9 shRNA #503
Myh9 shRNA #504

Figure S11

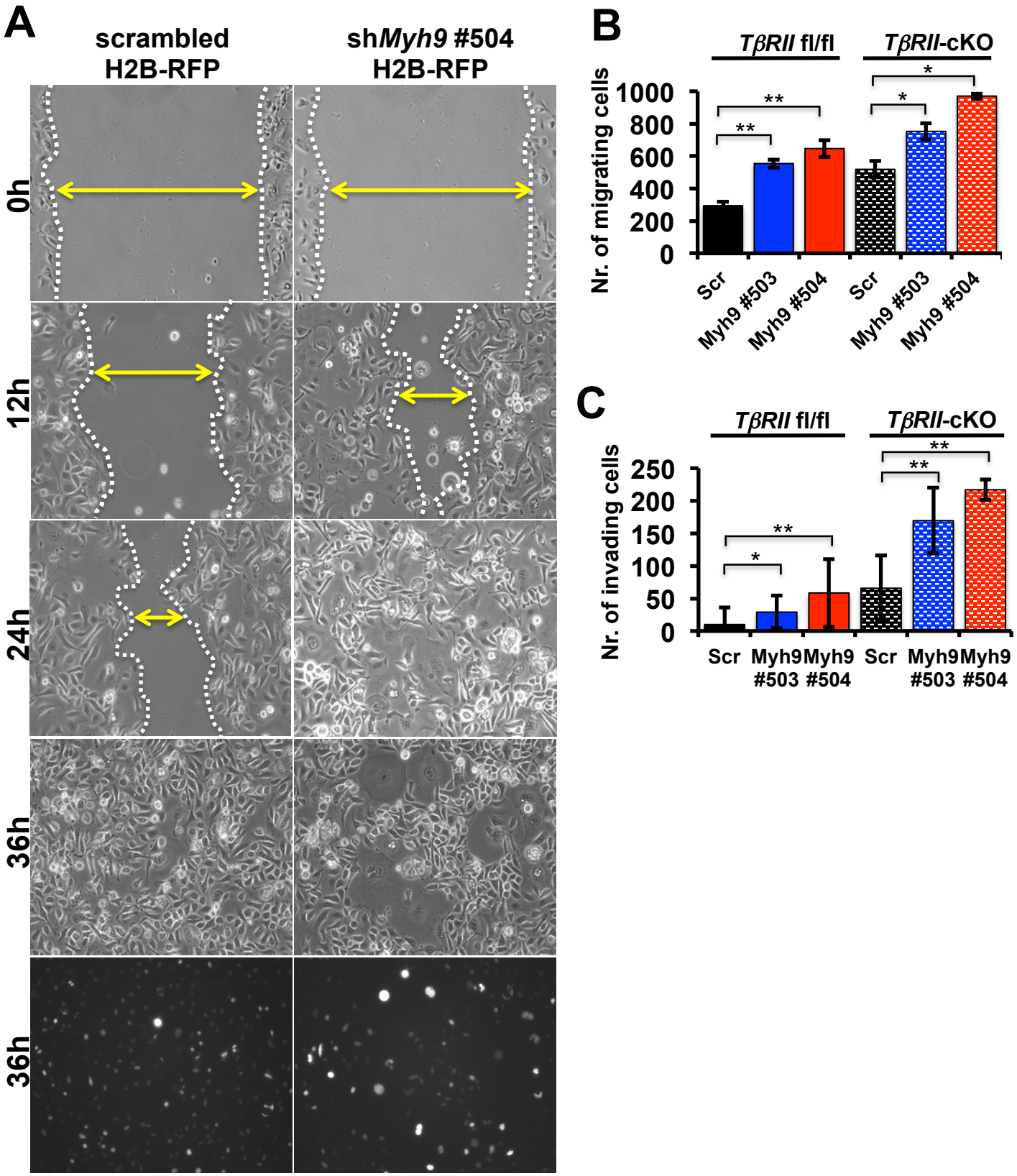
A
scrambled
H2B-RFP
shMyh9 #504
H2B-RFP
0h
12h
24h
36h
36h
B
TβRII fl/fl
TβRII-cKO
Nr. of migrating cells
1000
800
600
400
200
0
**
**
*
*
Scr
Myh9 #503
Myh9 #504
Scr
Myh9 #503
Myh9 #504
C
TβRII fl/fl
TβRII-cKO
Nr. of invading cells
250
200
150
100
50
0
*
**
**
**
Scr
Myh9 #503
Myh9 #504
Scr
Myh9 #503
Myh9 #504

Figure S12

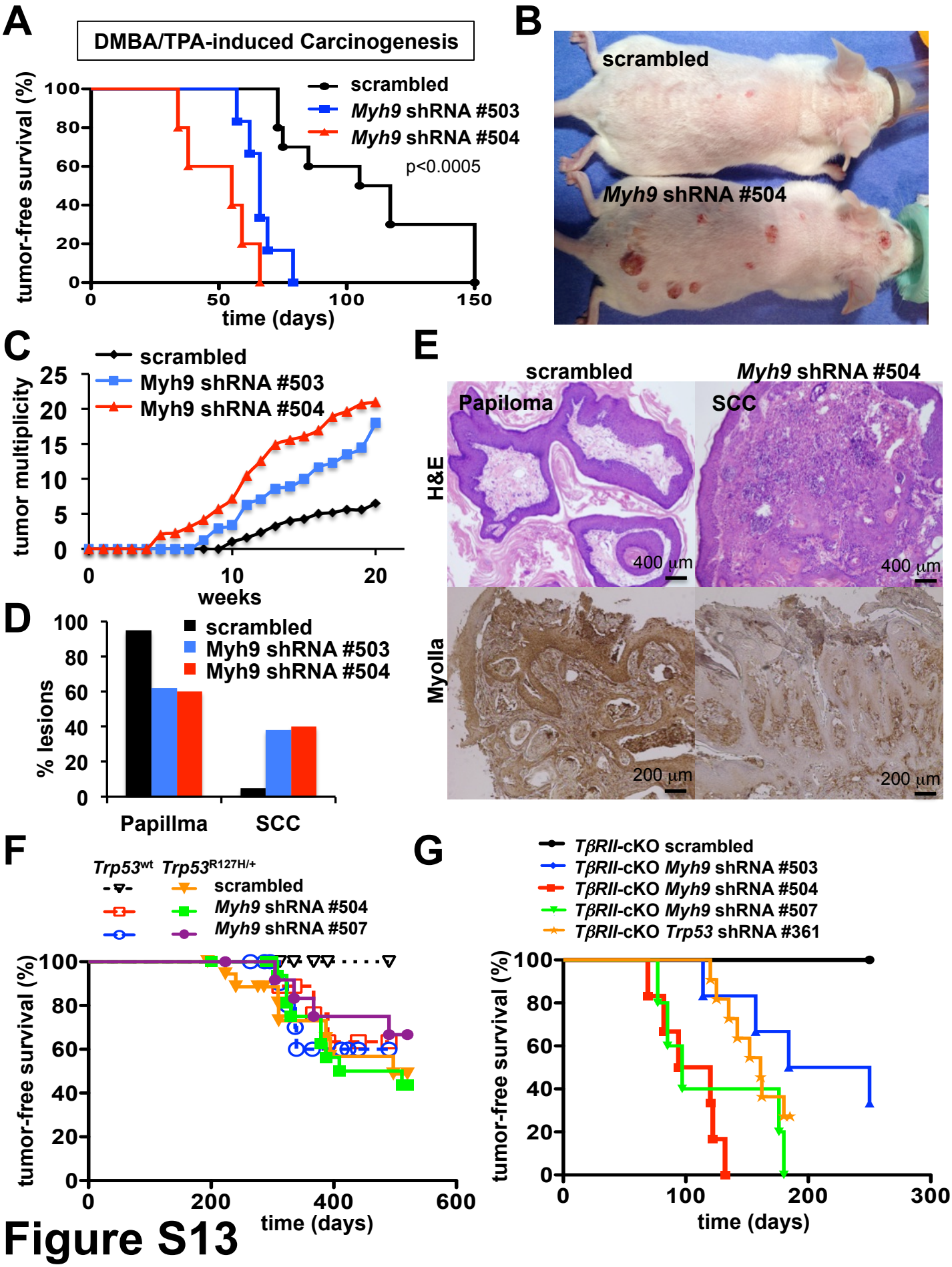
A
DMBA/TPA-induced Carcinogenesis
tumor-free survival (%)
time (days)
scrambled
Myh9 shRNA #503
Myh9 shRNA #504
p<0.0005
B
scrambled
Myh9 shRNA #504
C
tumor multiplicity
weeks
scrambled
Myh9 shRNA #503
Myh9 shRNA #504
D
% lesions
Papillma
SCC
scrambled
Myh9 shRNA #503
Myh9 shRNA #504
E
scrambled
Myh9 shRNA #504
H&E
Myolla
Papiloma
SCC
400 μm
200 μm
F
Trp53wt
Trp53R127H/+
scrambled
Myh9 shRNA #504
Myh9 shRNA #507
tumor-free survival (%)
time (days)
G
TβRII-cKO scrambled
TβRII-cKO Myh9 shRNA #503
TβRII-cKO Myh9 shRNA #504
TβRII-cKO Myh9 shRNA #507
TβRII-cKO Trp53 shRNA #361
tumor-free survival (%)
time (days)

Figure S13

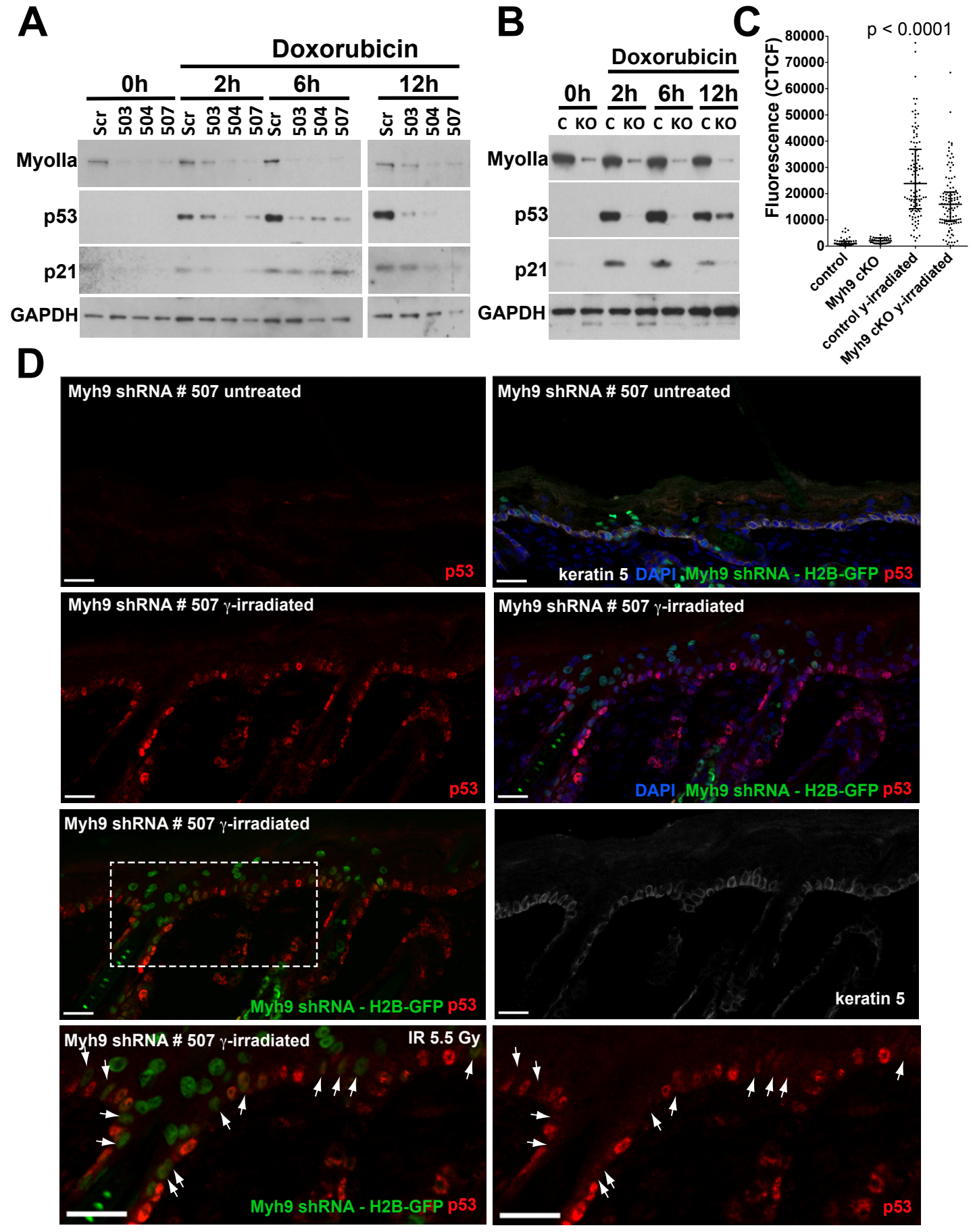
A
Doxorubicin
0h
2h
6h
12h
Scr
503
504
507
Myolla
p53
p21
GAPDH
B
Doxorubicin
0h
2h
6h
12h
C
KO
Myolla
p53
p21
GAPDH
C
p < 0.0001
Fluorescence (CTCF)
80000
70000
60000
50000
40000
30000
20000
10000
0
control
Myh9 cKO
control γ-irradiated
Myh9 cKO γ-irradiated
D
Myh9 shRNA # 507 untreated
p53
Myh9 shRNA # 507 untreated
keratin 5 DAPI Myh9 shRNA - H2B-GFP p53
Myh9 shRNA # 507 γ-irradiated
p53
Myh9 shRNA # 507 γ-irradiated
DAPI Myh9 shRNA - H2B-GFP p53
Myh9 shRNA # 507 γ-irradiated
Myh9 shRNA - H2B-GFP p53
keratin 5
Myh9 shRNA # 507 γ-irradiated
IR 5.5 Gy
Myh9 shRNA - H2B-GFP p53
p53

Figure S14

A

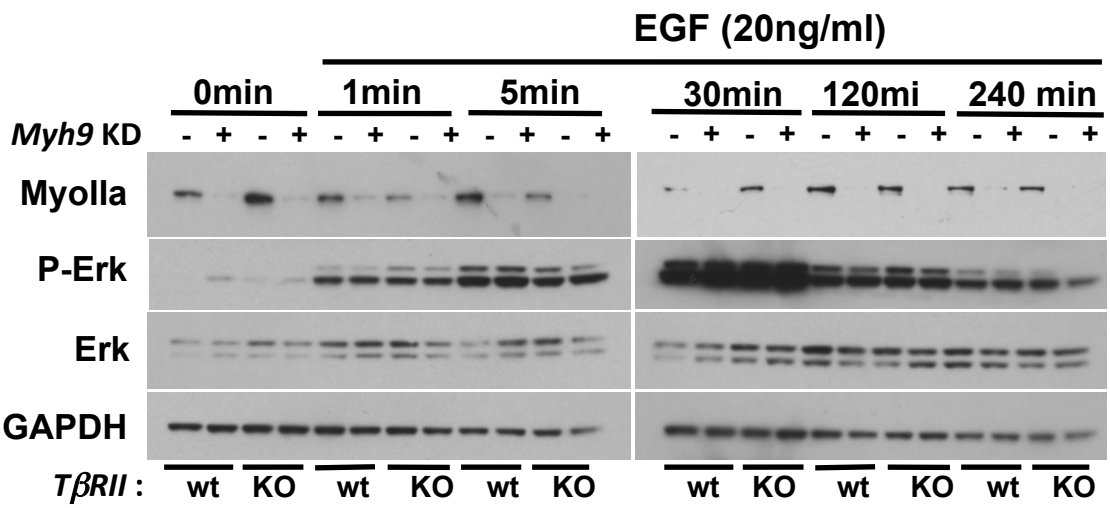
EGF (20ng/ml)
0min
1min
5min
30min
120mi
240 min
Myh9 KD
- + - + - + - + - + - + - + - + - + - + - +
Myolla
P-Erk
Erk
GAPDH
TβRII :
wt KO wt KO wt KO wt KO wt KO wt KO

Figure S15

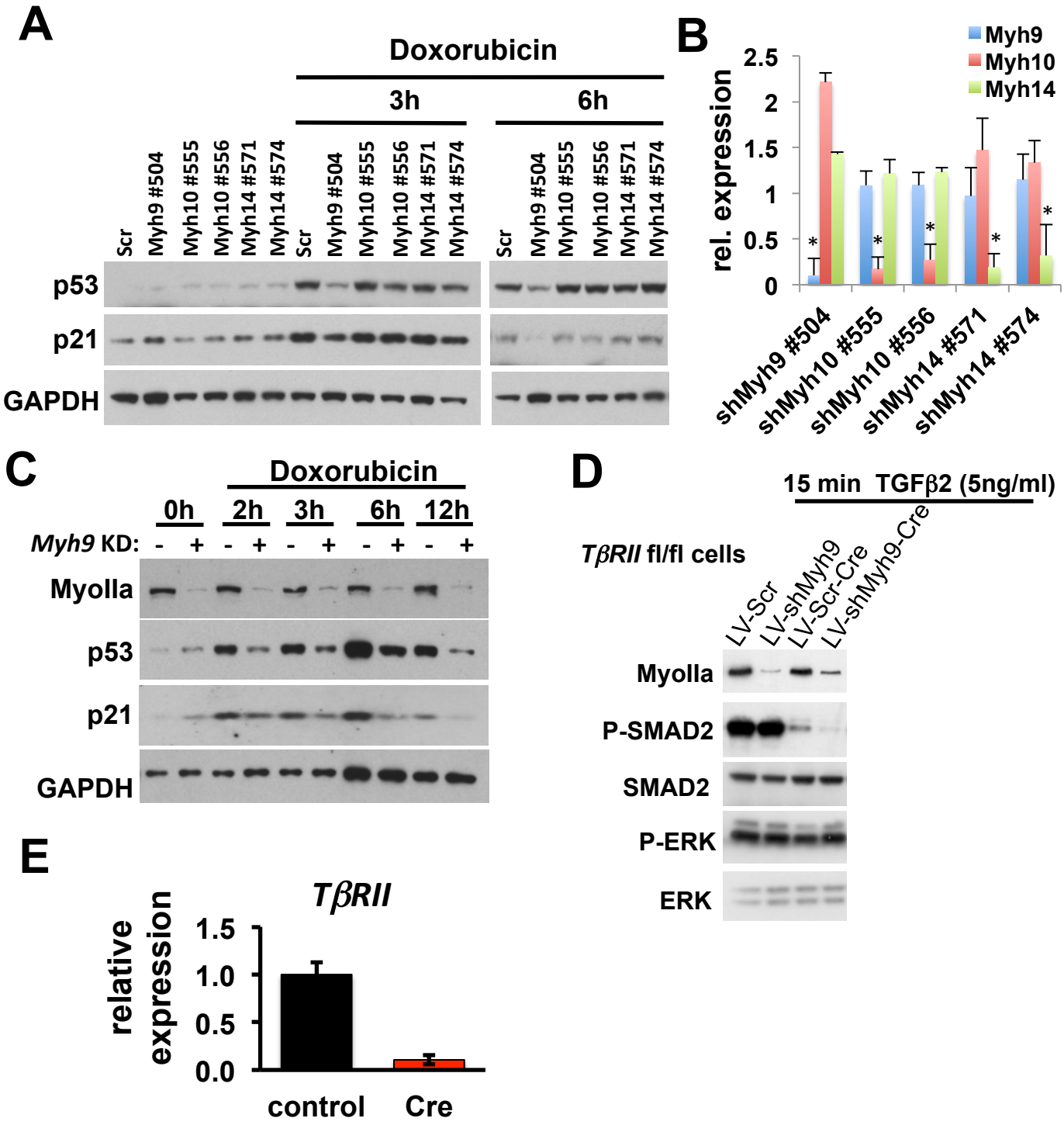
A
Doxorubicin
3h
6h
Scr
Myh9 #504
Myh10 #555
Myh10 #556
Myh14 #571
Myh14 #574
p53
p21
GAPDH
B
Myh9
Myh10
Myh14
rel. expression
2.5
2
1.5
1
0.5
0
shMyh9 #504
shMyh10 #555
shMyh10 #556
shMyh14 #571
shMyh14 #574
C
Doxorubicin
0h
2h
3h
6h
12h
Myh9 KD: - + - + - + - + - +
Myolla
p53
p21
GAPDH
D
15 min TGFβ2 (5ng/ml)
TβRII fl/fl cells
LV-Scr
LV-shMyh9
LV-Scr-Cre
LV-shMyh9-Cre
Myolla
P-SMAD2
SMAD2
P-ERK
ERK
E
TβRII
relative expression
1.5
1.0
0.5
0.0
control
Cre

Figure S16

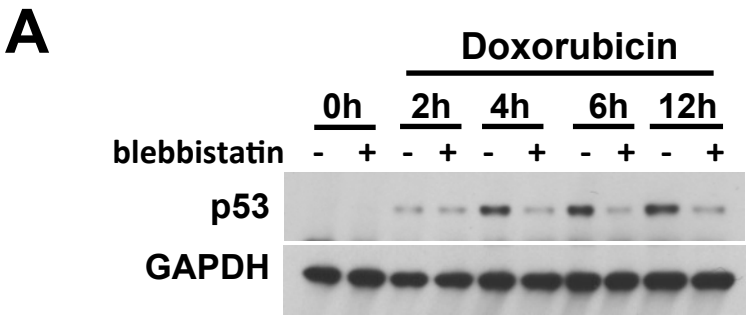
A
Doxorubicin
0h
2h
4h
6h
12h
blebbistatin - + - + - + - + - +
p53
GAPDH

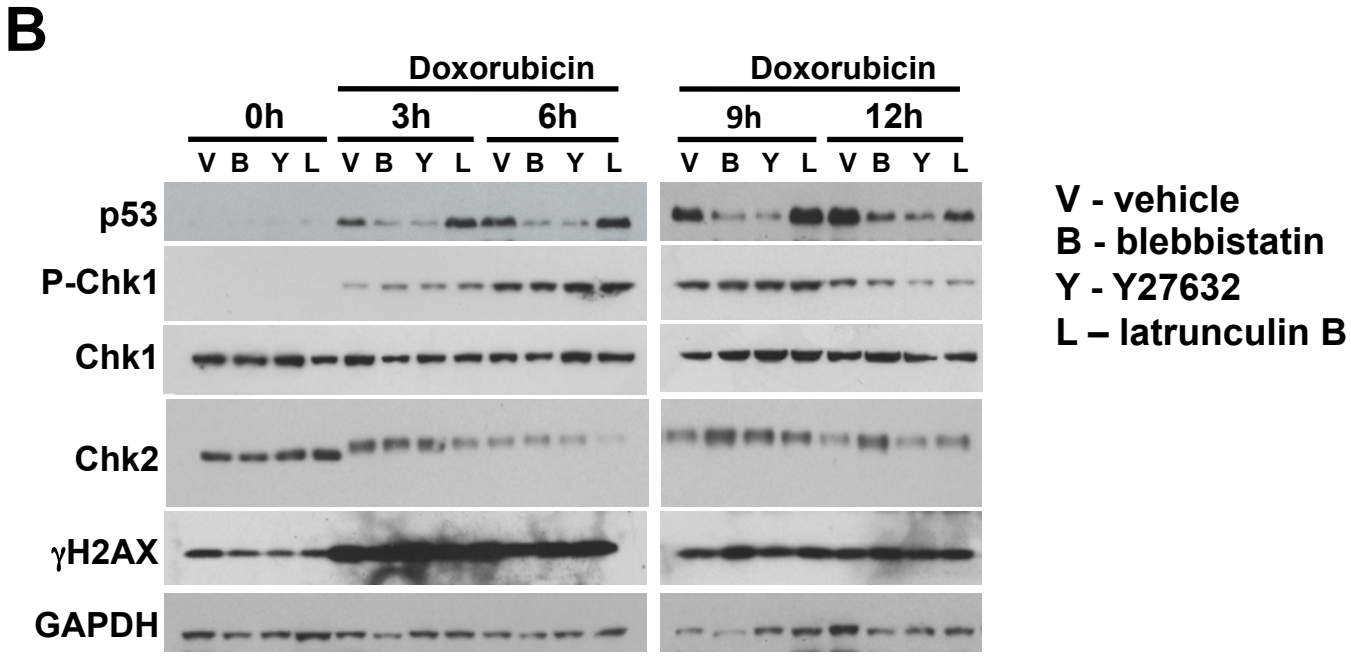
B
Doxorubicin
Doxorubicin
0h
3h
6h
9h
12h
V B Y L V B Y L V B Y L V B Y L V B Y L
p53
P-Chk1
Chk1
Chk2
γH2AX
GAPDH
V - vehicle
B - blebbistatin
Y - Y27632
L – latrunculin B

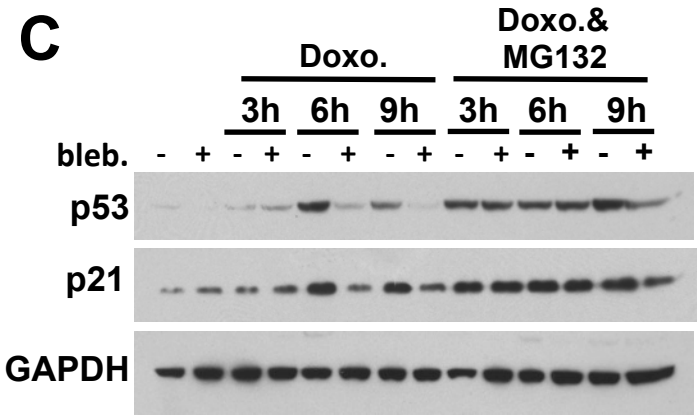
C
Doxo.
Doxo.& MG132
3h 6h 9h 3h 6h 9h
bleb. - + - + - + - + - + - + - +
p53
p21
GAPDH

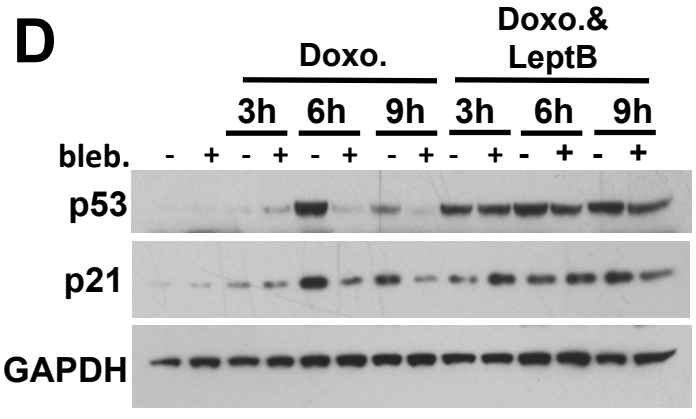
D
Doxo.
Doxo.& LeptB
3h 6h 9h 3h 6h 9h
bleb. - + - + - + - + - + - + - +
p53
p21
GAPDH

Figure S17

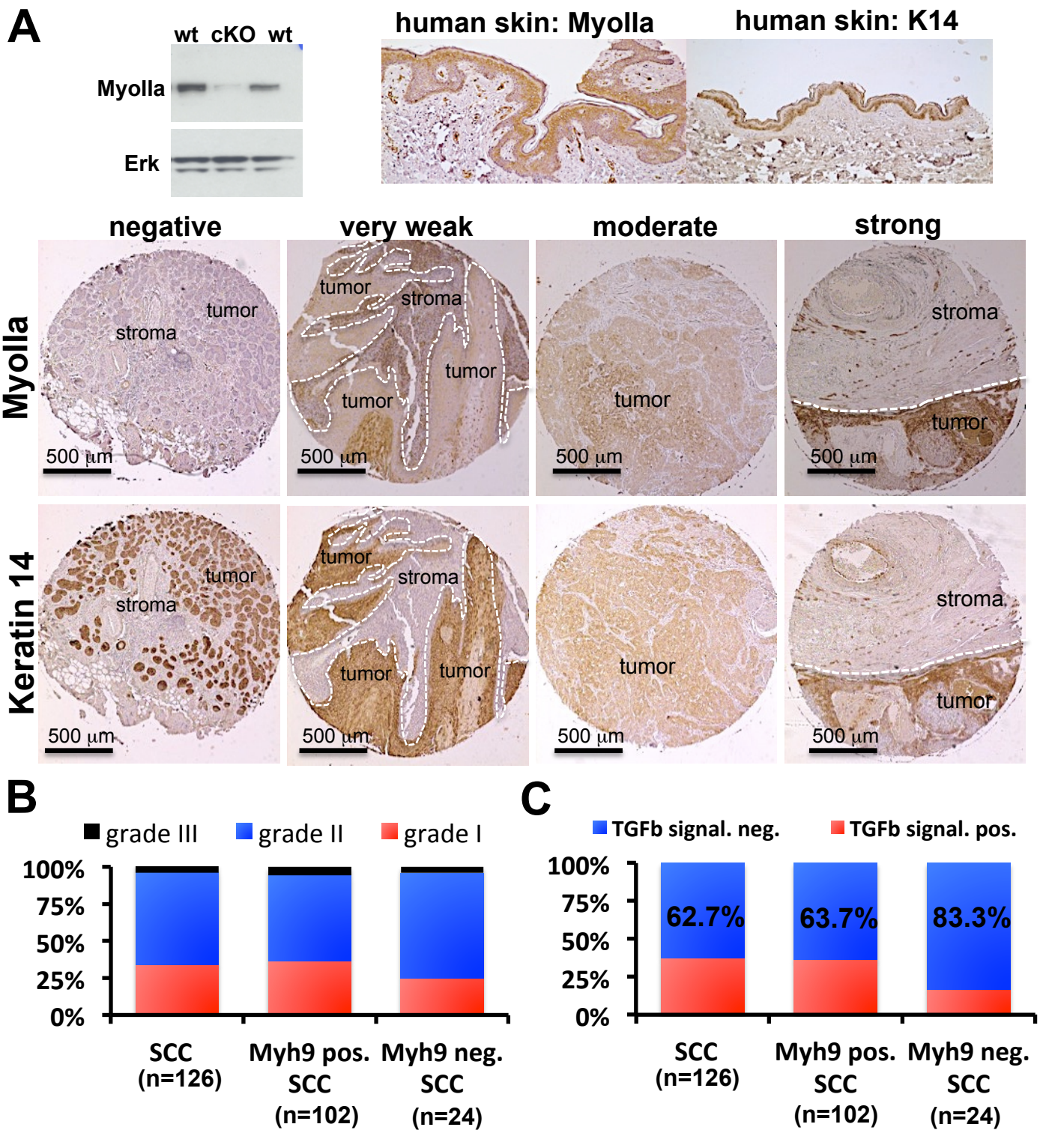
A
wt cKO wt
Myolla
Erk
human skin: Myolla
human skin: K14
negative
very weak
moderate
strong
Myolla
Keratin 14
tumor
stroma
500 μm
B
grade III
grade II
grade I
100%
75%
50%
25%
0%
SCC (n=126)
Myh9 pos. SCC (n=102)
Myh9 neg. SCC (n=24)
C
TGFb signal. neg.
TGFb signal. pos.
62.7%
63.7%
83.3%

Figure S18

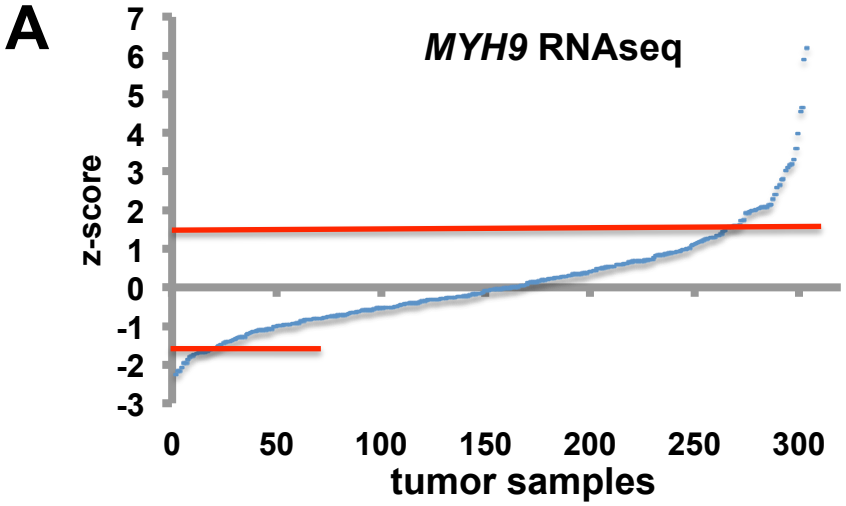
A
MYH9 RNAseq
z-score
7
6
5
4
3
2
1
0
-1
-2
-3
0
50
100
150
200
250
300
tumor samples

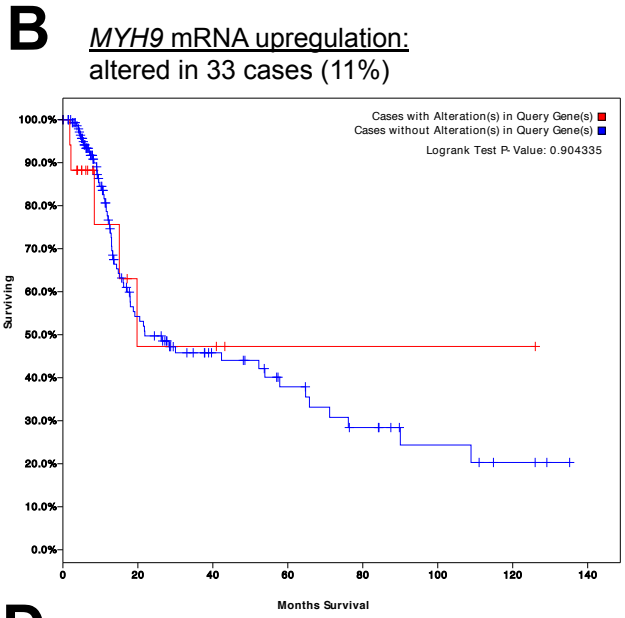
B
MYH9 mRNA upregulation:
altered in 33 cases (11%)
Cases with Alteration(s) in Query Gene(s)
Cases without Alteration(s) in Query Gene(s)
Logrank Test P-Value: 0.904335
Surviving
Months Survival

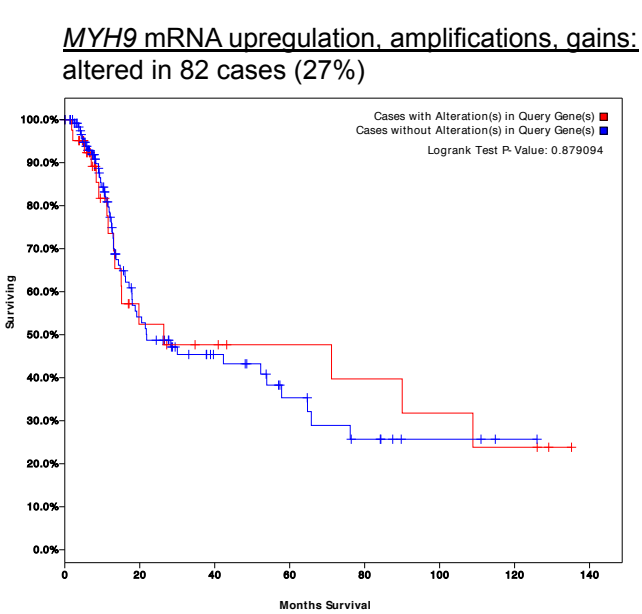
C
MYH9 mRNA upregulation, amplifications, gains:
altered in 82 cases (27%)
Cases with Alteration(s) in Query Gene(s)
Cases without Alteration(s) in Query Gene(s)
Logrank Test P-Value: 0.879094
Surviving
Months Survival

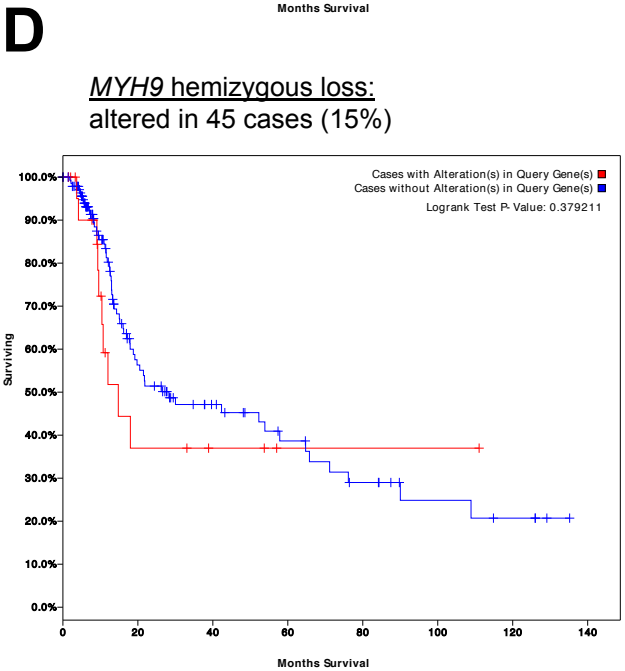
D
MYH9 hemizygous loss:
altered in 45 cases (15%)
Cases with Alteration(s) in Query Gene(s)
Cases without Alteration(s) in Query Gene(s)
Logrank Test P-Value: 0.379211
Surviving
Months Survival

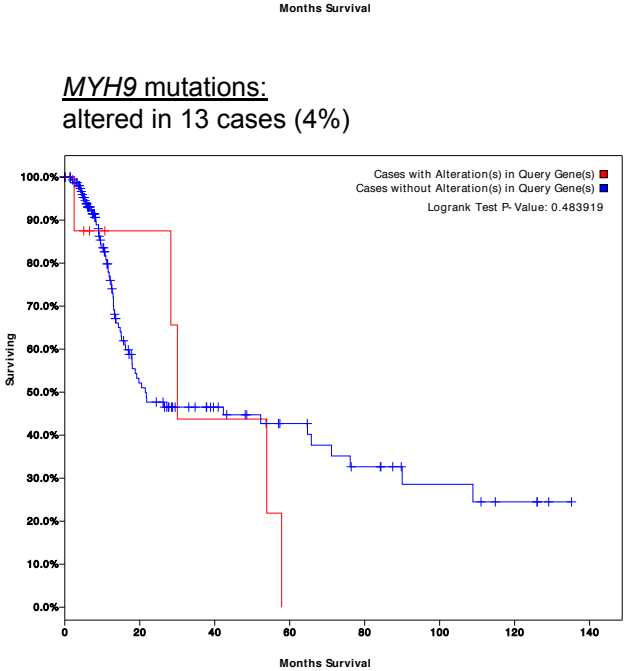
E
MYH9 mutations:
altered in 13 cases (4%)
Cases with Alteration(s) in Query Gene(s)
Cases without Alteration(s) in Query Gene(s)
Logrank Test P-Value: 0.483919
Surviving
Months Survival

Figure S19

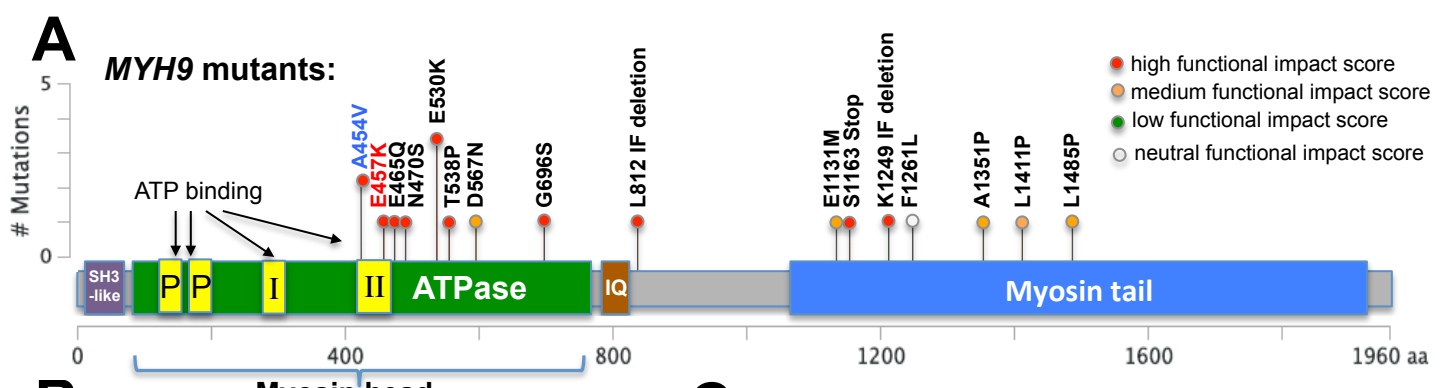

B

	Mutation	AA variant	Gene	MSA	PDB	Func. Impact	FI score
1	MYH9_HUMAN A454V	A454V	MYH9	msa	pdb	high	4.345
2	MYH9_HUMAN E457K	E457K	MYH9	msa	pdb	high	4.97
3	MYH9_HUMAN E465Q	E465Q	MYH9	msa	pdb	high	4.325
4	MYH9_HUMAN N470S	N470S	MYH9	msa	pdb	high	3.84
5	MYH9_HUMAN E530K	E530K	MYH9	msa	pdb	high	4.265
6	MYH9_HUMAN T538P	T538P	MYH9	msa	pdb	high	3.885
7	MYH9_HUMAN D567N	D567N	MYH9	msa	pdb	medium	2.33
8	MYH9_HUMAN G696S	G696S	MYH9	msa	pdb	high	3.67
9	MYH9_HUMAN L812X	L812X	MYH9	msa	pdb	high	
10	MYH9_HUMAN E1131M	E1131M	MYH9	msa		medium	3.5
11	MYH9_HUMAN S1163X	S1163X	MYH9	msa		high	
12	MYH9_HUMAN K1249E	K1249E	MYH9	msa		medium	2.3
13	MYH9_HUMAN F1261L	F1261L	MYH9	msa		neutral	-0.865
14	MYH9_HUMAN A1351P	A1351P	MYH9	msa		medium	2.89
15	MYH9_HUMAN L1411P	L1411P	MYH9	msa		medium	3.455
16	MYH9_HUMAN L1485P	L1485P	MYH9	msa		medium	3.09

C

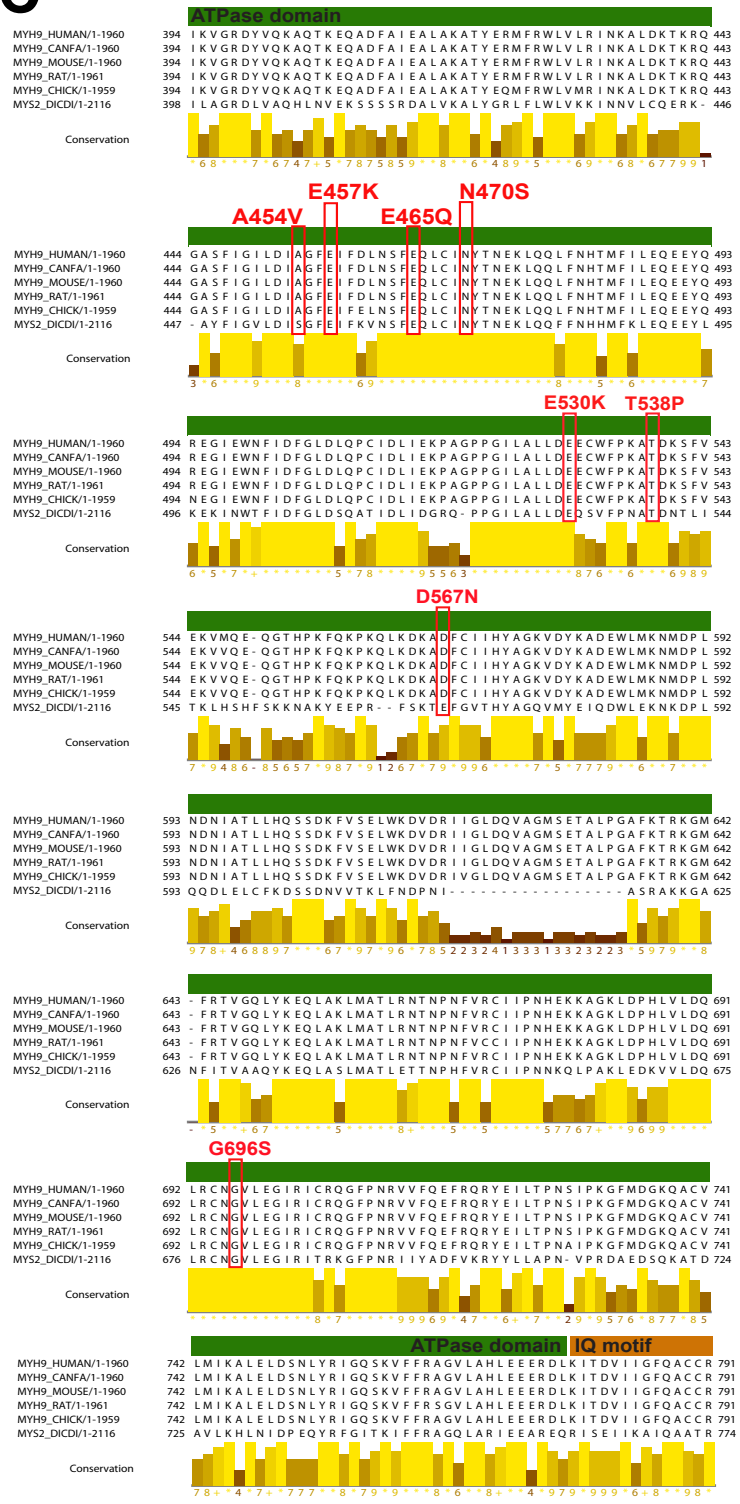

Figure S20

A

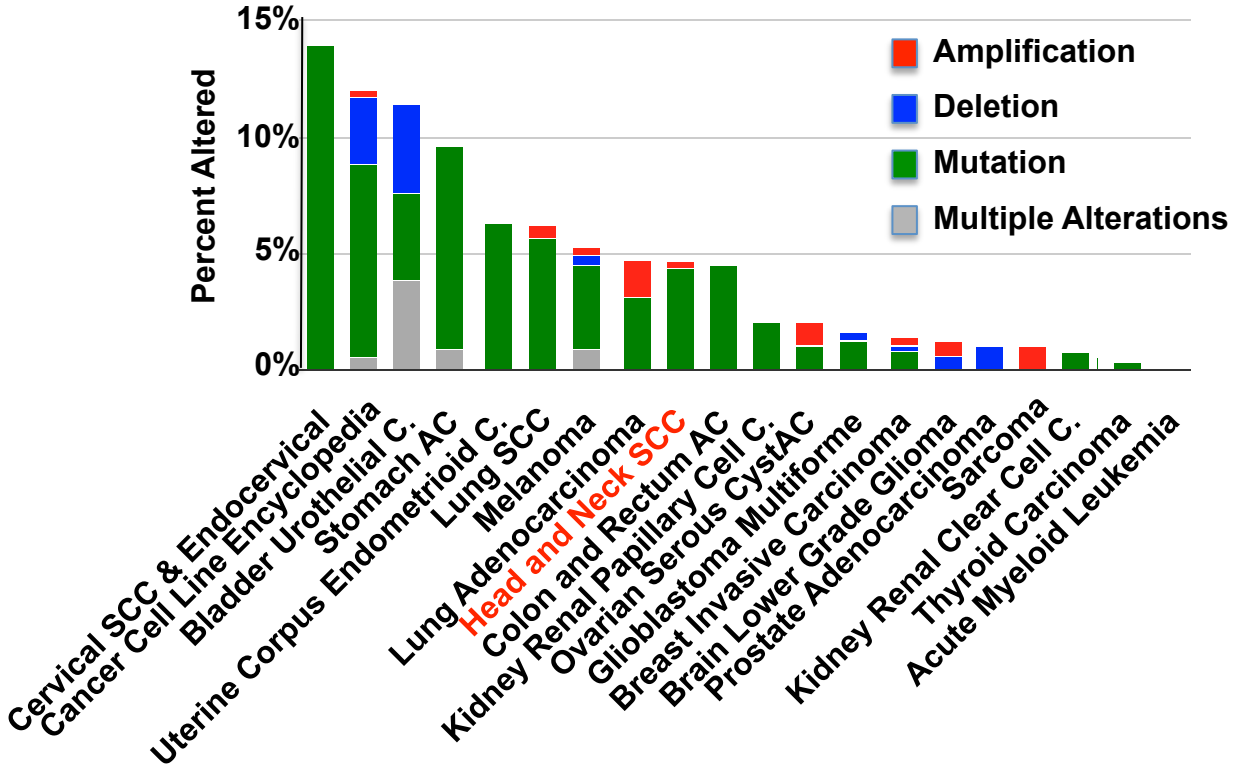
15%
10%
5%
0%
Percent Altered
Amplification
Deletion
Mutation
Multiple Alterations
Cervical SCC & Endocervical
Cancer Cell Line Encyclopedia
Bladder Urothelial C.
Stomach AC
Uterine Corpus Endometrioid C.
Lung SCC
Melanoma
Lung Adenocarcinoma
Head and Neck SCC
Colon and Rectum AC
Kidney Renal Papillary Cell C.
Ovarian Serous CystAC
Glioblastoma Multiforme
Breast Invasive Carcinoma
Brain Lower Grade Glioma
Prostate Adenocarcinoma
Kidney Renal Clear Cell C.
Sarcoma
Thyroid Carcinoma
Acute Myeloid Leukemia

Figure S21

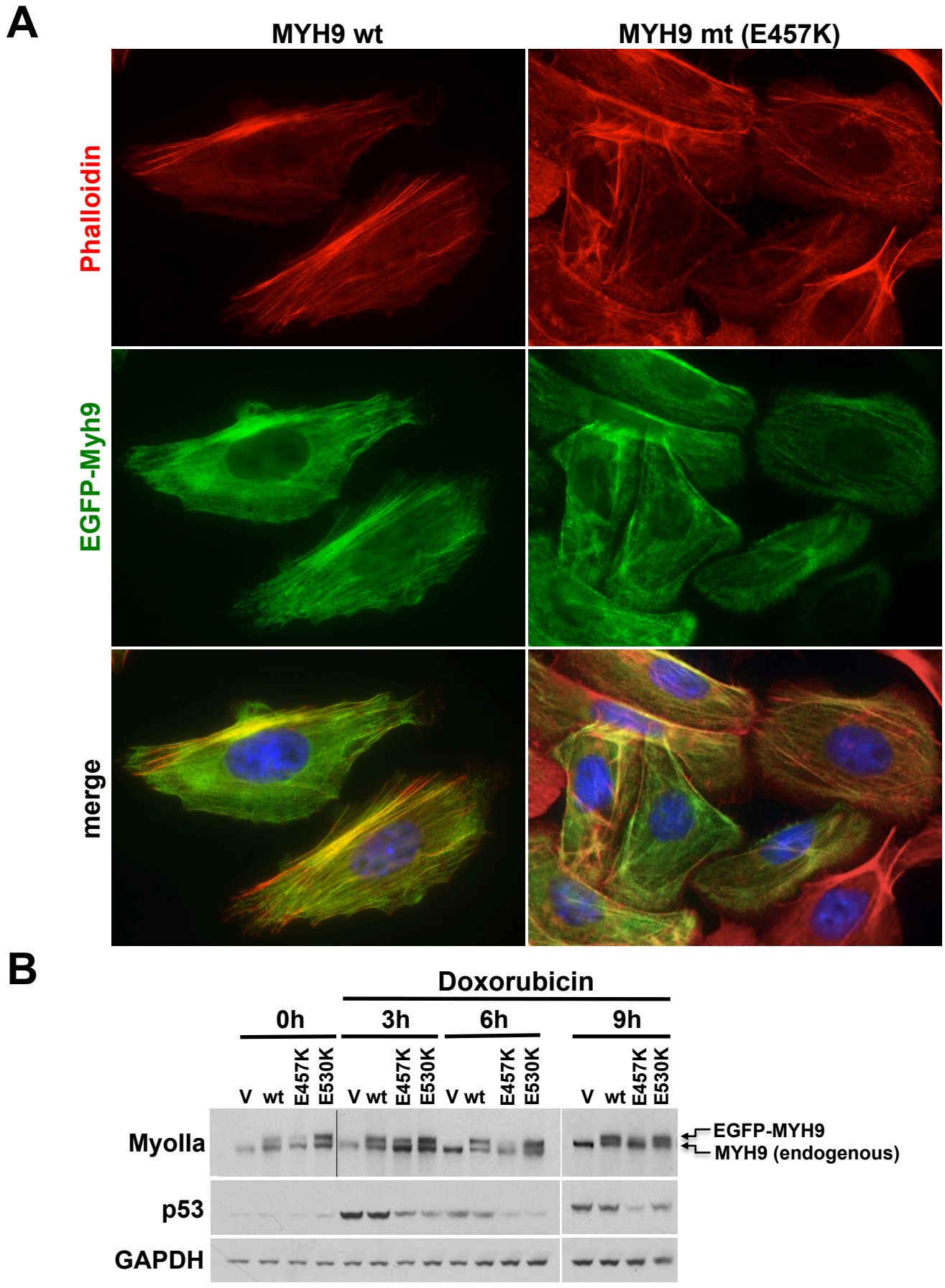
A
MYH9 wt
MYH9 mt (E457K)
Phalloidin
EGFP-Myh9
merge
B
Doxorubicin
0h
3h
6h
9h
V
wt
E457K
E530K
Myolla
p53
GAPDH
EGFP-MYH9
MYH9 (endogenous)

Figure S22

A

HNSCC: p53 mutations and p53 inactivating mutations are not mutually exclusive

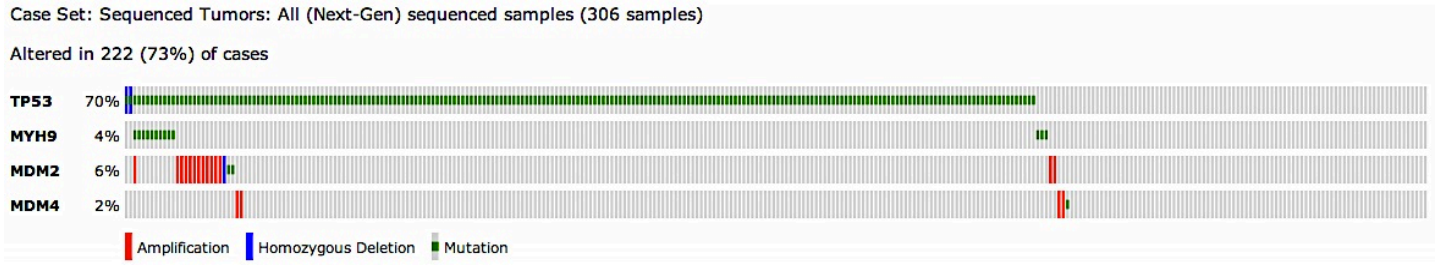

Gene	TP53	MDM2	MYH9	MDM4
TP53	---	0.070863	0.415401	0.162199
MDM2		---	0.531626	0.749961
MYH9			---	0.803702
MDM4				---

Legend
Strong tendency towards mutual exclusivity (0 < Odds Ratio < 0.1)
Some tendency towards mutual exclusivity (0.1 < Odds Ratio < 0.5)
No association (0.5 < Odds Ratio < 2)
Tendency toward co-occurrence (2 < Odds Ratio < 10)
Strong tendendency towards co-occurrence (Odds Ratio > 10)
No events recorded for one or both genes

B

Glioblastoma: p53 mutations and p53 inactivating mutations are mutually exclusive

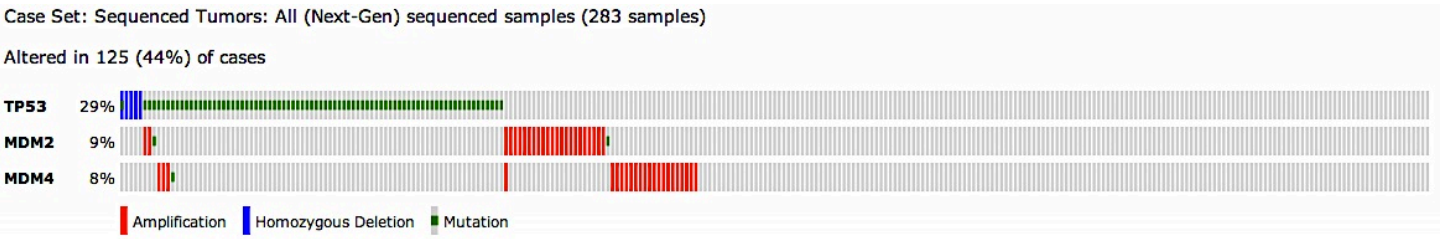

Gene	TP53	MDM2	MDM4
TP53	---	0.025041	0.114155
MDM2		---	0.326795
MDM4			---

p-values <0.05, as derived via Fisher's Exact test are outlined in red.
p-values are *not* adjusted for FDR.

Legend
Strong tendency towards mutual exclusivity (0 < Odds Ratio < 0.1)
Some tendency towards mutual exclusivity (0.1 < Odds Ratio < 0.5)
No association (0.5 < Odds Ratio < 2)
Tendency toward co-occurrence (2 < Odds Ratio < 10)
Strong tendendency towards co-occurrence (Odds Ratio > 10)
No events recorded for one or both genes

Figure S23

Table S1. Genes and shRNA construct included in the shRNA library

Gene	Construct	Clone	gene
1	1	TRCN0000179370	1500026B10Rik
	2	TRCN0000179624	1500026B10Rik
	3	TRCN0000179770	1500026B10Rik
	4	TRCN0000184447	1500026B10Rik
	5	TRCN0000184474	1500026B10Rik
2	6	TRCN0000126479	2010107G23Rik
	7	TRCN0000126480	2010107G23Rik
	8	TRCN0000126481	2010107G23Rik
	9	TRCN0000126482	2010107G23Rik
	10	TRCN0000126483	2010107G23Rik
3	11	TRCN0000176661	2310057J16Rik
	12	TRCN0000177579	2310057J16Rik
	13	TRCN0000182145	2310057J16Rik
	14	TRCN0000182145	2310057J16Rik
	15	TRCN0000182753	2310057J16Rik
4	16	TRCN0000113435	Abca6
	17	TRCN0000113436	Abca6
	18	TRCN0000113437	Abca6
	19	TRCN0000113438	Abca6
	20	TRCN0000113439	Abca6
5	21	TRCN0000113440	Abca9
	22	TRCN0000113442	Abca9
	23	TRCN0000113443	Abca9
	24	TRCN0000113444	Abca9
6	25	TRCN0000105260	Abcd4
	26	TRCN0000105261	Abcd4
	27	TRCN0000105262	Abcd4
	28	TRCN0000105263	Abcd4
	29	TRCN0000105264	Abcd4
7	30	TRCN0000087968	Abi3
	31	TRCN0000087969	Abi3
	32	TRCN0000087970	Abi3
	33	TRCN0000087971	Abi3
	34	TRCN0000087972	Abi3
8	35	TRCN0000022604	Acvr1c
	36	TRCN0000022605	Acvr1c
	37	TRCN0000022606	Acvr1c
	38	TRCN0000022607	Acvr1c
	39	TRCN0000022608	Acvr1c
9	40	TRCN0000032274	Adamts12
	41	TRCN0000032275	Adamts12
	42	TRCN0000032276	Adamts12
	43	TRCN0000032277	Adamts12
	44	TRCN0000032278	Adamts12
10	45	TRCN0000114956	Adcy8
	46	TRCN0000114957	Adcy8
	47	TRCN0000114958	Adcy8
	48	TRCN0000114959	Adcy8
	49	TRCN0000114960	Adcy8
11	50	TRCN0000086608	Aff3
	51	TRCN0000086609	Aff3
	52	TRCN0000086610	Aff3
	53	TRCN0000086612	Aff3
12	54	TRCN0000071348	Ahctf1
	55	TRCN0000071349	Ahctf1
	56	TRCN0000071350	Ahctf1
	57	TRCN0000071351	Ahctf1
	58	TRCN0000071352	Ahctf1
13	59	TRCN0000101420	Allc
	60	TRCN0000101421	Allc
	61	TRCN0000101422	Allc
	62	TRCN0000101423	Allc
	63	TRCN0000101424	Allc
14	64	TRCN0000022614	Amhr2
	65	TRCN0000022615	Amhr2
	66	TRCN0000022616	Amhr2
	67	TRCN0000022617	Amhr2
	68	TRCN0000022618	Amhr2
15	69	TRCN0000090053	Ank3
	70	TRCN0000090054	Ank3
	71	TRCN0000090055	Ank3
	72	TRCN0000090056	Ank3
	73	TRCN0000090057	Ank3
16	74	TRCN0000090263	Anln
	75	TRCN0000090264	Anln
	76	TRCN0000090265	Anln
	77	TRCN0000090266	Anln
17	78	TRCN0000110725	Anxa3
	79	TRCN0000110726	Anxa3
	80	TRCN0000110727	Anxa3
	81	TRCN0000110728	Anxa3
	82	TRCN0000110729	Anxa3
18	83	TRCN0000012278	Apaf1
	84	TRCN0000012280	Apaf1
	85	TRCN0000012281	Apaf1
	86	TRCN0000012282	Apaf1
19	87	TRCN0000026148	Ar
	88	TRCN0000026177	Ar
	89	TRCN0000026189	Ar
	90	TRCN0000026195	Ar
	91	TRCN0000026211	Ar
20	92	TRCN0000022609	Araf
	93	TRCN0000022610	Araf
	94	TRCN0000022611	Araf
	95	TRCN0000022612	Araf
	96	TRCN0000022613	Araf
21	97	TRCN0000109960	Arhgef12
	98	TRCN0000109961	Arhgef12
	99	TRCN0000109962	Arhgef12
	100	TRCN0000109963	Arhgef12
	101	TRCN0000109964	Arhgef12
22	102	TRCN0000075553	Atf5
	103	TRCN0000075554	Atf5
	104	TRCN0000075555	Atf5
	105	TRCN0000075556	Atf5
	106	TRCN0000075557	Atf5
23	107	TRCN0000012643	Atm
	108	TRCN0000012644	Atm
	109	TRCN0000012645	Atm
	110	TRCN0000012646	Atm
	111	TRCN0000012647	Atm
24	112	TRCN0000101520	Atp10d
	113	TRCN0000101521	Atp10d
	114	TRCN0000101522	Atp10d
	115	TRCN0000101523	Atp10d
25	116	TRCN0000115396	Azin1
	117	TRCN0000115397	Azin1
	118	TRCN0000115398	Azin1
	119	TRCN0000115399	Azin1
	120	TRCN0000115400	Azin1
26	121	TRCN0000070508	Barx2
	122	TRCN0000070509	Barx2
	123	TRCN0000070510	Barx2
	124	TRCN0000070511	Barx2
	125	TRCN0000070512	Barx2
27	126	TRCN0000004678	Bcl2
	127	TRCN0000004679	Bcl2

	128	TRCN0000004680	Bcl2
	129	TRCN0000004681	Bcl2
28	130	TRCN0000042553	Bcl3
	131	TRCN0000042554	Bcl3
	132	TRCN0000042555	Bcl3
	133	TRCN0000042556	Bcl3
	134	TRCN0000042557	Bcl3
29	135	TRCN0000012563	Bmi1
	136	TRCN0000012564	Bmi1
	137	TRCN0000012565	Bmi1
	138	TRCN0000012566	Bmi1
	139	TRCN0000012567	Bmi1
30	140	TRCN0000025877	Bmp2
	141	TRCN0000025878	Bmp2
	142	TRCN0000025923	Bmp2
	143	TRCN0000025939	Bmp2
	144	TRCN0000025949	Bmp2
31	145	TRCN0000025875	Bmp4
	146	TRCN0000025905	Bmp4
	147	TRCN0000025922	Bmp4
	148	TRCN0000025936	Bmp4
	149	TRCN0000025957	Bmp4
32	150	TRCN0000022619	Bmpr1a
	151	TRCN0000022620	Bmpr1a
	152	TRCN0000022621	Bmpr1a
	153	TRCN0000022622	Bmpr1a
	154	TRCN0000022623	Bmpr1a
33	155	TRCN0000022529	Bmpr2
	156	TRCN0000022530	Bmpr2
	157	TRCN0000022531	Bmpr2
	158	TRCN0000022532	Bmpr2
	159	TRCN0000022533	Bmpr2
34	160	TRCN0000009687	Bnip3
	161	TRCN0000009688	Bnip3
	162	TRCN0000009689	Bnip3
	163	TRCN0000009690	Bnip3
	164	TRCN0000009691	Bnip3
35	165	TRCN0000022589	Braf
	166	TRCN0000022590	Braf
	167	TRCN0000022591	Braf
	168	TRCN0000022592	Braf
	169	TRCN0000022593	Braf
36	170	TRCN0000042558	Brca1
	171	TRCN0000042559	Brca1
	172	TRCN0000042560	Brca1
	173	TRCN0000042561	Brca1
	174	TRCN0000042562	Brca1
37	175	TRCN0000071008	Brca2
	176	TRCN0000071009	Brca2
	177	TRCN0000071010	Brca2
	178	TRCN0000071011	Brca2
	179	TRCN0000071012	Brca2
38	180	TRCN0000103285	C130053K05Rik
	181	TRCN0000103286	C130053K05Rik
	182	TRCN0000103287	C130053K05Rik
	183	TRCN0000103288	C130053K05Rik
	184	TRCN0000103289	C130053K05Rik
39	185	TRCN0000024114	Camk1d
	186	TRCN0000024115	Camk1d
	187	TRCN0000024116	Camk1d
	188	TRCN0000024117	Camk1d
	189	TRCN0000024118	Camk1d
40	190	TRCN0000114461	Car2
	191	TRCN0000114462	Car2
	192	TRCN0000114463	Car2
	193	TRCN0000114464	Car2
	194	TRCN0000114465	Car2
41	195	TRCN0000012243	Casp8
	196	TRCN0000012244	Casp8
	197	TRCN0000012245	Casp8
	198	TRCN0000012246	Casp8
	199	TRCN0000012247	Casp8
42	200	TRCN0000042568	Cbl
	201	TRCN0000042569	Cbl
	202	TRCN0000042570	Cbl
	203	TRCN0000042571	Cbl
	204	TRCN0000042572	Cbl
43	205	TRCN0000071028	Cbx1
	206	TRCN0000071029	Cbx1
	207	TRCN0000071030	Cbx1
	208	TRCN0000071031	Cbx1
	209	TRCN0000071032	Cbx1
44	210	TRCN0000071048	Cbx5
	211	TRCN0000071049	Cbx5
	212	TRCN0000071050	Cbx5
	213	TRCN0000071051	Cbx5
	214	TRCN0000071052	Cbx5
45	215	TRCN0000176503	Ccdc39
	216	TRCN0000176967	Ccdc39
	217	TRCN0000177337	Ccdc39
	218	TRCN0000182114	Ccdc39
	219	TRCN0000182268	Ccdc39
46	220	TRCN0000011978	Ccnd3
	221	TRCN0000011979	Ccnd3
	222	TRCN0000011980	Ccnd3
	223	TRCN0000011981	Ccnd3
47	224	TRCN0000119627	Cd320
	225	TRCN0000119629	Cd320
	226	TRCN0000119630	Cd320
	227	TRCN0000119631	Cd320
48	228	TRCN0000065353	Cd44
	229	TRCN0000065354	Cd44
	230	TRCN0000065355	Cd44
	231	TRCN0000065356	Cd44
	232	TRCN0000065357	Cd44
49	233	TRCN0000030109	Cdc14b
	234	TRCN0000030110	Cdc14b
	235	TRCN0000030111	Cdc14b
	236	TRCN0000030112	Cdc14b
	237	TRCN0000030113	Cdc14b
50	238	TRCN0000042578	Cdh1
	239	TRCN0000042579	Cdh1
	240	TRCN0000042580	Cdh1
	241	TRCN0000042581	Cdh1
	242	TRCN0000042582	Cdh1
51	243	TRCN0000094534	Cdh12
	244	TRCN0000094535	Cdh12
	245	TRCN0000094536	Cdh12
	246	TRCN0000094537	Cdh12
	247	TRCN0000094538	Cdh12
52	248	TRCN0000094729	Cdh4
	249	TRCN0000094730	Cdh4
	250	TRCN0000094731	Cdh4
	251	TRCN0000094732	Cdh4
	252	TRCN0000094733	Cdh4
53	253	TRCN0000094894	Cdh5
	254	TRCN0000094895	Cdh5
	255	TRCN0000094896	Cdh5
	256	TRCN0000094897	Cdh5
	257	TRCN0000094898	Cdh5
54	258	TRCN0000094784	Cdh7
	259	TRCN0000094785	Cdh7
	260	TRCN0000094786	Cdh7
	261	TRCN0000094787	Cdh7

	262	TRCN0000094788	Cdh7
55	263	TRCN0000023174	Cdk4
	264	TRCN0000023175	Cdk4
	265	TRCN0000023176	Cdk4
	266	TRCN0000023177	Cdk4
	267	TRCN0000023178	Cdk4
56	268	TRCN0000042583	Cdkn1a
	269	TRCN0000042585	Cdkn1a
	270	TRCN0000042586	Cdkn1a
	271	TRCN0000042587	Cdkn1a
	272	TRCN0000054898	Cdkn1a
	273	TRCN0000054899	Cdkn1a
	274	TRCN0000054900	Cdkn1a
	275	TRCN0000054901	Cdkn1a
	276	TRCN0000054902	Cdkn1a
57	277	TRCN0000071063	Cdkn1b
	278	TRCN0000071064	Cdkn1b
	279	TRCN0000071066	Cdkn1b
	280	TRCN0000071067	Cdkn1b
58	281	TRCN0000042588	Cdkn1c
	282	TRCN0000042589	Cdkn1c
	283	TRCN0000042590	Cdkn1c
	284	TRCN0000042592	Cdkn1c
59	285	TRCN0000077813	Cdkn2a
	286	TRCN0000077815	Cdkn2a
	287	TRCN0000077816	Cdkn2a
60	288	TRCN0000042598	Cdkn2b
	289	TRCN0000042599	Cdkn2b
	290	TRCN0000042600	Cdkn2b
	291	TRCN0000042601	Cdkn2b
	292	TRCN0000042602	Cdkn2b
61	293	TRCN0000085088	Cdkn2d
	294	TRCN0000085089	Cdkn2d
	295	TRCN0000085090	Cdkn2d
	296	TRCN0000085091	Cdkn2d
	297	TRCN0000085092	Cdkn2d
62	298	TRCN0000071654	Cebpd
	299	TRCN0000071655	Cebpd
	300	TRCN0000071657	Cebpd
63	301	TRCN0000094949	Celsr3
	302	TRCN0000094950	Celsr3
	303	TRCN0000094951	Celsr3
	304	TRCN0000094952	Celsr3
	305	TRCN0000094953	Celsr3
64	306	TRCN0000179809	Cep55
	307	TRCN0000182908	Cep55
	308	TRCN0000183083	Cep55
	309	TRCN0000183560	Cep55
65	310	TRCN0000012648	Chek1
	311	TRCN0000012649	Chek1
	312	TRCN0000012650	Chek1
	313	TRCN0000012651	Chek1
	314	TRCN0000012652	Chek1
66	315	TRCN0000012653	Chek2
	316	TRCN0000012654	Chek2
	317	TRCN0000012655	Chek2
	318	TRCN0000012656	Chek2
	319	TRCN0000012657	Chek2
67	320	TRCN0000103290	Chpt1
	321	TRCN0000103292	Chpt1
	322	TRCN0000103293	Chpt1
	323	TRCN0000103294	Chpt1
68	324	TRCN0000025883	Chrd
	325	TRCN0000025906	Chrd
	326	TRCN0000025914	Chrd
	327	TRCN0000025932	Chrd
	328	TRCN0000025944	Chrd
69	329	TRCN0000012348	Chuk
	330	TRCN0000012349	Chuk
	331	TRCN0000012350	Chuk
	332	TRCN0000012351	Chuk
	333	TRCN0000012352	Chuk
70	334	TRCN0000069708	Clca2
	335	TRCN0000069709	Clca2
	336	TRCN0000069710	Clca2
	337	TRCN0000069711	Clca2
	338	TRCN0000069712	Clca2
71	339	TRCN0000069738	Clic1
	340	TRCN0000069739	Clic1
	341	TRCN0000069740	Clic1
	342	TRCN0000069741	Clic1
72	343	TRCN0000023189	Clk3
	344	TRCN0000023190	Clk3
	345	TRCN0000023191	Clk3
	346	TRCN0000023192	Clk3
	347	TRCN0000023193	Clk3
73	348	TRCN0000023194	Clk4
	349	TRCN0000023195	Clk4
	350	TRCN0000023196	Clk4
	351	TRCN0000023197	Clk4
	352	TRCN0000023198	Clk4
74	353	TRCN0000094734	Clstn2
	354	TRCN0000094735	Clstn2
	355	TRCN0000094736	Clstn2
	356	TRCN0000094737	Clstn2
	357	TRCN0000094738	Clstn2
75	358	TRCN0000039014	Cntn1
	359	TRCN0000039015	Cntn1
	360	TRCN0000039016	Cntn1
	361	TRCN0000039017	Cntn1
	362	TRCN0000039018	Cntn1
76	363	TRCN0000113645	Cntn3
	364	TRCN0000113646	Cntn3
	365	TRCN0000113647	Cntn3
	366	TRCN0000113648	Cntn3
	367	TRCN0000113649	Cntn3
77	368	TRCN0000094359	Cntnap1
	369	TRCN0000094360	Cntnap1
	370	TRCN0000094361	Cntnap1
	371	TRCN0000094362	Cntnap1
	372	TRCN0000094363	Cntnap1
78	373	TRCN0000094969	Cntnap2
	374	TRCN0000094970	Cntnap2
	375	TRCN0000094971	Cntnap2
	376	TRCN0000094972	Cntnap2
	377	TRCN0000094973	Cntnap2
79	378	TRCN0000094539	Cntnap4
	379	TRCN0000094540	Cntnap4
80	380	TRCN0000090503	Col1a1
	381	TRCN0000090504	Col1a1
	382	TRCN0000090505	Col1a1
	383	TRCN0000090506	Col1a1
	384	TRCN0000090507	Col1a1
81	385	TRCN0000090043	Col1a2
	386	TRCN0000090044	Col1a2
	387	TRCN0000090045	Col1a2
	388	TRCN0000090046	Col1a2
	389	TRCN0000090047	Col1a2
82	390	TRCN0000091163	Col22a1
	391	TRCN0000091164	Col22a1
	392	TRCN0000091165	Col22a1
	393	TRCN0000091166	Col22a1
	394	TRCN0000091167	Col22a1
83	395	TRCN0000091483	Col3a1

	396	TRCN0000091484	Col3a1
	397	TRCN0000091485	Col3a1
	398	TRCN0000091486	Col3a1
	399	TRCN0000091487	Col3a1
84	400	TRCN0000031319	Cpxm2
	401	TRCN0000031320	Cpxm2
	402	TRCN0000031321	Cpxm2
	403	TRCN0000031322	Cpxm2
	404	TRCN0000031323	Cpxm2
85	405	TRCN0000105235	Crabp2
	406	TRCN0000105236	Crabp2
	407	TRCN0000105237	Crabp2
	408	TRCN0000105238	Crabp2
	409	TRCN0000105239	Crabp2
86	410	TRCN0000042603	Crk
	411	TRCN0000042604	Crk
	412	TRCN0000042606	Crk
	413	TRCN0000042607	Crk
87	414	TRCN0000023734	Csk
	415	TRCN0000023735	Csk
	416	TRCN0000023736	Csk
	417	TRCN0000023737	Csk
	418	TRCN0000023738	Csk
88	419	TRCN0000087303	Csmd3
	420	TRCN0000087304	Csmd3
	421	TRCN0000087305	Csmd3
	422	TRCN0000087306	Csmd3
	423	TRCN0000087307	Csmd3
89	424	TRCN0000080278	Cst6
	425	TRCN0000080279	Cst6
	426	TRCN0000080280	Cst6
	427	TRCN0000080281	Cst6
	428	TRCN0000080282	Cst6
90	429	TRCN0000039019	Ctcf
	430	TRCN0000039020	Ctcf
	431	TRCN0000039021	Ctcf
	432	TRCN0000039022	Ctcf
	433	TRCN0000039023	Ctcf
91	434	TRCN0000109665	Ctgf
	435	TRCN0000109666	Ctgf
	436	TRCN0000109667	Ctgf
	437	TRCN0000109668	Ctgf
	438	TRCN0000109669	Ctgf
92	439	TRCN0000065368	Cxcl14
	440	TRCN0000065369	Cxcl14
	441	TRCN0000065370	Cxcl14
	442	TRCN0000065371	Cxcl14
	443	TRCN0000065372	Cxcl14
93	444	TRCN0000067258	Cxcl2
	445	TRCN0000067259	Cxcl2
	446	TRCN0000067260	Cxcl2
	447	TRCN0000067261	Cxcl2
94	448	TRCN0000028678	Cxcr4
	449	TRCN0000028704	Cxcr4
	450	TRCN0000028724	Cxcr4
	451	TRCN0000028749	Cxcr4
	452	TRCN0000028750	Cxcr4
95	453	TRCN0000125700	Cyp4f16
	454	TRCN0000125701	Cyp4f16
	455	TRCN0000125702	Cyp4f16
	456	TRCN0000125703	Cyp4f16
96	457	TRCN0000103750	Ddx3x
	458	TRCN0000103751	Ddx3x
	459	TRCN0000103752	Ddx3x
	460	TRCN0000103753	Ddx3x
	461	TRCN0000103754	Ddx3x
97	462	TRCN0000099475	Defb6
	463	TRCN0000099476	Defb6
	464	TRCN0000099477	Defb6
	465	TRCN0000099478	Defb6
98	466	TRCN0000028845	Dll1
	467	TRCN0000028864	Dll1
	468	TRCN0000028865	Dll1
	469	TRCN0000028890	Dll1
	470	TRCN0000028910	Dll1
99	471	TRCN0000028875	Dll3
	472	TRCN0000028879	Dll3
	473	TRCN0000028896	Dll3
	474	TRCN0000028907	Dll3
	475	TRCN0000028924	Dll3
100	476	TRCN0000028894	Dll4
	477	TRCN0000028916	Dll4
	478	TRCN0000028928	Dll4
101	479	TRCN0000070598	Dlx2
	480	TRCN0000070599	Dlx2
	481	TRCN0000070600	Dlx2
	482	TRCN0000070601	Dlx2
	483	TRCN0000070602	Dlx2
102	484	TRCN0000070608	Dlx3
	485	TRCN0000070609	Dlx3
	486	TRCN0000070610	Dlx3
	487	TRCN0000070611	Dlx3
	488	TRCN0000070612	Dlx3
103	489	TRCN0000070628	Dlx5
	490	TRCN0000070629	Dlx5
	491	TRCN0000070630	Dlx5
	492	TRCN0000070632	Dlx5
104	493	TRCN0000086488	Dmrta2
	494	TRCN0000086489	Dmrta2
	495	TRCN0000086490	Dmrta2
	496	TRCN0000086491	Dmrta2
105	497	TRCN0000008562	Dnajb9
	498	TRCN0000008563	Dnajb9
	499	TRCN0000008564	Dnajb9
	500	TRCN0000008565	Dnajb9
	501	TRCN0000008566	Dnajb9
106	502	TRCN0000039024	Dnmt1
	503	TRCN0000039025	Dnmt1
	504	TRCN0000039026	Dnmt1
	505	TRCN0000039027	Dnmt1
	506	TRCN0000039028	Dnmt1
107	507	TRCN0000039029	Dnmt2
	508	TRCN0000039030	Dnmt2
	509	TRCN0000039031	Dnmt2
	510	TRCN0000039032	Dnmt2
	511	TRCN0000039033	Dnmt2
108	512	TRCN0000039034	Dnmt3a
	513	TRCN0000039035	Dnmt3a
	514	TRCN0000039036	Dnmt3a
	515	TRCN0000039037	Dnmt3a
	516	TRCN0000039038	Dnmt3a
109	517	TRCN0000039104	Dnmt3l
	518	TRCN0000039105	Dnmt3l
	519	TRCN0000039106	Dnmt3l
	520	TRCN0000039107	Dnmt3l
	521	TRCN0000039108	Dnmt3l
110	522	TRCN0000054348	Dusp4
	523	TRCN0000054349	Dusp4
	524	TRCN0000054350	Dusp4
	525	TRCN0000054351	Dusp4
	526	TRCN0000054352	Dusp4
111	527	TRCN0000023479	Egfr
	528	TRCN0000023480	Egfr
	529	TRCN0000023481	Egfr

	530	TRCN0000023482	Egfr
	531	TRCN0000023483	Egfr
	532	TRCN0000055218	Egfr
	533	TRCN0000055219	Egfr
	534	TRCN0000055220	Egfr
	535	TRCN0000055221	Egfr
	536	TRCN0000055222	Egfr
112	537	TRCN0000009749	Egln3
	538	TRCN0000009750	Egln3
	539	TRCN0000009751	Egln3
	540	TRCN0000009752	Egln3
	541	TRCN0000009753	Egln3
113	542	TRCN0000081623	Egr1
	543	TRCN0000081624	Egr1
	544	TRCN0000081625	Egr1
	545	TRCN0000081626	Egr1
	546	TRCN0000081627	Egr1
114	547	TRCN0000081678	Egr2
	548	TRCN0000081679	Egr2
	549	TRCN0000081680	Egr2
	550	TRCN0000081681	Egr2
	551	TRCN0000081682	Egr2
115	552	TRCN0000081788	Ehf
	553	TRCN0000081789	Ehf
	554	TRCN0000081790	Ehf
	555	TRCN0000081791	Ehf
	556	TRCN0000081792	Ehf
116	557	TRCN0000081938	Elf5
	558	TRCN0000081939	Elf5
	559	TRCN0000081940	Elf5
	560	TRCN0000081941	Elf5
	561	TRCN0000081942	Elf5
117	562	TRCN0000042643	Elk3
	563	TRCN0000042644	Elk3
	564	TRCN0000042645	Elk3
	565	TRCN0000042646	Elk3
	566	TRCN0000042647	Elk3
118	567	TRCN0000023679	Epha7
	568	TRCN0000023680	Epha7
	569	TRCN0000023681	Epha7
	570	TRCN0000023682	Epha7
	571	TRCN0000023683	Epha7
119	572	TRCN0000092273	Eps8
	573	TRCN0000092274	Eps8
	574	TRCN0000092275	Eps8
	575	TRCN0000092276	Eps8
	576	TRCN0000092277	Eps8
120	577	TRCN0000190945	Esm1
	578	TRCN0000192471	Esm1
	579	TRCN0000192502	Esm1
	580	TRCN0000192617	Esm1
121	581	TRCN0000026176	Esr1
	582	TRCN0000026184	Esr1
	583	TRCN0000026197	Esr1
	584	TRCN0000026201	Esr1
	585	TRCN0000026214	Esr1
122	586	TRCN0000026150	Esr2
	587	TRCN0000026170	Esr2
	588	TRCN0000026192	Esr2
	589	TRCN0000026215	Esr2
123	590	TRCN0000111725	Exoc4
	591	TRCN0000111726	Exoc4
	592	TRCN0000111727	Exoc4
	593	TRCN0000111728	Exoc4
	594	TRCN0000111729	Exoc4
124	595	TRCN0000095694	Ezh1
	596	TRCN0000095695	Ezh1
	597	TRCN0000095696	Ezh1
	598	TRCN0000095697	Ezh1
	599	TRCN0000095698	Ezh1
125	600	TRCN0000039039	Ezh2
	601	TRCN0000039040	Ezh2
	602	TRCN0000039041	Ezh2
	603	TRCN0000039042	Ezh2
	604	TRCN0000039043	Ezh2
126	605	TRCN0000105190	Fabp3
	606	TRCN0000105191	Fabp3
	607	TRCN0000105192	Fabp3
	608	TRCN0000105193	Fabp3
	609	TRCN0000105194	Fabp3
127	610	TRCN0000105185	Fabp4
	611	TRCN0000105186	Fabp4
	612	TRCN0000105187	Fabp4
	613	TRCN0000105188	Fabp4
	614	TRCN0000105189	Fabp4
128	615	NM_010634.1-149s1c1	Fabp5
	616	NM_010634.1-592s1c1	Fabp5
	617	TRCN0000011894	Fabp5
	618	TRCN0000011896	Fabp5
	619	TRCN0000011897	Fabp5
129	620	TRCN0000114336	Fads2
	621	TRCN0000114337	Fads2
	622	TRCN0000114338	Fads2
	623	TRCN0000114340	Fads2
130	624	TRCN0000173476	Fancm
	625	TRCN0000173798	Fancm
	626	TRCN0000175001	Fancm
	627	TRCN0000176065	Fancm
	628	TRCN0000176066	Fancm
131	629	TRCN0000094844	Fath
	630	TRCN0000094845	Fath
	631	TRCN0000094846	Fath
	632	TRCN0000094847	Fath
	633	TRCN0000094848	Fath
132	634	TRCN0000012828	Fbxw7
	635	TRCN0000012829	Fbxw7
	636	TRCN0000012830	Fbxw7
	637	TRCN0000012831	Fbxw7
	638	TRCN0000012832	Fbxw7
133	639	TRCN0000004653	Ffar1
	640	TRCN0000004654	Ffar1
	641	TRCN0000004655	Ffar1
134	642	TRCN0000009606	Flt1
	643	TRCN0000009607	Flt1
	644	TRCN0000009608	Flt1
	645	TRCN0000009609	Flt1
	646	TRCN0000009610	Flt1
135	647	TRCN0000023739	Flt3
	648	TRCN0000023740	Flt3
	649	TRCN0000023741	Flt3
	650	TRCN0000023742	Flt3
	651	TRCN0000023743	Flt3
136	652	TRCN0000023754	Flt4
	653	TRCN0000023755	Flt4
	654	TRCN0000023756	Flt4
	655	TRCN0000023757	Flt4
	656	TRCN0000023758	Flt4
137	657	TRCN0000120512	Fmn2
	658	TRCN0000120513	Fmn2
	659	TRCN0000120514	Fmn2
	660	TRCN0000120515	Fmn2
	661	TRCN0000120516	Fmn2

138	662	TRCN0000084288	Foxj2
	663	TRCN0000084289	Foxj2
	664	TRCN0000084290	Foxj2
	665	TRCN0000084291	Foxj2
	666	TRCN0000084292	Foxj2
139	667	TRCN0000072003	Foxp1
	668	TRCN0000072004	Foxp1
	669	TRCN0000072005	Foxp1
	670	TRCN0000072006	Foxp1
	671	TRCN0000072007	Foxp1
140	672	TRCN0000108925	Fscn1
	673	TRCN0000108926	Fscn1
	674	TRCN0000108927	Fscn1
	675	TRCN0000108928	Fscn1
	676	TRCN0000108929	Fscn1
141	677	TRCN0000085478	Gata3
	678	TRCN0000085479	Gata3
	679	TRCN0000085480	Gata3
	680	TRCN0000085481	Gata3
	681	TRCN0000085482	Gata3
142	682	TRCN0000068823	Gjb5
	683	TRCN0000068824	Gjb5
	684	TRCN0000068825	Gjb5
	685	TRCN0000068826	Gjb5
	686	TRCN0000068827	Gjb5
143	687	TRCN0000027955	Gpr56
	688	TRCN0000027962	Gpr56
	689	TRCN0000027970	Gpr56
	690	TRCN0000027988	Gpr56
	691	TRCN0000027999	Gpr56
144	692	TRCN0000076528	Gpx2
	693	TRCN0000076529	Gpx2
	694	TRCN0000076530	Gpx2
	695	TRCN0000076531	Gpx2
	696	TRCN0000076532	Gpx2
145	697	TRCN0000103545	Grhl3
	698	TRCN0000103546	Grhl3
	699	TRCN0000103547	Grhl3
	700	TRCN0000103548	Grhl3
	701	TRCN0000103549	Grhl3
146	702	TRCN0000103040	Grid1
	703	TRCN0000103041	Grid1
	704	TRCN0000103042	Grid1
	705	TRCN0000103043	Grid1
	706	TRCN0000103044	Grid1
147	707	TRCN0000012613	Gsk3b
	708	TRCN0000012614	Gsk3b
	709	TRCN0000012615	Gsk3b
	710	TRCN0000012616	Gsk3b
	711	TRCN0000012617	Gsk3b
148	712	TRCN0000103310	Gsta1
	713	TRCN0000103311	Gsta1
	714	TRCN0000103312	Gsta1
	715	TRCN0000103313	Gsta1
	716	TRCN0000103314	Gsta1
149	717	TRCN0000103295	Gsta2
	718	TRCN0000103296	Gsta2
	719	TRCN0000103297	Gsta2
	720	TRCN0000103298	Gsta2
	721	TRCN0000103299	Gsta2
150	722	TRCN0000103280	Gsta3
	723	TRCN0000103281	Gsta3
	724	TRCN0000103282	Gsta3
	725	TRCN0000103283	Gsta3
	726	TRCN0000103284	Gsta3
151	727	TRCN0000103430	Gsta4
	728	TRCN0000103431	Gsta4
	729	TRCN0000103432	Gsta4
	730	TRCN0000103433	Gsta4
	731	TRCN0000103434	Gsta4
152	732	TRCN0000103240	Gstm1
	733	TRCN0000103241	Gstm1
	734	TRCN0000103242	Gstm1
	735	TRCN0000103243	Gstm1
	736	TRCN0000103244	Gstm1
153	737	TRCN0000103160	Gstm2
	738	TRCN0000103161	Gstm2
	739	TRCN0000103162	Gstm2
	740	TRCN0000103163	Gstm2
	741	TRCN0000103164	Gstm2
154	742	TRCN0000028854	Hes1
	743	TRCN0000028855	Hes1
	744	TRCN0000028881	Hes1
	745	TRCN0000028925	Hes1
	746	TRCN0000028927	Hes1
155	747	TRCN0000096954	Hist1h2bh
	748	TRCN0000096955	Hist1h2bh
	749	TRCN0000096956	Hist1h2bh
	750	TRCN0000096957	Hist1h2bh
	751	TRCN0000096958	Hist1h2bh
156	752	TRCN0000126044	Hmga2
	753	TRCN0000126045	Hmga2
	754	TRCN0000126046	Hmga2
	755	TRCN0000126047	Hmga2
	756	TRCN0000126048	Hmga2
157	757	TRCN0000075583	Hmgb2
	758	TRCN0000075584	Hmgb2
	759	TRCN0000075585	Hmgb2
	760	TRCN0000075586	Hmgb2
	761	TRCN0000075587	Hmgb2
158	762	TRCN0000070789	Hoxa4
	763	TRCN0000070790	Hoxa4
	764	TRCN0000070791	Hoxa4
	765	TRCN0000070792	Hoxa4
159	766	TRCN0000012518	Hoxa5
	767	TRCN0000012519	Hoxa5
	768	TRCN0000012520	Hoxa5
	769	TRCN0000012521	Hoxa5
	770	TRCN0000012522	Hoxa5
160	771	TRCN0000070863	Hoxb6
	772	TRCN0000070864	Hoxb6
	773	TRCN0000070865	Hoxb6
	774	TRCN0000070866	Hoxb6
	775	TRCN0000070867	Hoxb6
161	776	TRCN0000070888	Hoxb9
	777	TRCN0000070889	Hoxb9
	778	TRCN0000070890	Hoxb9
	779	TRCN0000070891	Hoxb9
	780	TRCN0000070892	Hoxb9
162	781	TRCN0000070908	Hoxc13
	782	TRCN0000070909	Hoxc13
	783	TRCN0000070910	Hoxc13
	784	TRCN0000070911	Hoxc13
163	785	TRCN0000070938	Hoxc6
	786	TRCN0000070939	Hoxc6
	787	TRCN0000070940	Hoxc6
	788	TRCN0000070941	Hoxc6
	789	TRCN0000070942	Hoxc6
164	790	TRCN0000070948	Hoxc8
	791	TRCN0000070949	Hoxc8
	792	TRCN0000070950	Hoxc8
	793	TRCN0000070951	Hoxc8
165	794	TRCN0000070468	Hoxd9
	795	TRCN0000070469	Hoxd9

	796	TRCN0000070470	Hoxd9
	797	TRCN0000070471	Hoxd9
	798	TRCN0000070472	Hoxd9
166	799	TRCN0000034379	Hras1
	800	TRCN0000034380	Hras1
	801	TRCN0000034381	Hras1
	802	TRCN0000034382	Hras1
	803	TRCN0000034383	Hras1
167	804	TRCN0000071433	Id1
	805	TRCN0000071435	Id1
	806	TRCN0000071437	Id1
168	807	TRCN0000071438	Id3
	808	TRCN0000071439	Id3
	809	TRCN0000071440	Id3
	810	TRCN0000071444	Id4
169	811	TRCN0000023489	Igf1r
	812	TRCN0000023490	Igf1r
	813	TRCN0000023491	Igf1r
	814	TRCN0000023492	Igf1r
	815	TRCN0000023493	Igf1r
170	816	TRCN0000096759	Igf2bp2
	817	TRCN0000096760	Igf2bp2
	818	TRCN0000096761	Igf2bp2
	819	TRCN0000096762	Igf2bp2
	820	TRCN0000096763	Igf2bp2
171	821	TRCN0000012858	Igfbp2
	822	TRCN0000012859	Igfbp2
	823	TRCN0000012860	Igfbp2
	824	TRCN0000012861	Igfbp2
	825	TRCN0000012862	Igfbp2
172	826	TRCN0000026867	Ikbkb
	827	TRCN0000026891	Ikbkb
	828	TRCN0000026894	Ikbkb
	829	TRCN0000026913	Ikbkb
	830	TRCN0000026945	Ikbkb
173	831	TRCN0000088808	Ikbkg
	832	TRCN0000088809	Ikbkg
	833	TRCN0000088810	Ikbkg
	834	TRCN0000088811	Ikbkg
	835	TRCN0000088812	Ikbkg
174	836	TRCN0000068248	Il1r2
	837	TRCN0000068249	Il1r2
	838	TRCN0000068250	Il1r2
	839	TRCN0000068251	Il1r2
	840	TRCN0000068252	Il1r2
175	841	TRCN0000085328	Irf6
	842	TRCN0000085329	Irf6
	843	TRCN0000085330	Irf6
	844	TRCN0000085331	Irf6
	845	TRCN0000085332	Irf6
176	846	TRCN0000070478	Irx1
	847	TRCN0000070479	Irx1
	848	TRCN0000070480	Irx1
	849	TRCN0000070481	Irx1
	850	TRCN0000070482	Irx1
177	851	TRCN0000070403	Irx4
	852	TRCN0000070404	Irx4
	853	TRCN0000070405	Irx4
	854	TRCN0000070406	Irx4
	855	TRCN0000070407	Irx4
178	856	TRCN0000070418	Irx5
	857	TRCN0000070419	Irx5
	858	TRCN0000070420	Irx5
	859	TRCN0000070421	Irx5
	860	TRCN0000070422	Irx5
179	861	TRCN0000028850	Jag1
	862	TRCN0000028860	Jag1
	863	TRCN0000028869	Jag1
	864	TRCN0000028887	Jag1
	865	TRCN0000028933	Jag1
180	866	TRCN0000028871	Jag2
	867	TRCN0000028877	Jag2
	868	TRCN0000028897	Jag2
	869	TRCN0000028906	Jag2
181	870	TRCN0000075548	Jub
	871	TRCN0000075549	Jub
	872	TRCN0000075550	Jub
	873	TRCN0000075551	Jub
	874	TRCN0000075552	Jub
182	875	TRCN0000055203	Jun
	876	TRCN0000055204	Jun
	877	TRCN0000055205	Jun
	878	TRCN0000055206	Jun
	879	TRCN0000055207	Jun
183	880	TRCN0000069668	Kctd8
	881	TRCN0000069669	Kctd8
	882	TRCN0000069670	Kctd8
	883	TRCN0000069671	Kctd8
	884	TRCN0000069672	Kctd8
184	885	TRCN0000023744	Kdr
	886	TRCN0000023745	Kdr
	887	TRCN0000023746	Kdr
	888	TRCN0000023747	Kdr
	889	TRCN0000023748	Kdr
185	890	TRCN0000071468	Klf15
	891	TRCN0000071469	Klf15
	892	TRCN0000071470	Klf15
	893	TRCN0000071471	Klf15
	894	TRCN0000071472	Klf15
186	895	TRCN0000075558	Klf3
	896	TRCN0000075559	Klf3
	897	TRCN0000075560	Klf3
	898	TRCN0000075561	Klf3
	899	TRCN0000075562	Klf3
187	900	TRCN0000034384	Kras
	901	TRCN0000034385	Kras
	902	TRCN0000034386	Kras
	903	TRCN0000034387	Kras
	904	TRCN0000034388	Kras
188	905	TRCN0000022524	Ksr1
	906	TRCN0000022525	Ksr1
	907	TRCN0000022527	Ksr1
	908	TRCN0000022528	Ksr1
189	909	TRCN0000022594	Ksr2
	910	TRCN0000022595	Ksr2
	911	TRCN0000022596	Ksr2
	912	TRCN0000022597	Ksr2
	913	TRCN0000022598	Ksr2
190	914	TRCN0000075563	Lasp1
	915	TRCN0000075564	Lasp1
	916	TRCN0000075565	Lasp1
	917	TRCN0000075566	Lasp1
	918	TRCN0000075567	Lasp1
191	919	TRCN0000022704	Lats2
	920	TRCN0000022705	Lats2
	921	TRCN0000022706	Lats2
	922	TRCN0000022707	Lats2
	923	TRCN0000022708	Lats2
192	924	TRCN0000012673	Lef1
	925	TRCN0000012674	Lef1
	926	TRCN0000012675	Lef1
	927	TRCN0000012676	Lef1
	928	TRCN0000012677	Lef1
193	929	TRCN0000067908	Lefty1

	930	TRCN0000067909	Lefty1
	931	TRCN0000067911	Lefty1
	932	TRCN0000067912	Lefty1
194	933	TRCN0000070533	Lhx2
	934	TRCN0000070534	Lhx2
	935	TRCN0000070535	Lhx2
	936	TRCN0000070536	Lhx2
	937	TRCN0000070537	Lhx2
195	938	TRCN0000095669	Limd1
	939	TRCN0000095670	Limd1
	940	TRCN0000095671	Limd1
	941	TRCN0000095672	Limd1
	942	TRCN0000095673	Limd1
196	943	TRCN0000084373	Lmo4
	944	TRCN0000084374	Lmo4
	945	TRCN0000084375	Lmo4
	946	TRCN0000084376	Lmo4
	947	TRCN0000084377	Lmo4
197	948	TRCN0000070438	Lmx1a
	949	TRCN0000070439	Lmx1a
	950	TRCN0000070440	Lmx1a
	951	TRCN0000070441	Lmx1a
	952	TRCN0000070442	Lmx1a
198	953	TRCN0000119622	Lrp1
	954	TRCN0000119623	Lrp1
	955	TRCN0000119624	Lrp1
	956	TRCN0000119625	Lrp1
	957	TRCN0000119626	Lrp1
199	958	TRCN0000119607	Lrp1b
	959	TRCN0000119608	Lrp1b
	960	TRCN0000119609	Lrp1b
	961	TRCN0000119610	Lrp1b
	962	TRCN0000119611	Lrp1b
200	963	TRCN0000119632	Lrp4
	964	TRCN0000119633	Lrp4
	965	TRCN0000119634	Lrp4
	966	TRCN0000119635	Lrp4
	967	TRCN0000119636	Lrp4
201	968	TRCN0000109360	Lrp6
	969	TRCN0000109361	Lrp6
	970	TRCN0000109362	Lrp6
	971	TRCN0000109363	Lrp6
	972	TRCN0000109364	Lrp6
202	973	TRCN0000108455	Lrrc4c
	974	TRCN0000108456	Lrrc4c
	975	TRCN0000108457	Lrrc4c
	976	TRCN0000108458	Lrrc4c
	977	TRCN0000108459	Lrrc4c
203	978	TRCN0000102225	Lrrfip1
	979	TRCN0000102226	Lrrfip1
	980	TRCN0000102227	Lrrfip1
	981	TRCN0000102229	Lrrfip1
204	982	TRCN0000189740	Ly6g6c
	983	TRCN0000190117	Ly6g6c
	984	TRCN0000193012	Ly6g6c
	985	TRCN0000202432	Ly6g6c
205	986	TRCN0000012608	Map2k7
	987	TRCN0000012609	Map2k7
	988	TRCN0000012610	Map2k7
	989	TRCN0000012611	Map2k7
	990	TRCN0000012612	Map2k7
206	991	TRCN0000012763	Map3k14
	992	TRCN0000012764	Map3k14
	993	TRCN0000012765	Map3k14
	994	TRCN0000012766	Map3k14
	995	TRCN0000012767	Map3k14
207	996	TRCN0000012758	Map4k1
	997	TRCN0000012759	Map4k1
	998	TRCN0000012761	Map4k1
	999	TRCN0000012762	Map4k1
208	1000	TRCN0000055223	Mapk14
	1001	TRCN0000055224	Mapk14
	1002	TRCN0000055225	Mapk14
	1003	TRCN0000055226	Mapk14
	1004	TRCN0000055227	Mapk14
209	1005	TRCN0000023184	Mapk3
	1006	TRCN0000023185	Mapk3
	1007	TRCN0000023186	Mapk3
	1008	TRCN0000023187	Mapk3
	1009	TRCN0000023188	Mapk3
210	1010	TRCN0000023179	Mapk4
	1011	TRCN0000023180	Mapk4
	1012	TRCN0000023181	Mapk4
	1013	TRCN0000023182	Mapk4
	1014	TRCN0000023183	Mapk4
211	1015	TRCN0000023199	Mapk6
	1016	TRCN0000023200	Mapk6
	1017	TRCN0000023201	Mapk6
	1018	TRCN0000023202	Mapk6
	1019	TRCN0000023203	Mapk6
212	1020	TRCN0000012599	Mapk8ip1
	1021	TRCN0000012600	Mapk8ip1
213	1022	TRCN0000004691	Mcl1
	1023	TRCN0000004692	Mcl1
	1024	TRCN0000004693	Mcl1
	1025	TRCN0000004694	Mcl1
	1026	TRCN0000004695	Mcl1
214	1027	TRCN0000012068	Mef2c
	1028	TRCN0000012069	Mef2c
	1029	TRCN0000012070	Mef2c
	1030	TRCN0000012071	Mef2c
	1031	TRCN0000012072	Mef2c
215	1032	TRCN0000012523	Meis1
	1033	TRCN0000012524	Meis1
	1034	TRCN0000012525	Meis1
	1035	TRCN0000012526	Meis1
	1036	TRCN0000012527	Meis1
216	1037	TRCN0000022599	Mlkl
	1038	TRCN0000022600	Mlkl
	1039	TRCN0000022601	Mlkl
	1040	TRCN0000022602	Mlkl
	1041	TRCN0000022603	Mlkl
217	1042	TRCN0000034424	Mll1
	1043	TRCN0000034428	Mll1
218	1044	TRCN0000032834	Mmp16
	1045	TRCN0000032835	Mmp16
	1046	TRCN0000032836	Mmp16
	1047	TRCN0000032837	Mmp16
	1048	TRCN0000032838	Mmp16
219	1049	TRCN0000071523	Morf4l1
	1050	TRCN0000071524	Morf4l1
	1051	TRCN0000071525	Morf4l1
	1052	TRCN0000071526	Morf4l1
	1053	TRCN0000071527	Morf4l1
195	1054	TRCN0000012663	Mre11a
	1055	TRCN0000012664	Mre11a
	1056	TRCN0000012665	Mre11a
	1057	TRCN0000012667	Mre11a
196	1058	TRCN0000070623	Msx1
	1059	TRCN0000070624	Msx1
	1060	TRCN0000070625	Msx1
	1061	TRCN0000070626	Msx1
	1062	TRCN0000070627	Msx1
197	1063	TRCN0000075943	Mthfd1l

	1064	TRCN0000075944	Mthfd1l
	1065	TRCN0000075945	Mthfd1l
	1066	TRCN0000075946	Mthfd1l
	1067	TRCN0000075947	Mthfd1l
198	1068	TRCN0000042513	Myc
	1069	TRCN0000042514	Myc
	1070	TRCN0000042515	Myc
	1071	TRCN0000042516	Myc
	1072	TRCN0000042517	Myc
	1073	TRCN0000054853	Myc
	1074	TRCN0000054854	Myc
	1075	TRCN0000054855	Myc
	1076	TRCN0000054856	Myc
199	1077	TRCN0000011993	Myef2
	1078	TRCN0000011994	Myef2
	1079	TRCN0000011995	Myef2
	1080	TRCN0000011996	Myef2
	1081	TRCN0000011997	Myef2
200	1082	TRCN0000071503	Myh9
	1083	TRCN0000071504	Myh9
	1084	TRCN0000071505	Myh9
	1085	TRCN0000071506	Myh9
	1086	TRCN0000071507	Myh9
201	1087	TRCN0000125409	Nav1
	1088	TRCN0000125410	Nav1
	1089	TRCN0000125411	Nav1
	1090	TRCN0000125412	Nav1
	1091	TRCN0000125413	Nav1
202	1092	TRCN0000009791	Nedd9
	1093	TRCN0000009792	Nedd9
	1094	TRCN0000009793	Nedd9
	1095	TRCN0000009794	Nedd9
	1096	TRCN0000009795	Nedd9
203	1097	TRCN0000087559	Neto1
	1098	TRCN0000087560	Neto1
	1099	TRCN0000087561	Neto1
	1100	TRCN0000087562	Neto1
204	1101	TRCN0000086943	Neto2
	1102	TRCN0000086944	Neto2
	1103	TRCN0000086945	Neto2
	1104	TRCN0000086946	Neto2
	1105	TRCN0000086947	Neto2
205	1106	TRCN0000034339	Nf1
	1107	TRCN0000034340	Nf1
	1108	TRCN0000034341	Nf1
	1109	TRCN0000034342	Nf1
	1110	TRCN0000034343	Nf1
206	1111	TRCN0000075343	Nfe2l1
	1112	TRCN0000075344	Nfe2l1
	1113	TRCN0000075345	Nfe2l1
	1114	TRCN0000075346	Nfe2l1
	1115	TRCN0000075347	Nfe2l1
207	1116	TRCN0000012128	Nfe2l2
	1117	TRCN0000012129	Nfe2l2
	1118	TRCN0000012130	Nfe2l2
	1119	TRCN0000012131	Nfe2l2
	1120	TRCN0000012132	Nfe2l2
	1121	TRCN0000054658	Nfe2l2
	1122	TRCN0000054659	Nfe2l2
	1123	TRCN0000054660	Nfe2l2
	1124	TRCN0000054661	Nfe2l2
	1125	TRCN0000054662	Nfe2l2
208	1126	TRCN0000012088	Nfib
	1127	TRCN0000012089	Nfib
	1128	TRCN0000012090	Nfib
	1129	TRCN0000012091	Nfib
	1130	TRCN0000012092	Nfib
209	1131	TRCN0000075348	Nfix
	1132	TRCN0000075349	Nfix
	1133	TRCN0000075350	Nfix
	1134	TRCN0000075351	Nfix
	1135	TRCN0000075352	Nfix
210	1136	TRCN0000096119	Nfkbia
	1137	TRCN0000096120	Nfkbia
	1138	TRCN0000096121	Nfkbia
	1139	TRCN0000096122	Nfkbia
	1140	TRCN0000096123	Nfkbia
211	1141	TRCN0000025895	Notch1
	1142	TRCN0000025902	Notch1
	1143	TRCN0000025908	Notch1
	1144	TRCN0000025918	Notch1
	1145	TRCN0000025935	Notch1
212	1146	TRCN0000012063	Nr1d2
	1147	TRCN0000012064	Nr1d2
	1148	TRCN0000012065	Nr1d2
	1149	TRCN0000012066	Nr1d2
	1150	TRCN0000012067	Nr1d2
213	1151	TRCN0000034389	Nras
	1152	TRCN0000034390	Nras
	1153	TRCN0000034391	Nras
	1154	TRCN0000034392	Nras
	1155	TRCN0000034393	Nras
214	1156	TRCN0000025299	Nrk
	1157	TRCN0000025300	Nrk
	1158	TRCN0000025301	Nrk
	1159	TRCN0000025302	Nrk
	1160	TRCN0000025303	Nrk
215	1161	TRCN0000029859	Nrp1
	1162	TRCN0000029860	Nrp1
	1163	TRCN0000029861	Nrp1
	1164	TRCN0000029862	Nrp1
	1165	TRCN0000029863	Nrp1
216	1166	TRCN0000028974	Nrp2
	1167	TRCN0000028975	Nrp2
	1168	TRCN0000028976	Nrp2
	1169	TRCN0000028977	Nrp2
	1170	TRCN0000028978	Nrp2
217	1171	TRCN0000094624	Nrxn1
	1172	TRCN0000094625	Nrxn1
	1173	TRCN0000094626	Nrxn1
	1174	TRCN0000094627	Nrxn1
	1175	TRCN0000094628	Nrxn1
218	1176	TRCN0000094486	Nrxn2
	1177	TRCN0000094487	Nrxn2
	1178	TRCN0000094488	Nrxn2
219	1179	TRCN0000094189	Nrxn3
	1180	TRCN0000094190	Nrxn3
	1181	TRCN0000094191	Nrxn3
	1182	TRCN0000094192	Nrxn3
	1183	TRCN0000094193	Nrxn3
220	1184	TRCN0000114176	Nudt14
	1185	TRCN0000114177	Nudt14
	1186	TRCN0000114178	Nudt14
	1187	TRCN0000114179	Nudt14
	1188	TRCN0000114180	Nudt14
221	1189	TRCN0000072128	Numa1
	1190	TRCN0000072129	Numa1
	1191	TRCN0000072130	Numa1
	1192	TRCN0000072131	Numa1
222	1193	TRCN0000075838	Oas1f
	1194	TRCN0000075839	Oas1f
	1195	TRCN0000075840	Oas1f
	1196	TRCN0000075841	Oas1f
	1197	TRCN0000075842	Oas1f

223	1198	TRCN0000071193	Orc3l
	1199	TRCN0000071194	Orc3l
	1200	TRCN0000071195	Orc3l
	1201	TRCN0000071197	Orc3l
224	1202	TRCN0000025154	Pak3
	1203	TRCN0000025155	Pak3
	1204	TRCN0000025156	Pak3
	1205	TRCN0000025157	Pak3
	1206	TRCN0000025158	Pak3
225	1207	TRCN0000032809	Pappa2
	1208	TRCN0000032810	Pappa2
	1209	TRCN0000032811	Pappa2
	1210	TRCN0000032812	Pappa2
	1211	TRCN0000032813	Pappa2
226	1212	TRCN0000012573	Pbx1
	1213	TRCN0000012574	Pbx1
	1214	TRCN0000012577	Pbx1
227	1215	TRCN0000094899	Pcdh15
	1216	TRCN0000094900	Pcdh15
	1217	TRCN0000094901	Pcdh15
	1218	TRCN0000094902	Pcdh15
	1219	TRCN0000094903	Pcdh15
228	1220	TRCN0000111680	Pclo
	1221	TRCN0000111681	Pclo
	1222	TRCN0000111682	Pclo
	1223	TRCN0000111683	Pclo
	1224	TRCN0000111684	Pclo
229	1225	TRCN0000174416	Pdpn
	1226	TRCN0000174621	Pdpn
	1227	TRCN0000175972	Pdpn
	1228	TRCN0000176005	Pdpn
230	1229	TRCN0000025977	Pgr
	1230	TRCN0000025996	Pgr
	1231	TRCN0000026003	Pgr
	1232	TRCN0000026032	Pgr
231	1233	TRCN0000055083	Phlda2
	1234	TRCN0000055084	Phlda2
	1235	TRCN0000055085	Phlda2
	1236	TRCN0000055086	Phlda2
	1237	TRCN0000055087	Phlda2
232	1238	TRCN0000088628	Pik3ap1
	1239	TRCN0000088629	Pik3ap1
	1240	TRCN0000088630	Pik3ap1
	1241	TRCN0000088631	Pik3ap1
	1242	TRCN0000088632	Pik3ap1
233	1243	TRCN0000025614	Pik3ca
	1244	TRCN0000025615	Pik3ca
	1245	TRCN0000025616	Pik3ca
	1246	TRCN0000025617	Pik3ca
	1247	TRCN0000025618	Pik3ca
234	1248	TRCN0000024584	Pip5k1a
	1249	TRCN0000024585	Pip5k1a
	1250	TRCN0000024586	Pip5k1a
	1251	TRCN0000024587	Pip5k1a
	1252	TRCN0000024588	Pip5k1a
235	1253	TRCN0000054653	Pitx1
	1254	TRCN0000054654	Pitx1
	1255	TRCN0000054655	Pitx1
	1256	TRCN0000054656	Pitx1
	1257	TRCN0000054657	Pitx1
236	1258	TRCN0000072083	Pkd1
	1259	TRCN0000072084	Pkd1
	1260	TRCN0000072085	Pkd1
	1261	TRCN0000072086	Pkd1
	1262	TRCN0000072087	Pkd1
237	1263	TRCN0000123359	Pkp4
	1264	TRCN0000123360	Pkp4
	1265	TRCN0000123361	Pkp4
	1266	TRCN0000123362	Pkp4
	1267	TRCN0000123363	Pkp4
238	1268	TRCN0000076908	Plcb1
	1269	TRCN0000076909	Plcb1
	1270	TRCN0000076910	Plcb1
	1271	TRCN0000076911	Plcb1
	1272	TRCN0000076912	Plcb1
239	1273	TRCN0000105980	Ppp1r9a
	1274	TRCN0000105981	Ppp1r9a
	1275	TRCN0000105982	Ppp1r9a
	1276	TRCN0000105983	Ppp1r9a
	1277	TRCN0000105984	Ppp1r9a
240	1278	TRCN0000081058	Ppp3ca
	1279	TRCN0000081059	Ppp3ca
	1280	TRCN0000081060	Ppp3ca
	1281	TRCN0000081061	Ppp3ca
	1282	TRCN0000081062	Ppp3ca
241	1283	TRCN0000085193	Prdm9
	1284	TRCN0000085194	Prdm9
	1285	TRCN0000085195	Prdm9
	1286	TRCN0000085196	Prdm9
	1287	TRCN0000085197	Prdm9
242	1288	TRCN0000091048	Prickle2
	1289	TRCN0000091049	Prickle2
	1290	TRCN0000091050	Prickle2
	1291	TRCN0000091051	Prickle2
	1292	TRCN0000091052	Prickle2
243	1293	TRCN0000022875	Prkca
	1294	TRCN0000022878	Prkca
	1295	TRCN0000022754	Prkci
244	1296	TRCN0000022755	Prkci
	1297	TRCN0000022756	Prkci
	1298	TRCN0000022757	Prkci
	1299	TRCN0000022758	Prkci
245	1300	TRCN0000022717	Prkg2
	1301	TRCN0000022718	Prkg2
246	1302	TRCN0000115318	Prom1 (CD133)
	1303	TRCN0000115316	Prom1 (CD133)
	1304	TRCN0000115317	Prom1 (CD133)
	1305	TRCN0000115319	Prom1 (CD133)
	1306	TRCN0000115320	Prom1 (CD133)
247	1307	TRCN0000025359	Prpf4b
	1308	TRCN0000025360	Prpf4b
	1309	TRCN0000025361	Prpf4b
	1310	TRCN0000025362	Prpf4b
	1311	TRCN0000025363	Prpf4b
248	1312	TRCN0000012113	Psip1
	1313	TRCN0000012114	Psip1
	1314	TRCN0000012115	Psip1
	1315	TRCN0000012116	Psip1
	1316	TRCN0000012117	Psip1
249	1317	TRCN0000042538	Ptch1
	1318	TRCN0000042539	Ptch1
	1319	TRCN0000042540	Ptch1
	1320	TRCN0000042541	Ptch1
	1321	TRCN0000042542	Ptch1
250	1322	TRCN0000028989	Pten
	1323	TRCN0000028991	Pten
	1324	TRCN0000028993	Pten
251	1325	TRCN0000011913	Ptgds
	1326	TRCN0000011914	Ptgds
	1327	TRCN0000011915	Ptgds
	1328	TRCN0000011916	Ptgds
	1329	TRCN0000011917	Ptgds
252	1330	TRCN0000067938	Ptgs2
	1331	TRCN0000067939	Ptgs2

	1332	TRCN0000067940	Ptgs2
	1333	TRCN0000067941	Ptgs2
	1334	TRCN0000067942	Ptgs2
253	1335	TRCN0000023484	Ptk2
	1336	TRCN0000023485	Ptk2
	1337	TRCN0000023486	Ptk2
	1338	TRCN0000023487	Ptk2
	1339	TRCN0000023488	Ptk2
254	1340	TRCN0000081068	Ptprz1
	1341	TRCN0000081069	Ptprz1
	1342	TRCN0000081070	Ptprz1
	1343	TRCN0000081071	Ptprz1
	1344	TRCN0000081072	Ptprz1
255	1345	TRCN0000100435	Rab31
	1346	TRCN0000100436	Rab31
	1347	TRCN0000100437	Rab31
	1348	TRCN0000100438	Rab31
	1349	TRCN0000100439	Rab31
256	1350	TRCN0000055188	Rac1
	1351	TRCN0000055189	Rac1
	1352	TRCN0000055190	Rac1
	1353	TRCN0000055191	Rac1
	1354	TRCN0000055192	Rac1
257	1355	TRCN0000012658	Rad51
	1356	TRCN0000012659	Rad51
	1357	TRCN0000012660	Rad51
	1358	TRCN0000012661	Rad51
	1359	TRCN0000012662	Rad51
258	1360	TRCN0000012628	Raf1
	1361	TRCN0000012629	Raf1
	1362	TRCN0000012630	Raf1
	1363	TRCN0000012631	Raf1
	1364	TRCN0000012632	Raf1
	1365	TRCN0000055138	Raf1
	1366	TRCN0000055139	Raf1
	1367	TRCN0000055140	Raf1
	1368	TRCN0000055141	Raf1
	1369	TRCN0000055142	Raf1
259	1370	TRCN0000071953	Rapgef3
	1371	TRCN0000071954	Rapgef3
	1372	TRCN0000071955	Rapgef3
	1373	TRCN0000071956	Rapgef3
	1374	TRCN0000071957	Rapgef3
	1375	TRCN0000077653	Rasa1
	1376	TRCN0000077654	Rasa1
	1377	TRCN0000077655	Rasa1
	1378	TRCN0000077656	Rasa1
	1379	TRCN0000077657	Rasa1
260	1380	TRCN0000042543	Rb1
	1381	TRCN0000042544	Rb1
	1382	TRCN0000042545	Rb1
	1383	TRCN0000042546	Rb1
	1384	TRCN0000042547	Rb1
	1385	TRCN0000055378	Rb1
	1386	TRCN0000055379	Rb1
	1387	TRCN0000055380	Rb1
	1388	TRCN0000055381	Rb1
	1389	TRCN0000055382	Rb1
261	1390	TRCN0000071273	Rbl2
	1391	TRCN0000071274	Rbl2
	1392	TRCN0000071275	Rbl2
	1393	TRCN0000071276	Rbl2
	1394	TRCN0000071277	Rbl2
262	1395	TRCN0000042548	Rel
	1396	TRCN0000042549	Rel
	1397	TRCN0000042550	Rel
	1398	TRCN0000042551	Rel
	1399	TRCN0000042552	Rel
263	1400	TRCN0000120627	Reln
	1401	TRCN0000120628	Reln
	1402	TRCN0000120629	Reln
	1403	TRCN0000120630	Reln
	1404	TRCN0000120631	Reln
264	1405	TRCN0000071343	Rest
	1406	TRCN0000071344	Rest
	1407	TRCN0000071345	Rest
	1408	TRCN0000071346	Rest
	1409	TRCN0000071347	Rest
265	1410	TRCN0000106155	Rims2
	1411	TRCN0000106156	Rims2
	1412	TRCN0000106157	Rims2
	1413	TRCN0000106158	Rims2
	1414	TRCN0000106159	Rims2
266	1415	TRCN0000022634	Ripk4
	1416	TRCN0000022635	Ripk4
	1417	TRCN0000022636	Ripk4
	1418	TRCN0000022637	Ripk4
	1419	TRCN0000022638	Ripk4
267	1420	TRCN0000027509	Rxfp3
	1421	TRCN0000027517	Rxfp3
	1422	TRCN0000027523	Rxfp3
	1423	TRCN0000027528	Rxfp3
	1424	TRCN0000027574	Rxfp3
268	1425	TRCN0000011858	S100a4
	1426	TRCN0000011859	S100a4
	1427	TRCN0000011860	S100a4
	1428	TRCN0000011861	S100a4
	1429	TRCN0000011862	S100a4
269	1430	TRCN0000072043	S100a9
	1431	TRCN0000072044	S100a9
	1432	TRCN0000072045	S100a9
	1433	TRCN0000072046	S100a9
	1434	TRCN0000072047	S100a9
270	1435	TRCN0000071628	Sfrs3
	1436	TRCN0000071629	Sfrs3
	1437	TRCN0000071630	Sfrs3
	1438	TRCN0000071631	Sfrs3
	1439	TRCN0000071632	Sfrs3
271	1440	TRCN0000071933	Sfrs7
	1441	TRCN0000071934	Sfrs7
	1442	TRCN0000071935	Sfrs7
	1443	TRCN0000071936	Sfrs7
	1444	TRCN0000071937	Sfrs7
272	1445	TRCN0000022884	Sgk
	1446	TRCN0000022885	Sgk
	1447	TRCN0000022886	Sgk
	1448	TRCN0000022887	Sgk
273	1449	TRCN0000022879	Sgk2
	1450	TRCN0000022880	Sgk2
	1451	TRCN0000022881	Sgk2
	1452	TRCN0000022882	Sgk2
	1453	TRCN0000022883	Sgk2
274	1454	TRCN0000011953	Si
	1455	TRCN0000011954	Si
	1456	TRCN0000011955	Si
	1457	TRCN0000011956	Si
	1458	TRCN0000011957	Si
275	1459	TRCN0000042563	Ski
	1460	TRCN0000042564	Ski
	1461	TRCN0000042565	Ski
	1462	TRCN0000042566	Ski
	1463	TRCN0000042567	Ski
276	1464	TRCN0000079543	Slc16a1
	1465	TRCN0000079544	Slc16a1

	1466	TRCN0000079545	Slc16a1
	1467	TRCN0000079546	Slc16a1
	1468	TRCN0000079547	Slc16a1
277	1469	TRCN0000079308	Slc6a2
	1470	TRCN0000079309	Slc6a2
	1471	TRCN0000079310	Slc6a2
	1472	TRCN0000079311	Slc6a2
	1473	TRCN0000079312	Slc6a2
278	1474	TRCN0000079253	Slco3a1
	1475	TRCN0000079254	Slco3a1
	1476	TRCN0000079255	Slco3a1
	1477	TRCN0000079256	Slco3a1
	1478	TRCN0000079257	Slco3a1
279	1479	TRCN0000106575	Slit1
	1480	TRCN0000106576	Slit1
	1481	TRCN0000106577	Slit1
	1482	TRCN0000106578	Slit1
	1483	TRCN0000106579	Slit1
280	1484	TRCN0000120817	Slit2
	1485	TRCN0000120818	Slit2
	1486	TRCN0000120819	Slit2
	1487	TRCN0000120820	Slit2
	1488	TRCN0000120821	Slit2
281	1489	TRCN0000114071	Slitrk3
	1490	TRCN0000114073	Slitrk3
	1491	TRCN0000114074	Slitrk3
	1492	TRCN0000114075	Slitrk3
282	1493	TRCN0000025884	Smad1
	1494	TRCN0000025910	Smad1
	1495	TRCN0000025933	Smad1
	1496	TRCN0000025963	Smad1
283	1497	TRCN0000025881	Smad4
	1498	TRCN0000025885	Smad4
	1499	TRCN0000025900	Smad4
	1500	TRCN0000025953	Smad4
284	1501	TRCN0000025891	Smad9
	1502	TRCN0000025893	Smad9
	1503	TRCN0000025912	Smad9
	1504	TRCN0000025913	Smad9
	1505	TRCN0000025937	Smad9
285	1506	TRCN0000071398	Smarca2
	1507	TRCN0000071399	Smarca2
	1508	TRCN0000071400	Smarca2
	1509	TRCN0000071401	Smarca2
	1510	TRCN0000071402	Smarca2
286	1511	TRCN0000085748	Sox2
	1512	TRCN0000085749	Sox2
	1513	TRCN0000085750	Sox2
	1514	TRCN0000085751	Sox2
	1515	TRCN0000085752	Sox2
287	1516	TRCN0000086338	Spic
	1517	TRCN0000086339	Spic
	1518	TRCN0000086340	Spic
	1519	TRCN0000086341	Spic
	1520	TRCN0000086342	Spic
288	1521	TRCN0000087743	Spink5
	1522	TRCN0000087744	Spink5
	1523	TRCN0000087745	Spink5
	1524	TRCN0000087746	Spink5
	1525	TRCN0000087747	Spink5
289	1526	TRCN0000009601	Spp1
	1527	TRCN0000009602	Spp1
	1528	TRCN0000009603	Spp1
	1529	TRCN0000009604	Spp1
	1530	TRCN0000009605	Spp1
	1531	TRCN0000054698	Spp1
	1532	TRCN0000054699	Spp1
	1533	TRCN0000054700	Spp1
	1534	TRCN0000054701	Spp1
	1535	TRCN0000054702	Spp1
290	1536	TRCN0000098415	Sprr1b
	1537	TRCN0000098416	Sprr1b
	1538	TRCN0000098417	Sprr1b
	1539	TRCN0000098418	Sprr1b
	1540	TRCN0000098419	Sprr1b
301	1541	TRCN0000065478	Spry1
	1542	TRCN0000065479	Spry1
	1543	TRCN0000065480	Spry1
	1544	TRCN0000065481	Spry1
	1545	TRCN0000065482	Spry1
302	1546	TRCN0000103591	Spry2
	1547	TRCN0000103592	Spry2
	1548	TRCN0000103593	Spry2
	1549	TRCN0000103594	Spry2
303	1550	TRCN0000065538	Spry3
	1551	TRCN0000065539	Spry3
	1552	TRCN0000065540	Spry3
	1553	TRCN0000065541	Spry3
	1554	TRCN0000065542	Spry3
304	1555	TRCN0000065934	Spry4
	1556	TRCN0000065935	Spry4
	1557	TRCN0000065936	Spry4
	1558	TRCN0000065937	Spry4
305	1559	TRCN0000103170	Sptlc2
	1560	TRCN0000103171	Sptlc2
	1561	TRCN0000103172	Sptlc2
	1562	TRCN0000103173	Sptlc2
	1563	TRCN0000103174	Sptlc2
306	1564	TRCN0000125734	Steap1
	1565	TRCN0000125735	Steap1
	1566	TRCN0000125736	Steap1
	1567	TRCN0000125737	Steap1
	1568	TRCN0000125738	Steap1
307	1569	TRCN0000023729	Styk1
	1570	TRCN0000023730	Styk1
	1571	TRCN0000023731	Styk1
	1572	TRCN0000023732	Styk1
	1573	TRCN0000023733	Styk1
308	1574	TRCN0000072048	Sub1
	1575	TRCN0000072049	Sub1
	1576	TRCN0000072050	Sub1
	1577	TRCN0000072051	Sub1
	1578	TRCN0000072052	Sub1
309	1579	TRCN0000125999	Susd2
	1580	TRCN0000126000	Susd2
	1581	TRCN0000126001	Susd2
	1582	TRCN0000126002	Susd2
	1583	TRCN0000126003	Susd2
310	1584	TRCN0000108875	Syne1
	1585	TRCN0000108876	Syne1
	1586	TRCN0000108877	Syne1
	1587	TRCN0000108878	Syne1
	1588	TRCN0000108879	Syne1
311	1589	TRCN0000042573	Tal1
	1590	TRCN0000042574	Tal1
	1591	TRCN0000042575	Tal1
	1592	TRCN0000042576	Tal1
	1593	TRCN0000042577	Tal1
312	1594	TRCN0000176581	Tanc1
	1595	TRCN0000176582	Tanc1
	1596	TRCN0000178012	Tanc1
	1597	TRCN0000178631	Tanc1
313	1598	TRCN0000012093	Tcf4
	1599	TRCN0000012094	Tcf4

	1600	TRCN0000012095	Tcf4
	1601	TRCN0000012096	Tcf4
	1602	TRCN0000012097	Tcf4
314	1603	TRCN0000012178	Tcf7l2
	1604	TRCN0000012179	Tcf7l2
	1605	TRCN0000012180	Tcf7l2
	1606	TRCN0000012181	Tcf7l2
315	1607	TRCN0000075508	Tcfap2c
	1608	TRCN0000075509	Tcfap2c
	1609	TRCN0000075510	Tcfap2c
	1610	TRCN0000075511	Tcfap2c
	1611	TRCN0000075512	Tcfap2c
316	1612	TRCN0000086223	Tcfap2e
	1613	TRCN0000086224	Tcfap2e
	1614	TRCN0000086225	Tcfap2e
	1615	TRCN0000086227	Tcfap2e
317	1616	TRCN0000071308	Terf2ip
	1617	TRCN0000071309	Terf2ip
	1618	TRCN0000071310	Terf2ip
	1619	TRCN0000071311	Terf2ip
	1620	TRCN0000071312	Terf2ip
318	1621	TRCN0000054809	Tgfbi
	1622	TRCN0000054811	Tgfbi
319	1623	TRCN0000022624	Tgfbr2
	1624	TRCN0000022625	Tgfbr2
	1625	TRCN0000022626	Tgfbr2
	1626	TRCN0000022627	Tgfbr2
	1627	TRCN0000022628	Tgfbr2
320	1628	TRCN0000075523	Tgif2
	1629	TRCN0000075524	Tgif2
	1630	TRCN0000075525	Tgif2
	1631	TRCN0000075526	Tgif2
	1632	TRCN0000075527	Tgif2
321	1633	TRCN0000042593	Tiam1
	1634	TRCN0000042595	Tiam1
	1635	TRCN0000042596	Tiam1
	1636	TRCN0000042597	Tiam1
322	1637	TRCN0000112785	Tm4sf1
	1638	TRCN0000112786	Tm4sf1
	1639	TRCN0000112787	Tm4sf1
	1640	TRCN0000112788	Tm4sf1
	1641	TRCN0000112789	Tm4sf1
323	1642	TRCN0000174268	Tm7sf3
	1643	TRCN0000174778	Tm7sf3
	1644	TRCN0000193418	Tm7sf3
	1645	TRCN0000193467	Tm7sf3
	1646	TRCN0000193517	Tm7sf3
324	1647	TRCN0000110735	Tnc
	1648	TRCN0000110736	Tnc
	1649	TRCN0000110737	Tnc
	1650	TRCN0000110738	Tnc
	1651	TRCN0000110739	Tnc
325	1652	TRCN0000023749	Tnk2
	1653	TRCN0000023750	Tnk2
	1654	TRCN0000023751	Tnk2
	1655	TRCN0000023752	Tnk2
	1656	TRCN0000023753	Tnk2
326	1657	TRCN0000070163	Tnpo2
	1658	TRCN0000070164	Tnpo2
	1659	TRCN0000070165	Tnpo2
	1660	TRCN0000070166	Tnpo2
	1661	TRCN0000070167	Tnpo2
327	1662	TRCN0000012362	Trp53
	1663	TRCN0000054551	Trp53
	1664	TRCN0000054552	Trp53
328	1665	TRCN0000012748	Trp63
	1666	TRCN0000012749	Trp63
	1667	TRCN0000012750	Trp63
	1668	TRCN0000012751	Trp63
	1669	TRCN0000012752	Trp63
329	1670	TRCN0000012753	Trp73
	1671	TRCN0000012754	Trp73
	1672	TRCN0000012755	Trp73
	1673	TRCN0000012756	Trp73
	1674	TRCN0000012757	Trp73
330	1675	TRCN0000094629	Tspan6
	1676	TRCN0000094630	Tspan6
	1677	TRCN0000094631	Tspan6
	1678	TRCN0000094632	Tspan6
	1679	TRCN0000094633	Tspan6
331	1680	TRCN0000094474	Tspan8
	1681	TRCN0000094475	Tspan8
	1682	TRCN0000094477	Tspan8
	1683	TRCN0000094478	Tspan8
332	1684	TRCN0000088743	Ttn
	1685	TRCN0000088744	Ttn
	1686	TRCN0000088745	Ttn
	1687	TRCN0000088746	Ttn
	1688	TRCN0000088747	Ttn
333	1689	TRCN0000071573	Usf2
	1690	TRCN0000071574	Usf2
	1691	TRCN0000071575	Usf2
	1692	TRCN0000071576	Usf2
	1693	TRCN0000071577	Usf2
334	1694	TRCN0000042608	Vav1
	1695	TRCN0000042609	Vav1
	1696	TRCN0000042610	Vav1
	1697	TRCN0000042611	Vav1
	1698	TRCN0000042612	Vav1
335	1699	TRCN0000027068	Vdr
	1700	TRCN0000027098	Vdr
	1701	TRCN0000027101	Vdr
	1702	TRCN0000027104	Vdr
	1703	TRCN0000027123	Vdr
336	1704	TRCN0000066818	Vegfa
	1705	TRCN0000066819	Vegfa
	1706	TRCN0000066820	Vegfa
	1707	TRCN0000066821	Vegfa
	1708	TRCN0000066822	Vegfa
337	1709	TRCN0000097084	Was
	1710	TRCN0000097085	Was
	1711	TRCN0000097086	Was
	1712	TRCN0000097087	Was
	1713	TRCN0000097088	Was
338	1714	TRCN0000012403	Wasf1
	1715	TRCN0000012404	Wasf1
	1716	TRCN0000012405	Wasf1
	1717	TRCN0000012406	Wasf1
	1718	TRCN0000012407	Wasf1
339	1719	TRCN0000099640	Wasl
	1720	TRCN0000099641	Wasl
	1721	TRCN0000099642	Wasl
	1722	TRCN0000099643	Wasl
	1723	TRCN0000099644	Wasl
340	1724	TRCN0000183172	Waspip
	1725	TRCN0000183384	Waspip
	1726	TRCN0000184459	Waspip
	1727	TRCN0000195856	Waspip
341	1728	TRCN0000115481	Wdr63
	1729	TRCN0000115482	Wdr63
	1730	TRCN0000115483	Wdr63
	1731	TRCN0000115484	Wdr63
	1732	TRCN0000115485	Wdr63
342	1733	TRCN0000080203	Wfdc1

	1734	TRCN0000080204	Wfdc1
	1735	TRCN0000080205	Wfdc1
	1736	TRCN0000080206	Wfdc1
	1737	TRCN0000080207	Wfdc1
343	1738	TRCN0000080198	Wfdc2
	1739	TRCN0000080199	Wfdc2
	1740	TRCN0000080200	Wfdc2
	1741	TRCN0000080201	Wfdc2
	1742	TRCN0000080202	Wfdc2
344	1743	TRCN0000042113	Wwox
	1744	TRCN0000042114	Wwox
	1745	TRCN0000042115	Wwox
	1746	TRCN0000042116	Wwox
	1747	TRCN0000042117	Wwox
345	1748	TRCN0000095864	Yap1
	1749	TRCN0000095865	Yap1
	1750	TRCN0000095866	Yap1
	1751	TRCN0000095867	Yap1
	1752	TRCN0000095868	Yap1
346	1753	TRCN0000071943	Zfp503
	1754	TRCN0000071944	Zfp503
	1755	TRCN0000071945	Zfp503
	1756	TRCN0000071946	Zfp503
	1757	TRCN0000071947	Zfp503
347	1758	TRCN0000096684	Zic1
	1759	TRCN0000096685	Zic1
	1760	TRCN0000096686	Zic1
	1761	TRCN0000096687	Zic1
	1762	TRCN0000096688	Zic1

Table S2. List of genes mutated in 306 HNSCC patients ranked by statistical significance of enrichment of these genes with predicted functional mutations. Number of genes displayed: 16.

MM is a number of missense mutations
TM is a number of truncating mutations
SM is a number of silent mutations
FIS≥2 is a number of missense mutations with the predicted functional score bigger than 2 [PMID: 21727090 PMCID: PMC3177186]
DD and D are, respectively, numbers of homozygous and hemizygous deletions
AA and A are, respectively, numbers DNA copy amplifications and DNA copy gains;
P-val (FIS≥2) is a probability to observe the obtained enrichment of predicted functional mutations in a given gene by chance taking as a background distribution the distribution of predicted functional mutations in all other genes. The significant enrichment of the functional mutations in a given gene as compared to the distribution of functional mutations across all other genes demonstrates the positive selection in tumor evolution and suggests that a given gene is a driver.
Q-val (FIS≥2) are P-values adjusted for false discovery rate by Benjamini and Hochberg method with values below 0.1 being considered significant.

Gene	Cytoband	TS/OG	CG	Samples	MM	TM	SM	FIS≥2.0	P val (FIS≥2.0)	Q val (FIS≥2.0)
TP53	17p13.1	1	9	302	171	128	6	160	0	0
NOTCH1	9q34.3	1	10	302	43	31	7	33	0	0
DNAH5	5p15.2	0	0	302	48	14	20	32	0	0
NFE2L2	2q31.2	0	2	302	24	0	0	24	0	0
CASP8	2q33.1	1	4	302	15	18	0	12	0	0
MYH8	17p13.1	0	0	302	21	2	4	15	0.000001	0.002
SMARCA4	19p13.2	1	4	302	16	1	1	12	0.000003	0.006
FAT1	4q35.2	1	1	302	22	89	2	13	0.000006	0.009
RAC1	7p22.1	0	4	302	10	0	0	9	0.000006	0.011
CUL3	2q36.2	0	0	302	9	5	1	8	0.000006	0.011
HIST1H2BD	6p22.1	0	0	302	6	1	0	6	0.000009	0.012
SCN3A	2q24.3	0	1	302	16	2	3	13	0.00001	0.016
PCDHGA1	5q31.3	0	0	302	10	2	1	9	0.00002	0.023
PRPF6	20q13.33	0	1	302	9	0	2	8	0.00002	0.023
EP300	22q13.2	0	10	302	22	8	1	14	0.00002	0.023
MYH9	22q12.3	0	5	302	16	2	4	12	0.00003	0.024

Table S3. Statistics of genomic alterations of *MYH9* across 10 cancer types found in the TCGA data set.

Gene	Cytoband	Cancer type	Samples	MM	TM	SM	FIS>=2.0	DD	D	AA	A	Cancers with DFTM enrichment	Cancers with FM enrichment	Cancers with FTM enrichment
MYH9	22q12.3	BLCA/ LUSC/ GBM/ KIRC/ COADREAD /UCEC/ HNSC/ BRCA/ OVC/ LUAD	3081	102	24	28	**58**	5	**1076**	16	323	LUSC	LUSC/ COADREAD/ UCEC/ HNSC	LUSC/ COADREAD / UCEC/ HNSC/ BRCA/ LUAD

Please, see table 2 for abbreviations.

FM - significant enrichment of predicted functional mutations
FTM significant enrichment of predicted functional and truncating mutations
DFTM - significant enrichment of predicted functional, truncating mutations and deletion

BLCA: bladder carcinoma; LUSC: lung squamous cell carcinoma; GBM: gliobastoma; KIRC: Kidney Renal Papillary Cell Carcinoma; COADREAD: colorectal carcinoma; UCEC: cervical SCC & endocervical carcinoma; HNSCC: head and neck SCC; BRCA: breast carcinoma; OVC: ovarian carcinoma; LUAD; lung adenocarcinoma

Table S4. Full list of cancer types with their respective percentage of *MYH9* hemizygosity

Human Cancers:	MYH9 hemizygosity		MYH9 hemizygosity
HNSCC	15%	Lung Adenocarcinoma	40%
		Lung Squamous Cell Carcinoma	9%
Acute Myeloid Leukemia	1%	Lymphoid Neoplasm Diffuse Large B-cell Lymphoma	6%
Bladder Urothelial Carcinoma	35%	Ovarian Serous Cystadenocarcinoma	79%
Brain Lower Grade Glioma	10%	Pancreatic Adenocarcinoma	15%
Breast Invasive Carcinoma	46%	Prostate Adenocarcinoma	8%
Cervical Squamous Cell Carcinoma and Endocervical Adenocarcinoma	26%	Sarcoma	42%
Colon and Rectum Adenocarcinoma	34%	Skin Cutaneous Melanoma	10%
Glioblastoma Multiforme	38%	Stomach Adenocarcinoma	29%
Kidney Renal Clear Cell Carcinoma	8%	Thyroid Carcinoma	17%
Kidney Renal Papillary Cell Carcinoma	26%	Uterine Corpus Endometrial Carcinoma	11%

Mouse:	Tumor incidence		Tumor incidence
heterozygous *Myh9* iKO *TbRII*-iKO mice	~26%	homozygous *Myh9* iKO *TbRII*-iKO mice	100%

References

1. C. R. Leemans, B. J. Braakhuis, R. H. Brakenhoff, The molecular biology of head and neck cancer. *Nat. Rev. Cancer* **11**, 9–22 (2011). doi:10.1038/nrc2982 Medline

2. N. Stransky, A. M. Egloff, A. D. Tward, A. D. Kostic, K. Cibulskis, A. Sivachenko, G. V. Kryukov, M. S. Lawrence, C. Sougnez, A. McKenna, E. Shefler, A. H. Ramos, P. Stojanov, S. L. Carter, D. Voet, M. L. Cortés, D. Auclair, M. F. Berger, G. Saksena, C. Guiducci, R. C. Onofrio, M. Parkin, M. Romkes, J. L. Weissfeld, R. R. Seethala, L. Wang, C. Rangel-Escareño, J. C. Fernandez-Lopez, A. Hidalgo-Miranda, J. Melendez-Zajgla, W. Winckler, K. Ardlie, S. B. Gabriel, M. Meyerson, E. S. Lander, G. Getz, T. R. Golub, L. A. Garraway, J. R. Grandis, The mutational landscape of head and neck squamous cell carcinoma. *Science* **333**, 1157–1160 (2011). doi:10.1126/science.1208130

3. N. Agrawal, M. J. Frederick, C. R. Pickering, C. Bettegowda, K. Chang, R. J. Li, C. Fakhry, T. X. Xie, J. Zhang, J. Wang, N. Zhang, A. K. El-Naggar, S. A. Jasser, J. N. Weinstein, L. Treviño, J. A. Drummond, D. M. Muzny, Y. Wu, L. D. Wood, R. H. Hruban, W. H. Westra, W. M. Koch, J. A. Califano, R. A. Gibbs, D. Sidransky, B. Vogelstein, V. E. Velculescu, N. Papadopoulos, D. A. Wheeler, K. W. Kinzler, J. N. Myers, Exome sequencing of head and neck squamous cell carcinoma reveals inactivating mutations in NOTCH1. *Science* **333**, 1154–1157 (2011). doi:10.1126/science.1206923 Medline

4. S. Beronja, G. Livshits, S. Williams, E. Fuchs, Rapid functional dissection of genetic networks via tissue-specific transduction and RNAi in mouse embryos. *Nat. Med.* **16**, 821–827 (2010). doi:10.1038/nm.2167 Medline

5. T. R. Berton, T. Matsumoto, A. Page, C. J. Conti, C. X. Deng, J. L. Jorcano, D. G. Johnson, Tumor formation in mice with conditional inactivation of Brca1 in epithelial tissues. *Oncogene* **22**, 5415–5426 (2003). doi:10.1038/sj.onc.1206825 Medline

6. G. Guasch, M. Schober, H. A. Pasolli, E. B. Conn, L. Polak, E. Fuchs, Loss of TGFβ signaling destabilizes homeostasis and promotes squamous cell carcinomas in stratified epithelia. *Cancer Cell* **12**, 313–327 (2007). doi:10.1016/j.ccr.2007.08.020 Medline

7. S. L. Lu, H. Herrington, D. Reh, S. Weber, S. Bornstein, D. Wang, A. G. Li, C. F. Tang, Y. Siddiqui, J. Nord, P. Andersen, C. L. Corless, X. J. Wang, Loss of transforming growth

factor-β type II receptor promotes metastatic head-and-neck squamous cell carcinoma. *Genes Dev.* **20**, 1331–1342 (2006). doi:10.1101/gad.1413306 Medline

8. M. Schober, E. Fuchs, Tumor-initiating stem cells of squamous cell carcinomas and their control by TGF-β and integrin/focal adhesion kinase (FAK) signaling. *Proc. Natl. Acad. Sci. U.S.A.* **108**, 10544–10549 (2011). doi:10.1073/pnas.1107807108 Medline

9. C. Caulin, T. Nguyen, G. A. Lang, T. M. Goepfert, B. R. Brinkley, W. W. Cai, G. Lozano, D. R. Roop, An inducible mouse model for skin cancer reveals distinct roles for gain- and loss-of-function p53 mutations. *J. Clin. Invest.* **117**, 1893–1901 (2007). doi:10.1172/JCI31721 Medline

10. D. Schramek, A. Kotsinas, A. Meixner, T. Wada, U. Elling, J. A. Pospisilik, G. G. Neely, R. H. Zwick, V. Sigl, G. Forni, M. Serrano, V. G. Gorgoulis, J. M. Penninger, The stress kinase MKK7 couples oncogenic stress to p53 stability and tumor suppression. *Nat. Genet.* **43**, 212–219 (2011). doi:10.1038/ng.767 Medline

11. B. Reva, Y. Antipin, C. Sander, Predicting the functional impact of protein mutations: Application to cancer genomics. *Nucleic Acids Res.* **39**, e118 (2011). doi:10.1093/nar/gkr407 Medline

12. C. T. Murphy, R. S. Rock, J. A. Spudich, A myosin II mutation uncouples ATPase activity from motility and shortens step size. *Nat. Cell Biol.* **3**, 311–315 (2001). doi:10.1038/35060110 Medline

13. S. Demehri, A. Turkoz, R. Kopan, Epidermal Notch1 loss promotes skin tumorigenesis by impacting the stromal microenvironment. *Cancer Cell* **16**, 55–66 (2009). doi:10.1016/j.ccr.2009.05.016 Medline

14. C. C. DuFort, M. J. Paszek, V. M. Weaver, Balancing forces: Architectural control of mechanotransduction. *Nat. Rev. Mol. Cell Biol.* **12**, 308–319 (2011). doi:10.1038/nrm3112 Medline

15. A. Fritsch, M. Höckel, T. Kiessling, K. D. Nnetu, F. Wetzel, M. Zink, J. A. Käs, Are biomechanical changes necessary for tumour progression? *Nat. Phys.* **6**, 730–732 (2010). doi:10.1038/nphys1800

16. S. Beronja, P. Janki, E. Heller, W.-H. Lien, B. E. Keyes, N. Oshimori, E. Fuchs, RNAi screens in mice identify physiological regulators of oncogenic growth. *Nature* **501**, 185–190 (2013). doi:10.1038/nature12464

17. P. Levéen, J. Larsson, M. Ehinger, C. M. Cilio, M. Sundler, L. J. Sjöstrand, R. Holmdahl, S. Karlsson, Induced disruption of the transforming growth factor β type II receptor gene in mice causes a lethal inflammatory disorder that is transplantable. *Blood* **100**, 560–568 (2002). doi:10.1182/blood.V100.2.560 Medline

18. V. Vasioukhin, L. Degenstein, B. Wise, E. Fuchs, The magical touch: Genome targeting in epidermal stem cells induced by tamoxifen application to mouse skin. *Proc. Natl. Acad. Sci. U.S.A.* **96**, 8551–8556 (1999). doi:10.1073/pnas.96.15.8551 Medline

19. S. Srinivas, T. Watanabe, C. S. Lin, C. M. William, Y. Tanabe, T. M. Jessell, F. Costantini, Cre reporter strains produced by targeted insertion of EYFP and ECFP into the ROSA26 locus. *BMC Dev. Biol.* **1**, 4 (2001). doi:10.1186/1471-213X-1-4 Medline

20. S. Beronja, G. Livshits, S. Williams, E. Fuchs, Rapid functional dissection of genetic networks via tissue-specific transduction and RNAi in mouse embryos. *Nat. Med.* **16**, 821–827 (2010). doi:10.1038/nm.2167 Medline

21. S. Beronja, E. Fuchs, RNAi-mediated gene function analysis in skin. *Methods Mol. Biol.* **961**, 351–361 (2013). doi:10.1007/978-1-62703-227-8_23 Medline

22. G. Guasch, M. Schober, H. A. Pasolli, E. B. Conn, L. Polak, E. Fuchs, Loss of TGFβ signaling destabilizes homeostasis and promotes squamous cell carcinomas in stratified epithelia. *Cancer Cell* **12**, 313–327 (2007). doi:10.1016/j.ccr.2007.08.020 Medline

23. J. Moffat, D. A. Grueneberg, X. Yang, S. Y. Kim, A. M. Kloepfer, G. Hinkle, B. Piqani, T. M. Eisenhaure, B. Luo, J. K. Grenier, A. E. Carpenter, S. Y. Foo, S. A. Stewart, B. R. Stockwell, N. Hacohen, W. C. Hahn, E. S. Lander, D. M. Sabatini, D. E. Root, A lentiviral RNAi library for human and mouse genes applied to an arrayed viral high-content screen. *Cell* **124**, 1283–1298 (2006). doi:10.1016/j.cell.2006.01.040 Medline

24. S. Beronja, G. Livshits, S. Williams, E. Fuchs, Rapid functional dissection of genetic networks via tissue-specific transduction and RNAi in mouse embryos. *Nat. Med.* **16**, 821–827 (2010). doi:10.1038/nm.2167 Medline

25. S. Beronja, P. Janki, E. Heller, W. H. Lien, B. E. Keyes, N. Oshimori, E. Fuchs, RNAi screens in mice identify physiological regulators of oncogenic growth. *Nature* **501**, 185–190 (2013). doi:10.1038/nature12464 Medline

26. S. E. Williams, S. Beronja, H. A. Pasolli, E. Fuchs, Asymmetric cell divisions promote Notch-dependent epidermal differentiation. *Nature* **470**, 353–358 (2011). doi:10.1038/nature09793 Medline

27. D. Schramek, A. Kotsinas, A. Meixner, T. Wada, U. Elling, J. A. Pospisilik, G. G. Neely, R. H. Zwick, V. Sigl, G. Forni, M. Serrano, V. G. Gorgoulis, J. M. Penninger, The stress kinase MKK7 couples oncogenic stress to p53 stability and tumor suppression. *Nat. Genet.* **43**, 212–219 (2011). doi:10.1038/ng.767 Medline

28. D. Schramek, A. Leibbrandt, V. Sigl, L. Kenner, J. A. Pospisilik, H. J. Lee, R. Hanada, P. A. Joshi, A. Aliprantis, L. Glimcher, M. Pasparakis, R. Khokha, C. J. Ormandy, M. Widschwendter, G. Schett, J. M. Penninger, Osteoclast differentiation factor RANKL controls development of progestin-driven mammary cancer. *Nature* **468**, 98–102 (2010). doi:10.1038/nature09387 Medline

29. C. Blanpain, W. E. Lowry, A. Geoghegan, L. Polak, E. Fuchs, Self-renewal, multipotency, and the existence of two cell populations within an epithelial stem cell niche. *Cell* **118**, 635–648 (2004). doi:10.1016/j.cell.2004.08.012 Medline

30. M. Schober, S. Raghavan, M. Nikolova, L. Polak, H. A. Pasolli, H. E. Beggs, L. F. Reichardt, E. Fuchs, Focal adhesion kinase modulates tension signaling to control actin and focal adhesion dynamics. *J. Cell Biol.* **176**, 667–680 (2007). doi:10.1083/jcb.200608010 Medline

31. E. Cerami, J. Gao, U. Dogrusoz, B. E. Gross, S. O. Sumer, B. A. Aksoy, A. Jacobsen, C. J. Byrne, M. L. Heuer, E. Larsson, Y. Antipin, B. Reva, A. P. Goldberg, C. Sander, N. Schultz, The cBio cancer genomics portal: An open platform for exploring multidimensional cancer genomics data. *Cancer Discov* **2**, 401–404 (2012). doi:10.1158/2159-8290.CD-12-0095 Medline

32. J. Gao, B. A. Aksoy, U. Dogrusoz, G. Dresdner, B. Gross, S. O. Sumer, Y. Sun, A. Jacobsen, R. Sinha, E. Larsson, E. Cerami, C. Sander, N. Schultz, Integrative analysis of complex

cancer genomics and clinical profiles using the cBioPortal. *Sci. Signal.* **6**, pl1 (2013). doi:10.1126/scisignal.2004088 Medline

33. B. Reva, Y. Antipin, C. Sander, Predicting the functional impact of protein mutations: application to cancer genomics. *Nucleic Acids Res.* **39**, e118 (2011). doi:10.1093/nar/gkr407 Medline

34. F. Gnad, A. Baucom, K. Mukhyala, G. Manning, Z. Zhang, Assessment of computational methods for predicting the effects of missense mutations in human cancers. *BMC Genomics* **14** (suppl. 3), S7 (2013). Medline

35. B. Reva, Revealing selection in cancer using the predicted functional impact of cancer mutations. Application to nomination of cancer drivers. *BMC Genomics* **14** (suppl. 3), S8 (2013). doi:10.1186/1471-2164-14-S3-S8 Medline

36. A. Gonzalez-Perez, N. Lopez-Bigas, Functional impact bias reveals cancer drivers. *Nucleic Acids Res.* **40**, e169 (2012). doi:10.1093/nar/gks743 Medline

37. Cancer Genome Atlas Research Network, Integrated genomic analyses of ovarian carcinoma. *Nature* **474**, 609–615 (2011). doi:10.1038/nature10166

38. Cancer Genome Atlas Research Network, Comprehensive genomic characterization defines human glioblastoma genes and core pathways. *Nature* **455**, 1061–1068 (2008). doi:10.1038/nature07385

39. B. S. Taylor, N. Schultz, H. Hieronymus, A. Gopalan, Y. Xiao, B. S. Carver, V. K. Arora, P. Kaushik, E. Cerami, B. Reva, Y. Antipin, N. Mitsiades, T. Landers, I. Dolgalev, J. E. Major, M. Wilson, N. D. Socci, A. E. Lash, A. Heguy, J. A. Eastham, H. I. Scher, V. E. Reuter, P. T. Scardino, C. Sander, C. L. Sawyers, W. L. Gerald, Integrative genomic profiling of human prostate cancer. *Cancer Cell* **18**, 11–22 (2010). doi:10.1016/j.ccr.2010.05.026 Medline

40. J. Barretina, B. S. Taylor, S. Banerji, A. H. Ramos, M. Lagos-Quintana, P. L. Decarolis, K. Shah, N. D. Socci, B. A. Weir, A. Ho, D. Y. Chiang, B. Reva, C. H. Mermel, G. Getz, Y. Antipin, R. Beroukhim, J. E. Major, C. Hatton, R. Nicoletti, M. Hanna, T. Sharpe, T. J. Fennell, K. Cibulskis, R. C. Onofrio, T. Saito, N. Shukla, C. Lau, S. Nelander, S. J. Silver, C. Sougnez, A. Viale, W. Winckler, R. G. Maki, L. A. Garraway, A. Lash, H. Greulich, D. E. Root, W. R. Sellers, G. K. Schwartz, C. R. Antonescu, E. S. Lander, H. E.

Varmus, M. Ladanyi, C. Sander, M. Meyerson, S. Singer, Subtype-specific genomic alterations define new targets for soft-tissue sarcoma therapy. *Nat. Genet.* **42**, 715–721 (2010). doi:10.1038/ng.619 Medline

41. L. Chin, W. C. Hahn, G. Getz, M. Meyerson, Making sense of cancer genomic data. *Genes Dev.* **25**, 534–555 (2011). doi:10.1101/gad.2017311 Medline